UNIVERSITÀ DEL PIEMONTE ORIENTALE

Scuola di Medicina e Chirurgia
Dipartimento di Medicina Traslazionale

Corso di Dottorato di Ricerca in Medical Sciences and Biotechnologies

Ciclo XXXIV

IDIOPATHIC PULMONARY FIBROSIS: FROM MONOCYTE AND MACROPHAGE INFLAMMATION TO A NOVEL, NON-INVASIVE MEASUREMENT OF PULMONARY DENSITY.

Settore Scientifico Disciplinare MED10

Coordinatore

Chiar.ma Prof.ssa Marisa Gariglio

Tutor

Chiar.mo Prof. Mario Malerba

Candidato

Dott. Filippo Patrucco

Summary

Introduction to PhD Project

My PhD project focused on different topics during these three years.

The first part was conducted at Sant'Andrea Hospital in Vercelli where I cooperated with Professor Valente, chief of the Pathology Unit. During this period, I conduced a research project evaluating both basal progenitor cells' markers and epithelial to mesenchymal transition markers on bronchial epithelial mucosal layer of endobronchial biopsies. We aimed to evaluate the different expression of these markers among chronic obstructive pulmonary disease (COPD) and non-COPD patients, as well as their correlation with pulmonary functional tests.

After the first year of research, due to the COIVD-19 pandemic, my research efforts were diverted on clinical and translational research on this field. Of note, in May 2020 I moved to the University Hospital Maggiore della Carità, Novara, where I continued clinical and translational research projects with the COVID-19 UPO team. During the second year, I conduced several clinical studies, mainly based on COVID-19 patients and I coordinated three clinical studies on bronchoalveolar lavage (BAL) of patients affected by SARS-COV-2: the first one was a multicentre study where we investigated the prevalence of SARS-CoV-2 viral infection on BAL fluid of patients with a double negative nasopharyngeal swab PCR test. In the second one, in cooperation with the University Radiology Institute, we demonstrated the correlation between BAL results and radiologic computed tomography pattern. The third study investigated the prevalence of mycotic co-infection, in particular *candida* spp and *aspergillus* spp. on BAL of patients who underwent bronchoscopy for suspected SARS-COV-2 infection.

During the 2020, in cooperation with the Pharmacology Institute of the University of Easter Piedmont, we submitted a research project to Boehringer Ingelheim International: the aim was to evaluate the effects of nintedanib on primary human monocytes and monocyte derived macrophages of patients with idiopathic pulmonary fibrosis (IPF) and healthy volunteers. In particular we aimed to evaluate, ex vivo, the ability of nintedanib to modify the responsiveness (evaluated with the production of oxygen free radicals) of monocytes and monocyte-derived macrophages and their phenotype in patients with IPF and healthy volunteers. In spring 2021 this project was funded by Boehringer Ingelheim International and approved by our local Ethical Committee. We then started the recruitment of both patients and healthy volunteers on August 2021; the results we present in this thesis represent the first part of the project. Finally, we had the possibility to use, first in Italy, a device measuring indirectly lung dielectric proprieties and deriving the fluid content. In cooperation with an international Italo-Israelian team, after the opportune mathematical verifications, we tested

the device on patients with IPF with the aim to evaluate possible correlations with functional, clinical and radiological parameters: here I present preliminary results of this research.

Title: Basal progenitor cells and epithelial to mesenchimal transition markers expression on bronchial biopsies in COPD patients

Background:

The natural history of chronic obstructive pulmonary disease (COPD), the major smokinginduced lung disorder, comprises several decades of accelerated decline in forced expiratory volume in 1 second (FEV1), a hallmark of airway obstruction [1]. Airway remodelling, a major histologic correlate of airway obstruction in COPD [2, 3] has been observed already at early stages of disease and even healthy smokers with COPD-like symptoms and minor decline in FEV1 [4-6]. Thus, an early time-point might exist in the developmental trajectory of COPD, when homeostatic regenerative mechanisms responsible for the maintenance of airway structure become ineffective and/or instead produce tissue remodelling phenotypes, a morphologic basis for airflow limitation.

The airway epithelium is essentially reliant on such homeostatic mechanism since it is continuously exposed to environmental stressors, including cigarette smoke. Basal progenitors (BPs), residing in the basal epithelial layer among basal cells (BCs), generate all cellular elements of the airway epithelium: BCs, via self-renewal, and ciliated, mucus-producing and non-mucous secretory cells via differentiation. In response to smoking, BPs produce remodelling patterns, including squamous met-aplasia, hyperplasia of BCs and mucus-producing cells, and loss of ciliated and nonmucous secretory cells (Figure 1) [7]. Reduced function of airway BPs has been observed in smokers with COPD [8]. Whether this occurs earlier in the natural history of COPD remained an open question.

Figure 1.

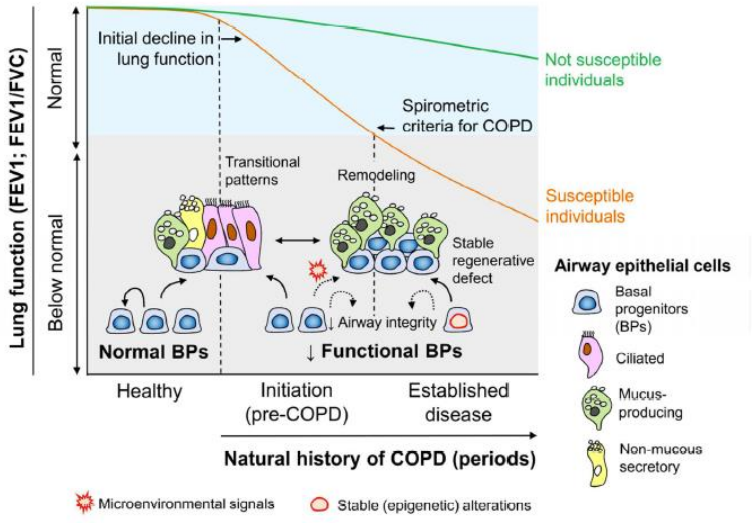

Figure 1. Conceptual model of airway basal progenitor cells (BPs) in the natural history of chronic obstructive

pulmonary disease (COPD). *Airway BPs play a critical role in airway homeostasis due to their ability to maintain the airway epithelium vis self-renewal and differentiation into ciliated, mucus-producing and non-mucous secretory cells. Alterations in BP function may occur in susceptible individuals at different stages of COPD development and contribute to various aspects of disease pathogenesis [7].*

p63 is a p53-homologous nuclear protein that appears to play a crucial role in regulation of stem cell commitment in squamous and other epithelia. The family of at least 13 proteins coded by these 3 genes displays overlapping as well as distinct biologic actions. p53 protein triggers cessation of cell division or apoptosis in response to DNA damage. p73 appears to play an essential role in nervous system development and is abnormally expressed in a number of malignancies. p63 proteins appear to play a critical role in maintaining stem cell populations in squamous and other stratified epithelia [9]. A study conduced on bronchial biopsies of COPD patients demonstrated that the there was 50% of p63 positive cells in COPD epithelia when compared to non-COPD; these cells were located on the basal layer of the epithelium (Figure 2) [10].

Figure 2.

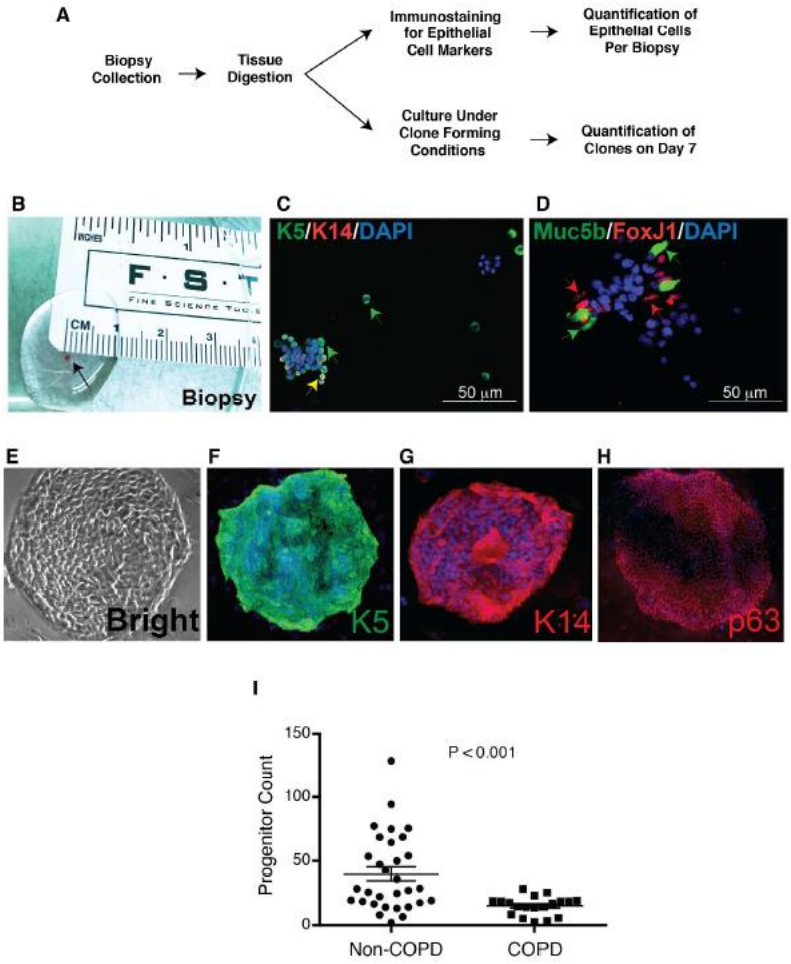

Figure 2. Airway progenitor counts in Non-COPD and COPD airways: *(A) Steps to grow and quantify clone forming basal progenitors from airway biopsies. (B) Representative image of an endobronchial biopsy (arrow). (C) Cytospin preparation of biopsy digest stained with antibodies to K5 (green), K14 (red), and DAPI (blue). K5/K14 dual positive cells are yellow. (D) Cytospin stained with antibodies to Muc5b (green), Fox J1 (red), and DAPI (blue). Scale bars are shown in the image and colored arrows point to each cell type shown in the image. (E – H) Pictures of clones generated by human airway basal progenitor cells. (E) Bright-field image, (F) K5 (green), (G) K14 (red) and (H) p63 (red) and DAPI (blue). Magnification 5x for all. (I) Progenitor counts (number of clones/103 epithelial cells) in Non-COPD (N = 31) and COPD (N = 19). P-value indicates results of Mann Whitney Test [10].*

One potential mechanism contributing to airway fibrosis is transition of airway epithelial cells to a mesenchymal phenotype with myofibroblast characteristics, which then migrate into the lamina propria, a process termed epithelial mesenchymal transition (EMT) (Figure 3) [11].

Figure 3.

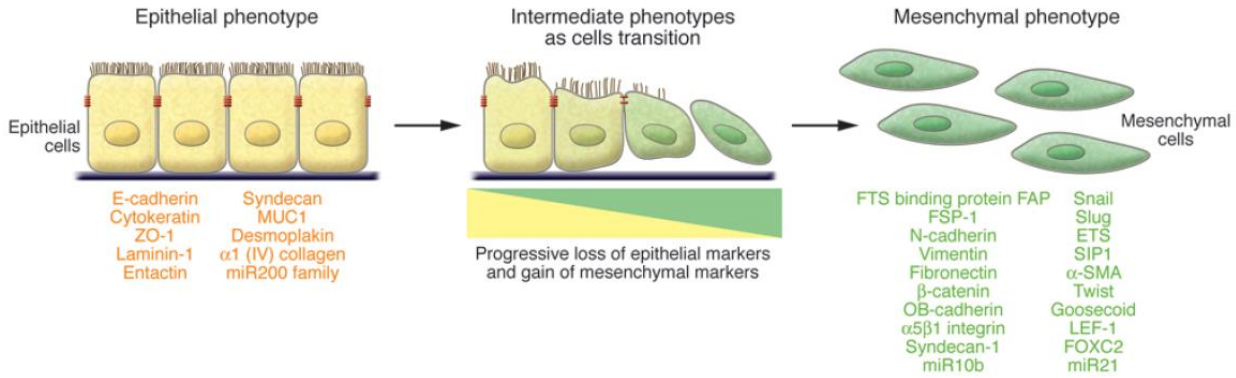

Figure 3, the EMT process: *an EMT involves a functional transition of polarized epithelial cells into mobile and ECM component–secreting mesenchymal cells. The epithelial and mesenchymal cell markers commonly used by EMT researchers are listed. Colocalization of these two sets of distinct markers defines an intermediate phenotype of EMT, indicating cells that have passed only partly through an EMT. Detection of cells expressing both sets of markers makes it impossible to identify all mesenchymal cells that originate from the epithelia via EMT, as many mesenchymal cells likely shed all epithelial markers once a transition is completed. For this reason, most studies in mice use irreversible epithelial cell–lineage tagging to address the full range of EMT-induced changes. ZO-1, zona occludens 1; MUC1, mucin 1, cell surface associated; miR200, microRNA 200; SIP1, survival of motor neuron protein interacting protein 1; FOXC2, forkhead box C2 [11].*

Studies conducted on biopsies performed on large airways of smokers and COPD demonstrated an active EMT observed in airways of smokers and in COPD subjects; this was supported by reticular basement membrane fragmentation both in current smoking patients and in ex-smokers with COPD. Moreover, the amount of staining of epithelial basal cells (marked with EGFR, S100A4 and MMP-9) was higher in all smoking or ex smoking groups [11-14]. Epithelial cells typically lose, transiently, their epithelial characteristics, with loss of polarity and junctional proteins, and acquire mesenchymal features such as vimentin filaments [15]. In a recent study, vimentin-expressing epithelial cells were then analysed as key markers of EMT-related de-differentiation. These cells

were increased in both large and small airways from COPD patients. In addition, epithelial expression of vimentin correlated with airway obstruction in terms of post-bronchodilator FEV1 and FEV1/vital capacity (VC) ratio (Figure 4) [16].

Figure 4.

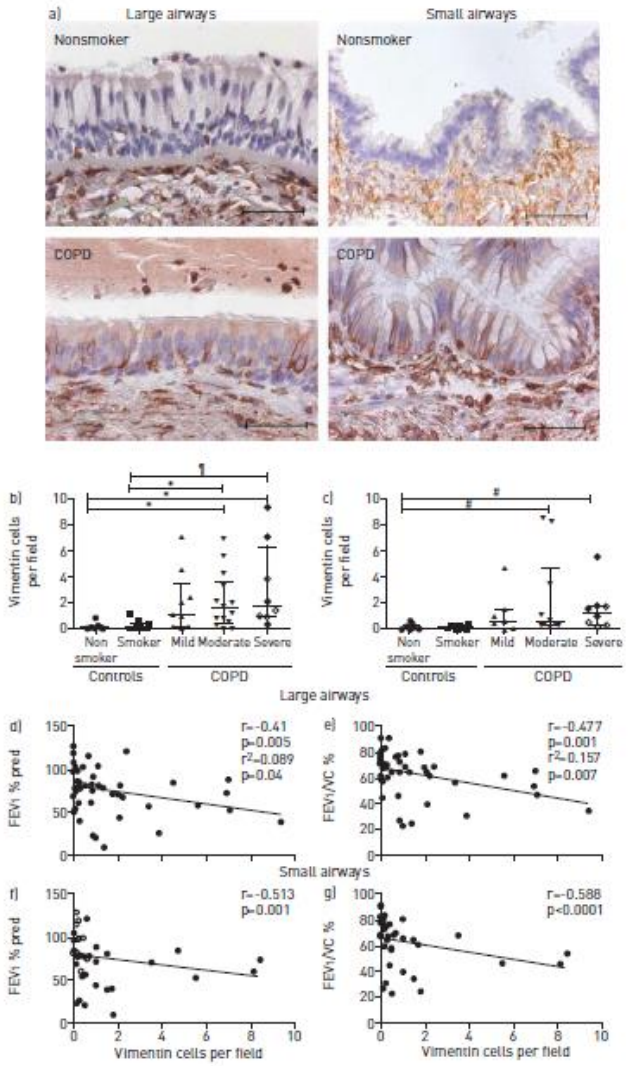

Figure 4, Vimentin immunostaining in lung tissue. *a) Immunohistochemistry for vimentin in large and small airways of a nonsmoker and a severe chronic obstructive pulmonary disease (COPD) patient. b) Quantification of vimentin staining in large airways. c) Quantification of vimentin staining in small. d) Correlation between vimentin staining and forced expiratory volume in 1 s (FEV1) in large airways. e) Correlation between vimentin staining and FEV1/vital capacity (VC) ratio in large airways. f) Correlation between vimentin staining and FEV1 in small airways. g) Correlation between vimentin staining and FEV1/VC ratio in small airways. *: p<0.05; #: p=0.011; ¶: p=0.01. [16]*

Objectives:

First endpoint was the evaluation of different expression of basal (p63) and mesenchymal (vimentin) cell markers in different included populations (COPD patients with or without

emphysematous pattern); secondary endpoint was to evaluate the correlation of p63 and vimentin expression with obstruction functional markers, different locations of bronchial biopsies and lung tumors histotypes.

Third endpoint was to evaluate p63 and vimentin as markers of early functional loss or presence of emphysema at CT scan.

Materials and methods:

Study subjects

We conducted a single center retrospective observational study including all patients who underwent bronchoscopy with bronchial biopsies for suspected lung tumors, between January 2018 and March 2020. We excluded from these analyses all peripheral lung tumors, including specimens only from endobronchial lesions. This study was conducted in cooperation with Universitary Pathology Unit of the same hospital. For each patient we retrieved demographic data, smoking habits, presence of comorbidities, histologic diagnosis of lung tumors, localization of pulmonary lesions at CT scan, presence or absence of emphysema [17], pulmonary function test (FEV1, % of the predicted values, Tiffeneau Index - TI), diagnosis of COPD and severity stratification with GOLD stages in mild, moderate, severe and very severe COPD.

Tissue sampling and processing

Bronchial biopsies have been obtained with forceps during bronchoscopy examinations; we obtained specimens of the suspected endobronchial neoplasms and of the nearby mucosa. Samples were then rapidly fixed in 10% neutral buffered formalin for at least 18 hours.

For staining, bronchial tissue was fixed in 4 % PFA prior to paraffin embedding. The 4 μm-sections were prepared with a microtome and mounted on Superfrost slides. Biopsies were stained by hematoxylin and eosin (H&E) and standard immunohistochemical (IHC) staining for immunophenotyping. We adopted specific p63 and vimentin IHC stainings to mark basal progenitor cells and mesenchymal differentiation respectively. Expression of p63 and vimentin on epithelial cells was expressed by the number of stained cells on one hundred of epithelial cells at microscope (100x enlargement magnification). Counting p63 and vimentin positive cells was performed manually. During the count of vimentin positive cells intraepithelial leukocytes, which also express vimentin, were excluded.

Statistical analysis

A preliminary statistical analysis was performed on included patients. Data are expressed as mean and standard deviations (SD), median (with interquartile ranges, IQR), percentages, as appropriate. The ability of p63 and vimentin expression to detect presence of COPD or emphysema was evaluated using receiver operating characteristic (ROC) curve, with respective sensibility and specificity. Correlation between p63 or vimentin expression and % predicted FEV1 was calculated with Pearson correlation test. Differences in mean marker expressions for each analysed variable were tested with Student's t test or Mann-Whitney U test as appropriate. All p-values were 2-tailed and a p-value <0.05 was considered as statistically significant. Statistical analysis was performed using GraphPad Prism 7 (GraphPad Software, San Diego, CA, USA).

Results

We included in our analysis 24 patients who underwent bronchoscopy with endobronchial biopsies: 15 of them were functionally diagnosed as COPD (62.5%) and 10 (10/15, 66.6%) had radiological signs of emphysema at computed tomography images. Samples were obtained from central airways (trachea and principal bronchi) in 41.6% of cases (10/24) and in 58.4% from peripheral lesions (lobar and segmental bronchi, 14/24). Final cancer diagnosis was non small cell lung cancer in the majority of cases (21/24, 87.5%), with 11 cases of squamocellular and 10 cases of adenocarcinoma; remaining 3 cases were small cell lung cancers (3/24, 12.5%%). Detailed characteristics of patients are represented in Table 1 (Table 1).

Table 1. Characteristics of patients included in the study.

	N (%)
N° of patients	24
Age (mean ± SD) in years	70.53 ± 7.8
COPD patients - Functional diagnosis - Combined functional and radiological	 10/24 (41.6) 14/24 (58.4)
% of predicted FEV1 (in %, ± SD)	73.45 ± 18.7

Site of biopsy (N, %) - Large airways - Small airways	 10/24 (41.6) 14/24 (58.4)
Cancer diagnosis - NSCLC - NSCLC, Adenocarcinoma - NSCLC, Squamocellular carcinoma - SCLC	 21/24 (87.5) 10/21 (47.6) 11/21 (52.4) 3/24 (12.5)
Mean p63 PBC (mean ± SD)	36.50 ± 9.1
Mean Vimentin PBC (mean ± SD)	24.00 ± 11.3

COPD: Chronic Obstructive Pulmonary Disease; FEV1: forced expiratory volume in the first second; NSCLC: non small cell lung cancer; PBC: positive bronchial cells; SCLC: small cell lung cancer

Mean expression of p63 positive bronchial cells (PBC) and vimentin were respectively 36.763 ± SD 7.436 cells and 22.388 ± SD 9.467 cells.

p63 expression

We found an inverse correlation among % predicted FEV1 and PBC expression, with r coefficient of -0.455 (p=0.02); an inverse correlation was found also among FEV1 of COPD patients (r -0.7053, p=0.003) but not in patients without COPD (r -0.396, p=0.291) (Table 2 and Figure 5).

Table 2. p63 PBC and FEV1 correlations in different subgroups.

	Coefficient correlation r	**95% IC**	**p**
% FEV1	**-0,4556**	-0,7256 to -0,06397	0,0253
% FEV1 COPD	**-0,7053**	-0,8944 to -0,3023	0,0033
% FEV1 non-COPD	-0,4445	-0,8559 to 0,3116	0,2306
% FEV1 Emphysema	-0,4260	-0,8324 to 0,2783	0,2196
% FEV1 non-Emphysema	-0,4761	-0,9860 to 0,8941	0,5239

Figure 5

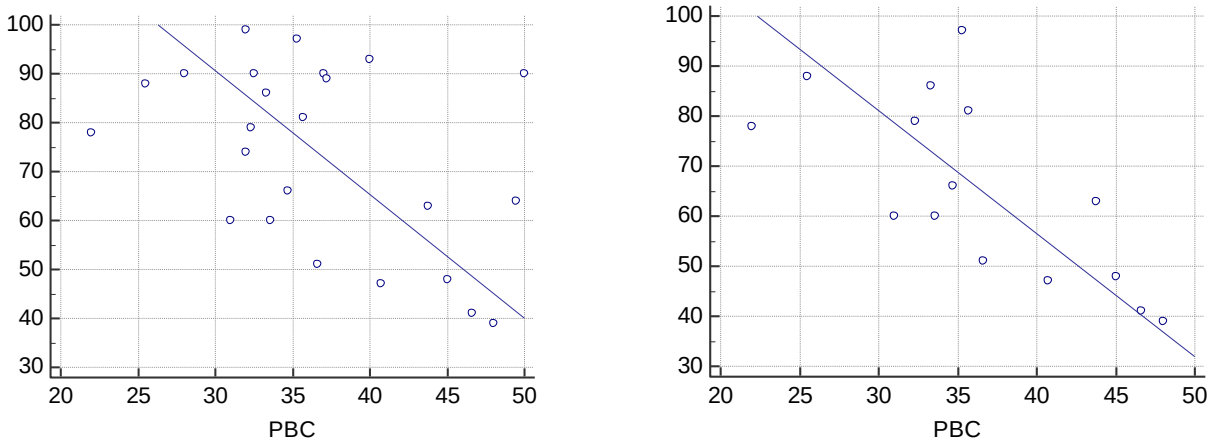

Figure 5: correlations between FEV1 in the whole population and COPD subgroup and p63 PBC.

Among COPD patients, mean p63 expression was slightly higher in emphysematous patients even if this difference was not significative; the same for SCLC versus NSCLC, adenocarcinomas versus squamocellular ones, central versus peripheral airways samples (Table 2) (Figure 6).

Table 2: differences of p63 PBC among different subgroups of samples.

	Mean	**SD**	**p**
COPD	36,2733	7,4632	0,6869
non-COPD	37,5778	7,7664	
Emphysematous	38,3000	5,7157	0,1886
non-Emphysematous	32,2000	10,9930	
Central airways	37,0800	8,6912	0,8060
Peripheral airways	36,2929	6,8318	
NSCLC	36,3857	7,1217	0,5234
SCLC	39,4000	10,8088	
Adenocarcinoma	34,1700	6,7021	0,1804

Squamocellular	38,4000	7,1861	

Figure 6.

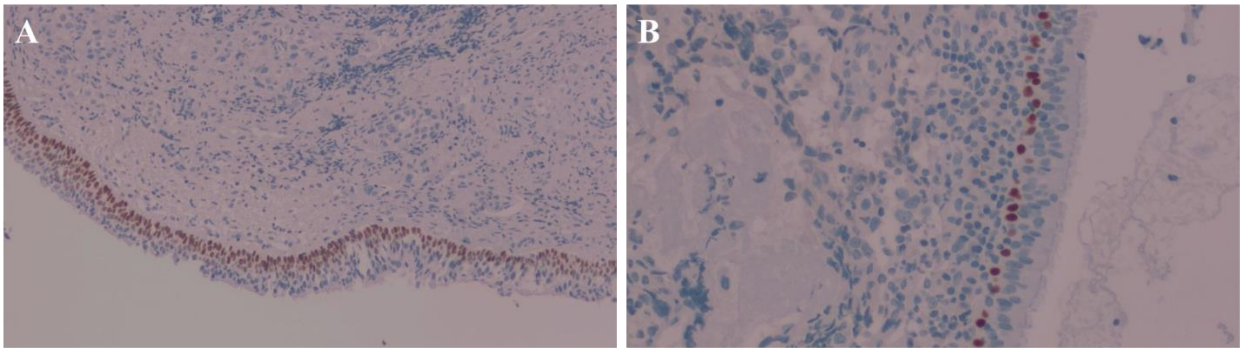

Figure6. p63 PBC stain of basal epithelial layer in non-COPD (A) and COPD (B) subgroups of patients.

ROC curve for COPD diagnosis showed an area under the ROC curve (AUC) of 0.659 (p=0.225); a cut-off of >40 PBC had sensitivity and specificity of 88.67% and 55.57% respectively.

Vimentin expression

We didn't find a direct correlation between % predicted FEV1 and vimentin expression (r coefficient of 0.0801, p=0.709). Even in this case, the correlation wasn't maintained considering separately COPD (r 0.161, p=0.565) and non COPD patients (r -0.150, p=0.701). The only correlation we observed was correlation between age and vimentin expression (r 0.472, p=0.019). Vimentin was highly expressed in emphysematous COPD patients respect non emphysematous COPD but this difference was not statistically significative (Table 3).

Table 3. Vimentin PBC and FEV1 correlations in different subgroups.

	Coefficient correlation r	**95% IC**	**p**
% FEV1	-0,2139	-0,5683 to 0,2074	0,3155
% FEV1 COPD	-0,1507	-0,6155 to 0,3918	0,5918

% FEV1 non-COPD	0,6224	-0,07115 to 0,9103	0,0735
% FEV1 Emphysema	-0,2269	-0,7495 to 0,4699	0,5284
% FEV1 non-Emphysema	0,6490	-0,8295 to 0,9916	0,3510

Vimentin was highly expressed in SCLC respect NSCLC; among NSCLC, expression was higher in adenocarcinoma than squamocelluar ones. Vimentin was highly expressed in peripheral lesion than in central ones, but the difference was not significant (Table 4).

Table 4: differences of vimentin PBC among different subgroups of samples.

	Mean	**SD**	**p**
COPD	22,4133	10,5502	0,9867
non-COPD	22,3444	7,9311	
Emphysematous	23,3400	8,4942	0,8565
non-Emphysematous	22,1250	16,6752	
Central airways	20,9200	11,1638	0,5450
Peripheral airways	23,3714	8,4057	
NSCLC	21,8238	9,9414	0,4526
SCLC	26,3333	3,9716	
Adenocarcinoma	22,9100	9,6454	0,6451
Squamocellular	20,8364	10,5678	

ROC curve for COPD diagnosis showed an area under the ROC curve (AUC) of 0.659 (p=0.225); a cut-off of >31 vimentin positive cells had sensitivity and specificity of 60.00% and 66.70% respectively.

Discussion:

Our results showed that there is an inverse correlation between p63 expression and FEV1; this basal progenitor marker expression increases with the loss of pulmonary function (measured with FEV1) indicating that the number of basal progenitor cells increase. In our cohort we didn't find a difference among COPD and non COPD patients but this could be due to the limited population included in the study. These results are in contrast with those previously published by Ghosh et al. [10] who demonstrated that p36 was less expressed in COPD patients compared to non COPD ones. This could be due to the limited number of patients included, a non highly selected population, the site of the sampling (usually near the endobronchial lesion); moreover in these patients we didn't evaluated the presence of squamous metaplasia (where p63 is hyper expressed).

Vimentin expression is only slightly correlated with FEV1; this data is surprisingly because we didn't expect a direct correlation but an inverse correlation to support the EMT paradigm, as previously demonstrated by Gohy et al [16]. In our cohort we found that COPD patients had an higher expression of vimentin respect those patients without COPD but the results were not statistically significant. Even in this case it could be due to the limited population included in the study or correlated to the site of the sampling.

As previously demonstrated, we confirm that vimentin is highly expressed in SCLC, a neuroendocrine differentiated histotype, than in NSCLC. In fact, the rise in vimentin expression has been reported to be associated with tumor migration, invasion and metastasis which are all factors typically found in SCLC; this reflects tumor cell heterogeneity and EMT during metastasis *in vivo*, accompanied by the development of refractory disease in relapse [18].

Due to previously reported limitations of our cohort, we will investigate basal progenitor cells with the evaluation of epidermal growth factor (EGFR) expression [19]; EMT will be evaluated with other mesenchymal markers (i.e. S100A, ß-catenin, N-cadherin).

Another interesting aspect that it would intriguing to study is the different expression of p63 and vimentin among those patients who have a normal pulmonary function (measured with FEV1 and FEV1/FVC) but that have emphysema at CT scan. In our cohort all non obstructed patients (considering FEV1/FVC ≥ were non emphysematous) and definitive conclusions can't be drawn. We expected that those patients would have similar p63 and vimentin expression than COPD ones with functional obstruction.

Finally, a comparison between results obtained from bronchial biopsies of central airways and distal ones (achieved from transbronchial biopsies or surgical samples) could led us to the evaluation possible early signs of basal or mesenchymal transition.

References

1. Vestbo J, Lange P. Natural history of COPD: Focusing on change in FEV1. Respirology 2016;21:34–43.
2. Hogg JC, Chu F, Utokaparch S, Woods R, Elliott WM, Buzatu L, Cherniack RM, Rogers RM, Sciurba FC, Coxson HO, Paré PD. The nature of small-airway obstruction in chronic obstructive pulmonary disease. N Engl J Med 2004;350:2645–53.
3. McDonough JE, Yuan R, Suzuki M, Seyednejad N, Elliott WM, Sanchez PG, Wright AC, Gefter WB, Litzky L, Coxson HO, Paré PD, Sin DD, Pierce RA, Woods JC, McWilliams AM, Mayo JR, Lam SC, Cooper JD, Hogg JC. Small-airway obstruction and emphysema in chronic obstructive pulmonary disease. N Engl J Med 2011;365:1567–75.
4. Regan EA, Lynch DA, Curran-Everett D, Curtis JL, Austin JHM, Grenier PA, Kauczor H- U, Bai-ley WC, DeMeo DL, Casaburi RH, Friedman P, Van Beek EJR, Hokanson JE, Bowler RP, Bea-ty TH, Washko GR, Han MK, Kim V, Kim SS, Yagihashi K, Washington L, McEvoy CE, Tanner C, Mannino DM, Make BJ, Silverman EK, Crapo JD. Clinical and Radiologic Disease in Smok-ers With Normal Spirometry. JAMA Intern Med 2015;175:1539.
5. Woodruff PG, Barr RG, Bleecker E, Christenson SA, Couper D, Curtis JL, Gouskova NA, Han-sel NN, Hoffman EA, Kanner RE, Kleerup E, Lazarus SC, Martinez FJ, Paine R, Rennard S, Tashkin DP, Han MK. Clinical Significance of Symptoms in Smokers with Preserved Pulmonary Function. N Engl J Med 2016;374:1811–1821.
6. Kirby M, Tanabe N, Tan W, Zhou G, Obeidat M, Hague C, Leipsic J, Bourbeau J, Sin D, Hogg JC, Coxson H, COLD Collaborative Research Group and the Canadian Respiratory Re-search Network. Total Airway Count on Computed Tomography and the Risk of COPD Progres-sion: Findings from a Population-based Study. Am J Respir Crit Care Med [online ahead of print] 08 Sept 2017; http://www.atsjournals.org/doi/abs/10.1164/rccm.201704-0692OC
7. Shaykhiev R, Crystal RG. Early events in the pathogenesis of chronic obstructive pulmonary disease: Smoking-induced reprogramming of airway epithelial basal progenitor cells. Ann Am Thorac Soc 2014;11:S252–S258.
8. Staudt MR, Buro-Auriemma LJ, Walters MS, Salit J, Vincent T, Shaykhiev R, Mezey JG, Tilley AE, Kaner RJ, Ho MWY, Crystal RG. Airway basal stem/progenitor cells

have diminished ca-pacity to regenerate airway epithelium in chronic obstructive pulmonary disease. Am J Respir Crit Care Med 2014;190:955–958.

9. Wang BY, Gil J, Kaufman D, Gan L, Kohtz DS, Burstein DE. P63 in pulmonary epithelium, pulmonary squamous neoplasms, and other pulmonary tumors. Hum Pathol. 2002 Sep;33(9):921-6.
10. Ghosh M, Miller YE, Nakachi I, Kwon JB, Barón AE, Brantley AE, et al. Exhaustion of Airway Basal Progenitor Cells in Early and Established COPD. Am J Respir Crit Care Med. 2018 Apr 1;197(7):885-896.
11. Kalluri R, Weinberg RA. The basics of epithelial-mesenchymal transition. J Clin Invest. 2009 Jun;119(6):1420-8.
12. Zeisberg M, Neilson EG. Biomarkers for epithelial–mesench- ymal transitions. J Clin Invest 2009;119:1429–37.
13. Kalluri R. EMT: when epithelial cells decide to become mesenchymal-like cells. J Clin Invest 2009;119:1417–9.
14. Ward C, Forrest IA, Murphy DM, et al. Phenotype of airway epithelial cells suggests epithelial to mesenchymal cell transition in clinically stable lung transplant recipients. Thorax 2005;60:865–71.
15. Puchelle E, Zahm JM, Tournier JM, et al. Airway epithelial repair, regeneration, and remodeling after injury in chronic obstructive pulmonary disease. Proc Am Thorac Soc 2006; 3: 726–733
16. Gohy ST, Hupin C, Fregimilicka C, Detry BR, Bouzin C, Gaide Chevronay H, et al. Imprinting of the COPD airway epithelium for dedifferentiation and mesenchymal transition. Eur Respir J. 2015 May;45(5):1258-72
17. Lynch DA, Al-Qaisi MA. Quantitative computed tomography in chronic obstructive pulmonary disease. J Thorac Imaging. 2013 Sep;28(5):284-90.
18. Krohn A, Ahrens T, Yalcin A, Plones T, Wehrle J, Taromi S, et al. Tumor Cell Heterogeneity in Small Cell Lung Cancer (SCLC): Phenotypical and Functional Differences Associated with Epithelial-Mesenchymal Transition (EMT) and DNA Methylation Changes. PLoS One. 2014 Jun 24;9(6):e100249
19. Zuo WL, Yang J, Gomi K, Chao I, Crystal RG, Shaykhiev R. EGF-Amphiregulin Interplay in Air-way Stem/Progenitor Cells Links the Pathogenesis of Smoking-Induced Lesions in the Human Airway Epithelium. Stem Cells. 2017 Mar;35(3):824-837

Title: Coronavirus disease 2019: role of bronchoalveolar lavage in SARS-CoV-2 pulmonary infection diagnosis in case of nasopharyngeal swat negativity

Background:

Severe Acute Respiratory Syndrome Coronavirus 2 (SARS-CoV-2) is the virus responsible for the Coronavirus disease 2019 (COVID-19) pandemic affecting millions of people worldwide [1]. The diagnosis of a suspected case is confirmed by the detection of the SARS-CoV-2 in real-time reverse-transcriptase-polymerase chain reaction (rRT-PCR) on biologic samples obtained from nasopharyngeal swabs [2]. However, this method, even if considered the gold standard, has some limitations due to the high rate of false-negative results [3]. It has been demonstrated that, when performed at the initial evaluation of COVID-19 patients, the sensitivity of computed tomography (CT) is significantly higher than that of rRT-PCR (respectively, 97.2 and 83.3%), thus reducing the number of false-negatives related to oropharyngeal swabs tests [4]. To date, no algorithms based on the integration of clinical, radiological, and laboratory data to define the diagnosis of SARSCoV-2 infection without a microbiological positive test have been developed. Many international societies have published documents and guidelines to define the role of bronchoscopy during the COVID-19 pandemic; these documents specify procedures, indications, setting, protection for healthcare workers and patients, and postprocedural disinfection recommendations [5].

Bronchoalveolar lavage (BAL), bronchial wash, as well as other diagnostic sampling procedures that provide fewer respiratory samples are not routinely indicated for COVID-19 diagnosis [6]. However, in a case of severe or progressive disease potentially requiring intubation, if additional specimens would be needed to establish a definitive diagnosis of COVID-19, or to rule out other diagnoses that could change patients' management, a bronchoscopy with BAL can be performed [7]. Recently, Torrego et al. [8] published a case series of 101 bronchoscopies performed on COVID-19 patients with severe acute hypoxemic respiratory failure requiring mechanical ventilation; the most common finding was the presence of a thick hypersecretion, and with guided mini-BAL, clinical suspicion of superinfection could be confirmed [8]. However, no study has reported the diagnostic yield of BAL in patients with suspected or confirmed pulmonary SARS-CoV-2.

The aims of our study were to: (i) evaluate the diagnostic rate of BAL in detecting SARS-CoV-2 pulmonary infection in patients undergoing bronchoscopy for different indications during COVID-19 pandemic, and (ii) describe CT radiological and endoscopic findings and the clinical characteristics of patients with a virological diagnosis of SARS-CoV-2 on BAL.

Materials and Methods

Study Design

This multicenter, retrospective, observational study was conducted in accordance with the STROBE (Strengthening the Reporting of Observational studies in Epidemiology) statement for observational studies [9]. We included all consecutive patients who underwent bronchoscopy with BAL for different indications as part of the research into SARS-CoV-2 between March 16th and May 27th, 2020. We retrospectively gathered data from 3 study centers in northwestern Italy who were actively involved in the emergency care of COVID-19 patients. We excluded cases with incomplete or nonretrievable data. For each patient, demographics (age and sex), in-hospital stay, number of days from the onset of symptoms, indications for bronchoscopy (an inconclusive noninvasive COVID-19 diagnosis, concerns about an alternative etiology of respiratory disease which would alter the management, suspicion of superinfection, or mucus plug-related atelectasis), nasopharyngeal swab result (positive or negative and the number of days before the bronchoscopy), radiological CT characteristics (bilateral, posterior, or multilobar involvement, peripheral distribution, ground-glass opacities, and consolidations), microbiological results of BAL (SARS-CoV-2 positivity/negativity, other respiratory viruses, or bacteria and fungi detected), endoscopic findings (secretions, bronchial inflammation, or lesions), technical procedure (the site where the bronchoscopy was performed, the length of the procedure, sedation, and anesthesia), and laboratory data on peripheral blood (white blood cell count, C-reactive protein level, and procalcitonin level) were collected. For each patient, the number of CT alterations was also calculated.

Statistical Analysis

In the descriptive analysis, n (%) were reported for categorical variables, and mean (SD) or medians (IQR) were used for numerical variables, based on the assumption of normality. To better understand the diagnostic result of BAL and compare the demographic and clinical characteristics between subjects in whom SARS-CoV-2 was or was not identified, Student's t test, Mann-Whitney U test, $\chi 2$ test, or Fisher's exact test were used as appropriate. Further analysis was performed to examine the association between the number of CT alterations and indications on bronchoscopy. A one-way ANOVA model was used and box plots were reported. To establish if sampling conducted at different time points can influence the rate of detection of SARS-CoV-2, firstly, the time was split into 6 intervals of 14 days each from March 16th to May 27th. Then, for each time interval, the

proportion of patients diagnosed with SARS-CoV-2 was calculated in all subjects as well as separately in those suspected of having COVID and all others. Finally, Pearson's correlation was estimated, and linear regression models were fitted to better interpret the trend in time. A two-sided α value < 0.05 was considered statistically significant. Statistical analyses were done using SAS software v9.4.

Results

Study Population

We included 131 consecutive patients in our study. Most of them were males (n = 93, 70.9%) and were hospitalized in an internal medicine ward (n = 83, 63.3%). All procedures were performed in accordance with the most recent recommendations [6]. Indications for bronchoscopy were: 65.5% (n = 86) suspected to have SARS-CoV-2 infection, 12.9% (n = 17) alternative diagnosis (i.e., hemoptysis or lung consolidations), 19.8% (n = 26) suspected superinfections, and 1.5% (n = 2) lung atelectasis. Most patients had previously had a double-negative nasopharyngeal swab for SARS-CoV-2 (n = 120, 91.6%) and bronchoscopy was performed at a median of 1 day (IQR 1–3) after the last nasopharyngeal swab. Bronchoscopies were mainly performed in a bronchoscopic suite (n = 60, 45.8%) with the patient conscious and under sedation (with midazolam or midazolam plus fentanyl, n = 116, 88.5%). Endobronchial secretions were reported only 46 times (36.22%) and 76.0% (n = 35) of them were nonpurulent. Endobronchial erythematous mucosa was observed 31 times (23.6%). In 4 cases (3.1%), a hemorrhagic BAL fluid recovery was recorded (Table 1).

Table 1: Demographic, clinical data. Number (percentages), percentages are referred to columns.

	All n=131	**SARS-CoV-2 not identified n=88**	**SARS-CoV-2 identified n=43**	**p-value**
DEMOGRAPHIC DATA				
Sex				
Female	38 (29.01)	26 (29.55)	12 (27.91)	0.846
Male	93 (70.99)	62 (70.45)	31 (72.09)	
Age				
<65	68 (51.91)	38 (43.18)	30 (69.77)	0.009
65-75	34 (25.95)	25 (28.41)	9 (20.93)	
>75	39 (22.14)	25 (28.41)	4 (9.30)	
Median [IQR]	64.65 [53.71-73.98]	67.01 [56.14-78.56]	55.85 [51.20-66.87]	0.004
Centre				
Novara	48 (36.64)	28 (31.82)	20 (46.51)	0.218
Torino	77 (58.78)	55 (62.50)	22 (51.16)	
Vercelli	6 (4.58)	5 (5.68)	1 (2.33)	
Hospital Unit				
Internistic ward	83 (63.36)	64 (72.73)	19 (44.19)	0.0008

Subintensive	36 (27.48)	21 (23.86)	15 (34.88)	
Intensive care unit	12 (9.16)	3 (3.41)	9 (20.93)	
CLINICAL DATA				
Days from nasopharyngeal swab to bronchoscopy				
Median [IQR]	1 [1-3]	1 [1-2]	2 [1-4]	0.0062
Days from symptoms' onset to bronchoscopy				
Median [IQR]	15 [8-31]	20 [9.5-33.5]	12 [7-20]	0.0221
Indications to bronchoscopy				
Suspected SARS-CoV-2 infection	86 (65.65)	54 (61.36)	32 (74.42)	0.034
Alternative diagnosis	17 (12.89)	15 (17.05)	2 (4.65)	
Suspected superinfection	26 (19.85)	19 (21.59)	7 (16.28)	
Lung atelectasis	2 (1.53)	0 (0)	2 (4.65)	
Nasopharyngeal swab				
Double negative	120 (91.60)	87 (98.86)	33 (76.74)	<0.0001
At least one positive	11 (8.40)	1 (1.14)	10 (23.26)	
Blood analysis, median [IQR]				
White Blood Cells, $x10^3/\mu L$	8.11 [5.98-13.27]	8.44 [6.48-13.40]	7.15 [5.88-10.90]	0.3364
C-reactive protein, mg/dL	7.40 [2-12.30]	6.80 [1.36-12.00]	8.74 [4.05-15.80]	0.0208
Procalcitonin, ng/mL	0.22 [0.080.9]	0.28 [0.08-0.80]	0.16 [0.08-0.90]	0.6675

SARS-CoV-2 Isolation

SARS-CoV-2 was isolated on BAL 43 times (32.8%). We did not find a statistically significant gender prevalence ($p = 0.846$) of SARS-CoV-2 positivity, but the positive patients were younger than the negative ones (55.85 vs. 67.01 years, $p = 0.004$) and the prevalence was higher in those younger than 65 years ($p = 0.009$). Of 120 patients with 2 negative swabs, we isolated SARS-CoV-2 33 times (27.5%), and 76% of these BAL-positive patients had a double-negative swab. For completeness, we note that, in 98.9% of the double-negative swabs, negativity was confirmed even on BAL ($p < 0.0001$). Interestingly, in 1 case with a positive swab, BAL did not detect the virus infection. The number of days from symptoms' onset to bronchoscopy was lower in patients with SARS-CoV-2 infection ($p = 0.022$). C-reactive protein was higher in SARS-CoV-2 positive patients ($p = 0.020$) (Table 1). Significant differences ($p = 0.034$) in the identification of SARS-CoV-2 were observed among the indications of bronchoscopy: in patients with successful virus isolation, the number of suspected COVID-19-positive patients was higher (74.4 vs. 61.36%), but the proportion of patients with suspected superinfections or an alternative diagnosis were lower (16.28 vs. 21.59%, and 4.65 vs. 17.05%) ($p = 0.034$). Remarkably, the virus was identified in only 32/86 (37.2%) patients with suspected SARS-CoV-2. In our cohort, the research of SARS-CoV-2 after a disobstructive bronchoscopy for mucus plugging was only performed twice, and we found the virus in both cases (2/2, 100%).

CT Scan Findings

We observed that, in patients with SARS-CoV-2 infection, the most frequent CT alterations were diffuse ground-glass opacities (n = 38, 88.3%) followed by posterior and peripheral ones (respectively, n = 37, 86.0% and n = 34, 79.0%). Peripheral, posterior, and multilobar alterations were most frequent in SARS-CoV-2-positive patients (respectively, p = 0.009, < 0.001, and 0.028). Moreover, SARS-CoV-2 patients presented with a higher number of CT alterations than patients without SARS-CoV-2 infection (median 5 vs. 4, p = 0.0001) (Table 2). Finally, when we considered 4 different indications on bronchoscopy, we observed that the group suspected of having SARS-CoV-2 presented a higher number of radiological alterations (p = 0.0001) (Figure 1).

Table 2. Radiologic, Bronchoscopic procedure and Microbiological data. Number (percentages), percentages are referred to columns.

	All n=131	**SARS-CoV-2 not identified n=88**	**SARS-CoV-2 identified n=43**	**p-value**
RADIOLOGIC DATA				
Radiological CT characteristics				
- Bilateral	95 (75.52)	62 (70.45)	33 (76.74)	0.4489
- Peripheral	83 (63.36)	49 (55.68)	34 (79.07)	0.0091
- Posterior	77 (58.78)	40 (45.45)	37 (86.05)	<0.001
- Ground-glass	108 (102.44)	70 (79.55)	38 (88.37)	0.2124
- Consolidation	76 (58.02)	49 (55.68)	27 (62.79)	0.4388
- Multilobar	80 (61.07)	48 (54.55)	32 /74.42)	0.0285
Number of CT characteristics per patient				
1	12 (9.16)	10 (11.36)	2 (4.65)	0.002
2	9 (6.87)	7 (7.95)	2 (4.65)	
3	23 (17.56)	19 (21.59)	4 (9.30)	
4	38 (29.01)	32 (36.36)	6 (13.95)	
5	26 (19.85)	11 (12.50)	15 (34.88)	
6	23 (17.56)	9 (10.23)	14 (32.56)	
Median [IQR]	4 [3-5]	4 [3-4]	5 [4-6]	<0.0001
BRONCHOSCOPY PROCEDURE DATA				
Setting				
Patient's bed side	57 (43.51)	37 (42.05)	20 (46.51)	0.0017
Broncoscopic suite	60 (45.80)	47 (53.41)	13 (30.23)	
Subintensive/ICU	14 (10.69)	4 (4.55)	10 (23.26)	
Sedation				
Conscious	116 (88.55)	84 (94.32)	33 (76.74)	0.0030
General anesthesia	15 (11.45)	5 (5.68)	10 (23.26)	
Procedure length, minutes				
Median [IQR]	8 [7-9]	8 [8-9.5]	8 [7-9]	0.0468
Endobronchial secretions	46 (36.22)	33 (39.29)	13 (30.23)	0.3151
Erythematous mucosa	31 (23.85)	21 (24.14)	10 (23.26)	>0.9999
MICROBIOLOGICAL DATA				
At least one germ*	46 (35.11)	33 (37.50)	13 (30.23)	0.4132

Virus (non SARS-CoV-2)	10 (7.75)	7 (8.14)	3 (6.98)	>0.9999
Bacteria	30 (22.90)	20 (22.73)	10 (23.26)	>0.9999
Fungi	19 (14.50)	16 (18.18)	3 (6.98)	0.0507

Figure 1. Mean number of CT characteristics in different indications for bronchoscopy.

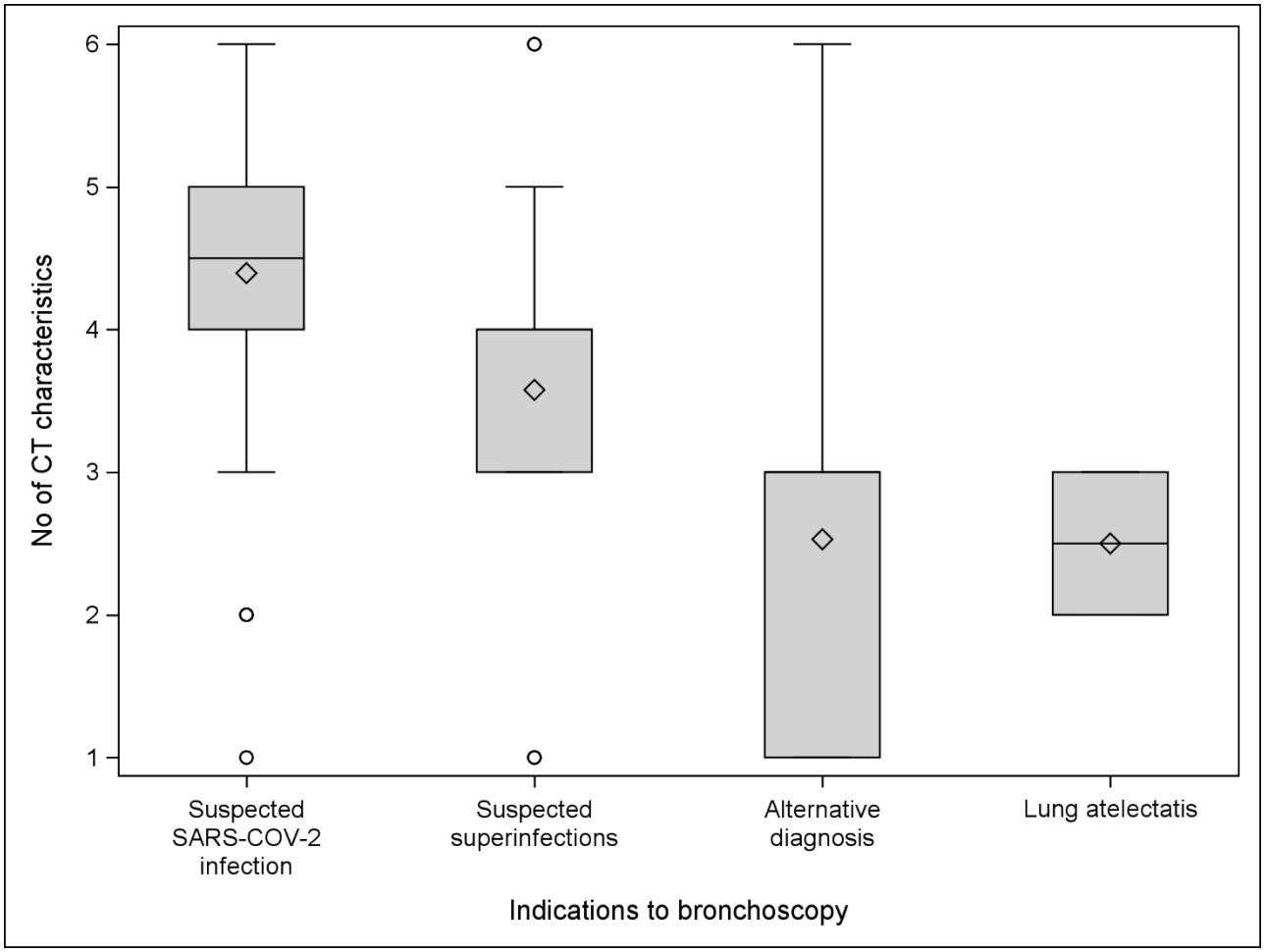

Time Course

When we divided all bronchoscopies performed during the observation period into intervals of 14 days, we observed that the proportion of bronchoscopies with SARS-CoV-2 isolation decreased over time (correlation –0.9687; p = 0.0066) (Figure 2). We observed the same trend when splitting patients into 2 groups, i.e., bronchoscopy for suspected SARS-CoV-2 infection and all other indications (Figure 3). In the subjects with suspected infection, a higher proportion of SARS-CoV-2 was isolated, but this was nearly zero at the end of the study. The last 2 observations (on May 26th and 27th) were excluded from this analysis due to their sparse data.

Figure 2. Proportion of SARS-CoV-2 isolation during the observation period divided into intervals of 14 days.

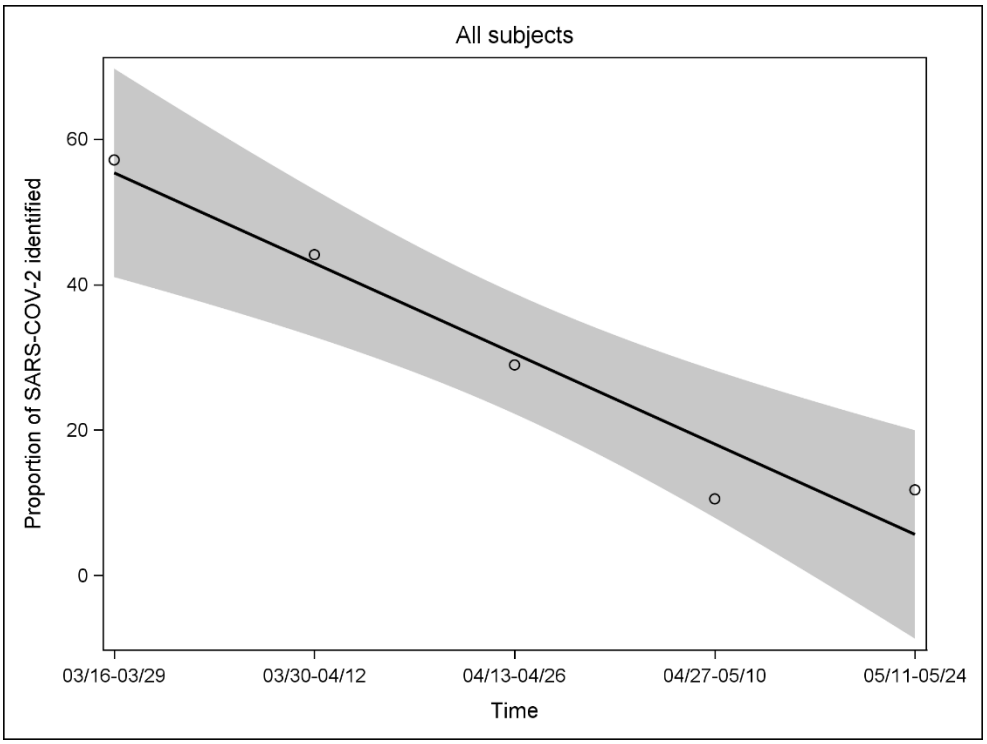

Figure 3. Proportion of SARS-CoV-2 isolation and the detection of other indications during the observation period divided into intervals of 14 days.

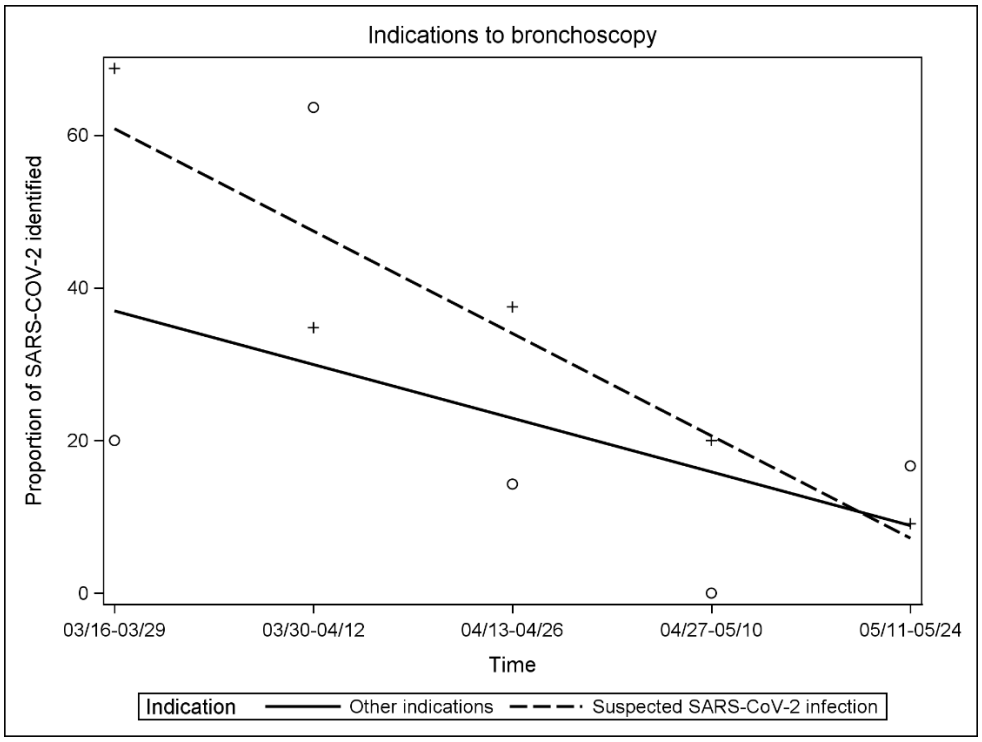

Other Microbiological Findings

Among the patients who underwent bronchoscopy for suspected SARS-CoV-2 infection, 26 other microbiological isolations were observed and 32 SARS-CoV-2-positives (i.e., 67%). Herpesviruses were the other most common viruses isolated (10/57,17.5%); of these, Cytomegalovirus and Human herpesvirus 6 were the most frequent (4× each). Among 30 isolated bacteria, Staphylococcus aureus, Escherichia coli, Klebsiella pneumoniae, and Pseudomonas aeruginosa were the most frequent. Fungi were identified 17 times (Candida albicans was isolated 11 times, i.e., 64.7%). No correlation was found between isolated bacteria, virus, or fungi and SARS-CoV-2-positive or SARS-CoV-2-negative patients (Table 3).

Table 3. Microbiological isolations

	N	**%**
Patients	131	
Viruses	57	
- SARS-CoV-2	43	75.44
- HHV-6	4	7.02
- HSV-1	2	3.51
- CMV	4	7.02
- EBV	2	3.51
- RSV	1	1.75
- Metapneumovirus	1	1.75
Bacteria	30	
- Staphylococcus aureus	9	30
- Escherichia coli	5	16.68
- Klebsiella pneumoniae	4	13.33
- Pseudomonas aeruginosa	4	13.33
- Chlamydia pneumoniae	1	3.33
- Mycoplasma pneumoniae	1	3.33
- Others	6	20
Fungi	17	
- Candida albicans	11	64.70
- Aspergillus spp.	4	23.54
- Others	2	11.77

CMV Cytomegalovirus, EBV Epstein-Barr Virus, HHV-6 Human Herpesvirus 6, HSV-1 Herpes Simplex Virus 1, RSV Respiratory Syncytial Virus, SARS-CoV-2 Severe Acute Respiratory Syndrome Coronavirus 2

Definitive Alternative Diagnosis

For completeness, a definitive alternative diagnosis was achieved in 15 cases. We diagnosed 8 primitive lung cancers, 4 alveolar hemorrhages, 2 cases of cryptogenic organizing pneumonia, and 1 of vasculitis. All cases of alveolar hemorrhage were SARS-CoV-2-negative with a sterile BAL recovery.

Discussion

During the COVID-19 pandemic, routine bronchoscopy with BAL to detect SARS-CoV-2 was not suggested as the first step of the diagnostic procedure, limiting the indications only to few cases [5]. In our cohort, the most frequent indication in the observation period was a suspected SARS-CoV-2 infection (65.5%) in patients with a double-negative nasopharyngeal swab. Interestingly, we confirmed a diagnosis of SARS-CoV-2 in only 37.2% of these patients. This result was probably influenced by several factors. First, the prevalence of SARS-CoV-2 infection changed over time. In fact, we observed that the overall proportion of positive bronchoscopies decreased during the weeks of observation, with a maximum in the first 3 weeks (16th March to 5th April). In Italy, in this lockdown period, we observed the highest incidence of COVID-19 infections (the peak was on the 20th March) [10]. Second, the knowledge about and the perception of the viral infection also changed over time, with several surveys demonstrating that Italian health workers had a good level of knowledge about SARS-CoV-2 and its clinical presentation [11, 12]. However, this was likely in contrast to the increased availability of diagnostic tools, with the fear of clinical and epidemiological implications due to a missed diagnosis [13]. Finally, we were asked to confirm or definitively exclude SARS-CoV-2 infection so as to isolate the infected patients. In cases with double-negative nasopharyngeal swabs, when the CT scan produced uncertain results, we decided to perform a bronchoscopy with BAL to confirm the diagnosis. This is probably the reason for the increased number of bronchoscopies with a negative SARS-CoV-2 outcome, lowering the positivity rate of this indication.

In this study population, the overall diagnostic rate of SARS-CoV-2 detection was 32.8%; this diagnostic yield is better than that reported in the literature in patients affected by viral community-acquired pneumonia, where BAL provided a specific diagnosis in 15% of patients [14, 15]. Up to now, only Wang et al. [16] reported the results of BAL in severely ill COVID-19 patients whose diagnosis was based on symptoms, radiology, and SARS-CoV-2 detection. SARS-CoV-2 was detected in specimens from multiple anatomic sites. They reported a SARS-CoV-2 diagnosis in 14/15 patients who underwent bronchoscopy with BAL (93%). These data suggest that, in patients with COVID-19, the viral load in cases of lower respiratory tract infection was higher and this could explain the high positivity rates for BAL [16]. There are various possible explanations for our different diagnostic rates. First, we mainly investigated patients with a suspected SARS-CoV-2 infection with 2 negative nasopharyngeal swabs. When we considered patients with at least 1 positive swab, we identified SARS-CoV-2 in 90.9% of cases (10/11 patients). Second, in our cohort, we observed significant differences as the days elapsed after symptoms' onset and bronchoscopy among patients with and without infection. It has been demonstrated that the viral

load, and consecutively the BAL diagnostic rate, decrease gradually from symptoms' onset, with a maximum of positive swabs after 5 days [17]. In our cohort, positive patients underwent bronchoscopy a median of 12 days after the development of symptoms. In the patients that tested negative, we cannot be absolutely certain about the absence of infection because more time had elapsed from symptoms' onset. Finally, when BAL results were negative for SARS-CoV-2 in 98% of the cases (87/88), we had a double-negative nasopharyngeal swab which confirmed the previously reported data [18]. On the other hand, when the BAL result was positive for SARS-CoV-2 in 76% of cases (33/43), we also had a double-negative nasopharyngeal swab. When we considered only those patients who underwent bronchoscopy for suspected SARS-CoV-2 infection, in 26 cases, we isolated other pathogens that could have influenced the suspicion of a viral infection. With these isolations, the diagnostic rate of BAL in clinical cases suspected for interstitial acute infectious diseases rose to 67% (58/86 bronchoscopies), which led to a correct therapeutic indication (COVID-19 or non-COVID-19) and admission to an appropriate setting. It must be noted that some isolated pathogens (viruses, in particular) can be innocent bystanders not representing an infectant agent. Among the noninfective diagnoses, we found 2 of cryptogenic organizing pneumonia [19]. In both these cases, BAL was negative for SARS-CoV-2; however, we can't completely rule out a previous viral infection because symptoms started 17 days before we performed the bronchoscopy.

There are several CT features that have been reported in COVID-19 patients, e.g., ground glass opacities, with or without consolidations in the peripheral and posterior lung zones. Their frequency and characteristics depend on when the patient undergoes the CT, and it has been demonstrated that the nature of the alterations can change during the course of an infection [20]. The number of CT findings has been used to predict SARS-CoV-2 infection in patients with moderate to severe symptoms, with a substantial interobserver agreement [21]. In our cohort, we confirmed that patients with SARS-CoV-2 infection presented with a higher number of CT alterations than the SARS-CoV-2-negative patients; moreover, peripheral, posterior, and multilobar alterations were observed most frequently. The patients who underwent bronchoscopy for a suspected SARS-CoV-2 infection presented with a higher number of CT alterations than patients with other indications. These results were likely biased by the variable indications used to perform the procedure; the higher the number of CT alterations, the higher the pretest probability of infection [21]. Nevertheless, we also tested for SARS-CoV-2 in patients with only 1 or 2 CT alterations and we could isolate the pathogen.

Our study has some limitations. First, we conducted a retrospective study; during the COVID-19 pandemic, due to the tumultuous course of the spread of the infection, once international guidelines become available, we gathered data about indications for bronchoscopy but with all the limitations of a retrospective study. Second, we did not collect data about the cycle threshold values of RT-PCR; such data would provide more information about the viral load in the BAL fluid. Wang et al. [16] demonstrated that BAL and nasal swabs had a lower cycle threshold, corresponding to the higher viral copy numbers. The final diagnosis of COVID-19 is difficult, particularly in patients with contrasting diagnostic test results, and so actually requires a multidisciplinary approach and discussion [22]. For this reason, we limited our study to the report of SARS-CoV-2 isolation in BAL fluid, and how these data influence the diagnostic rate of infection. Finally, regarding CT alterations, we calculated a score based on the sum of each CT finding by weighting each single alteration with the same value. Some features are more typical of SARS-CoV-2 infection (i.e., groundglass opacities) and so they should probably have a specific single score.

In conclusion, bronchoscopy with BAL should be reserved for cases that match the internationally suggested and widely accepted indications. In our multicenter experience, we reported a high number of bronchoscopies with BAL for suspected SARS-CoV-2 infection, in patients with 2 negative swabs, with a viral detection rate of 37.2%. Nevertheless, BAL led to a final microbiological diagnosis in 67% of the patients. The agreement of BAL with nasopharyngeal swabs was high, accounting for 90 and 98% positive and negative cases, respectively. CT alterations could predict the pretest probability of SARS-CoV-2 infection, but clinical suspicion of viral infection should always be considered due to the mutability of CT patterns during infection evolution and seasonal epidemiologic burn.

References

1. Luo F, Darwiche K, Singh S, Torrego A, Steinfort DP, Gasparini S, et al. Performing Bronchoscopy in Times of the COVID-19 Pandemic: Practice Statement From an International Expert Panel. Respiration. 2020;99(5):417-422. doi: 10.1159/000507898

2. Corman VM, Landt O, Kaiser M, Molenkamp R, Meijer A, Chu DK, et al. Detection of 2019 Novel Coronavirus (2019-nCoV) by Real-Time RT-PCR. Euro Surveill. 2020 Jan;25(3):2000045. doi: 10.2807/1560-7917.ES.2020.25.3.2000045.

3. Woloshin S, Patel N, Kesselheim A. False Negative Tests for SARS-CoV-2 Infection — Challenges and Implications. New Engl J Med. 2020. doi: 10.1056/NEJMp2015897

4. Long C, Xu H, Shen Q, Zhang X, Fan B, Wang C, et al. Diagnosis of the Coronavirus Disease (COVID-19): rRT-PCR or CT? Eur J Radiol. 2020 May;126:108961. doi: 10.1016/j.ejrad.2020.108961.

5. Lentz RJ, Colt H. Summarizing Societal Guidelines Regarding Bronchoscopy During the COVID-19 Pandemic. Respirology. 2020 Jun;25(6):574-577. doi: 10.1111/resp.13824.

6. Wahidi MM, Lamb C, Murgu S, Musani A, Shojaee S, Sachdeva A, et al. American Association for Bronchology and Interventional Pulmonology (AABIP) Statement on the Use of Bronchoscopy and Respiratory Specimen Collection in Patients with Suspected or Confirmed COVID-19 Infection. J Bronchology Interv Pulmonol. 2020 Mar 18;10.1097/LBR.0000000000000681. doi: 10.1097/LBR.0000000000000681.

7. Wahidi MM, Shojaee S, Lamb CR, Ost D, Maldonado F, Eapen G, et al. The Use of Bronchoscopy During the COVID-19 Pandemic: CHEST/AABIP Guideline and Expert Panel Report. Chest. 2020 May 1;S0012-3692(20)30850-3. doi: 10.1016/j.chest.2020.04.036.

8. Torrego A, Pajares V, Fernández-Arias C, Vera P, Mancebo J. Bronchoscopy in COVID-19 Patients With Invasive Mechanical Ventilation: A Center Experience. Am J Respir Crit Care Med. 2020 May 15. doi: 10.1164/rccm.202004-0945LE.

9. von Elm E, Altman DG, Egger M, Pocock SJ, Gøtzsche PC, Vandenbroucke JP, et al. The Strengthening the Reporting of Observational Studies in Epidemiology (STROBE) Statement: Guidelines for Reporting Observational Studies. J Clin Epidemiol. 2008 Apr;61(4):344-9. doi: 10.1016/j.jclinepi.2007.11.008.

10. Ministero della salute. [Internet] Covid-19 – Situazione in Italia, June 08, 2020. Available from: http://www.salute.gov.it/portale/nuovocoronavirus/dettaglioContenutiNuovoCoronavirus.jsp?area=nuovoCoronavirus&id=5351&lingua=italiano&menu=vuoto

11. Moro M, Vigezzi GP, Capraro M, Biancardi A, Nizzero P, Signorelli C, Odone A. 2019-novel coronavirus survey: knowledge and attitudes of hospital staff of a large Italian teaching hospital. Acta Bio Med. 2020;91(3-S):29-4.

12. Di Lorenzo G, Di Trolio R. Coronavirus Disease (COVID-19) in Italy: Analysis of Risk Factors and Proposed Remedial Measures. Front. Med. 2020;7:140. doi: 10.3389/fmed.2020.00140

13. Rosembaum L. Facing Covid-19 in Italy - Ethics, Logistics, and Therapeutics on the Epidemic's Front Line. N Engl J Med 2020; 382:1873-1875

14. Garbino J, Soccal PM, Aubert JD, Rochat T, Meylan P, Thomas Y, et al. Respiratory viruses in bronchoalveolar lavage: a hospital-based cohort study in adults. Thorax. 2009 May;64(5):399-404. doi: 10.1136/thx.2008.105155.

15. Oren I, Hardak E, Zuckerman T, Geffen Y, Hoffman R, Yigla M, et al. Does Molecular Analysis Increase the Efficacy of Bronchoalveolar Lavage in the Diagnosis and Management of Respiratory Infections in Hemato-Oncological Patients? Int J Infect Dis. 2016 Sep;50:48-53. doi: 10.1016/j.ijid.2016.07.011.

16. Wang W, Xu Y, Gao R, Lu R, Han K, Wu G, Tan W. Detection of SARS-CoV-2 in Different Types of Clinical Specimens. JAMA. 2020 Mar 11;323(18):1843-4. doi: 10.1001/jama.2020.3786.

17. Kucirka LM, Lauer SA, Laeyendecker O, Boon D, Lessler J. Variation in False-Negative Rate of Reverse Transcriptase Polymerase Chain Reaction–Based SARS-CoV-2 Tests by Time Since Exposure. Ann Intern Med. 2020 May 13;M20-1495. doi: 10.7326/M20-1495.

18. Simpson S, Kay FU, Abbara S, Bhalla S, Chung JH, Chung M, et al. Radiological Society of North America Expert Consensus Statement on Reporting Chest CT Findings Related to COVID-19. Endorsed by the Society of Thoracic Radiology, the American College of Radiology, and RSNA. J Thorac Imaging. 2020 Apr 28;10.1097/RTI.0000000000000524. doi: 10.1097/RTI.0000000000000524.

19. Prokop M, van Everdingen W, van Rees Vellinga T, van Ufford JQ, Stoger L, Beenen L, et al. CO-RADS – A categorical CT assessment scheme for patients with suspected COVID-19: definition and evaluation. Radiology. 2020 Apr 27;201473. doi: 10.1148/radiol.2020201473.

Title: COVID-19 diagnosis in case of two negative nasopharyngeal swabs: association between chest CT and bronchoalveolar lavage results.

Background

The final diagnosis of Severe Acute Respiratory Coronavirus 2 (SARS-CoV-2) infection is based on real-time reverse-transcriptase-polymerase reaction (rRT-PCR) virus positivity on nasopharyngeal swab [1]. However, this method is characterized by a high rate of false negative results, with a sensitivity ranging between 42% and 83% [2]. The role of computed tomography (CT) in the workup of patients is still debated and the Fleischner Society suggests a role in case of symptoms worsen or reduced availability for rRT-PCR [3]. Sensitivity and specificity of CT for Coronavirus Disease 2019 (COVID-19) are variable due to the lack of diagnostic criteria for viral infection. Positive and negative predictive value of CT for SARS-CoV-2 infection are respectively 92% and 42%; the low negative predictive value may indicate that in early phases CT wouldn't be the optimal screening test for COVID-19 diagnosis [4]. Very recently, the Society of Thoracic Radiology/Radiological Society of North America (STR/RSNA) proposed a structured report template to guide radiologists reporting CT findings potentially attributable to SARS-CoV-2 pneumonia. They suggested four categories based presence or absence of features: typical, with commonly reported imaging features for SARS-CoV-2 pneumonia; indeterminate, with nonspecific imaging features for SARS-CoV-2 pneumonia; atypical, with uncommonly or non-reported features of COVID-19 pneumonia; negative for pneumonia, without feature of pneumonia [4]. In a recent retrospective study conducted during the peak of the Italian epidemics the authors stated that the STR/RSNA criteria could increase the CT specificity up to 78.8% [5]. Prokop et al. introduced the COVID-19 Reporting and Data System (CO-RADS) for a standardized assessment of pulmonary involvement of SARS-CoV-2: CO-RADS indicates the suspicion of infection on a scale from 1 (very low) to 5 (very high) based on CT findings. The authors demonstrated a very good performance for predicting COVID-19 in patients with moderate to severe symptoms, with a substantial interobserver agreement [2].

Bronchoscopy during the COVID-19 pandemic should be reserved to a limited number of indications as suggested by international guidelines and recommendations [6]. Due to these limited indications and the absence of precise diagnostic criteria for SARS-CoV-2 infection based on endoscopic viral isolation, no prospective studies reported bronchoalveolar lavage (BAL) diagnostic yield neither the association between microbiological nor radiological findings.

Based on these assumption and to results that we previously demonstrated [7], we aimed to evaluate the association of two different chest CT probability scores for SARS-CoV-2 pulmonary infection, CO-RADS score and STR/RSNA categories with BAL results in patients with two negative nasopharyngeal swab RT-PCR tests.

Material and Methods

Study population

We conducted a single centre, retrospective and observational study, in accordance with Strengthening the Reporting of Observational studies in Epidemiology (STROBE) statement for observational studies [8]. We included all the consecutive patients who underwent in our institution both a bronchoscopy with BAL, for different indications, with the research of SARS-CoV-2 RNA, and a chest CT scan with two consecutive nasopharyngeal swabs in the Emergency setting. Data were collected between March 16th and May 19th, 2020. We excluded from the analysis those cases with incomplete or non-retrievable data or with at least one positive nasopharyngeal swab. The patients who performed the bronchoscopy more than 7 days after the chest CT scan were also excluded. The study was approved by the institutional committee on human research (approval protocol number CE 97/20).

Bronchoscopy and bronchoalveolar lavage technique

During flexible bronchoscopy the tip of the instrument is placed in wedge position through the tributary bronchus of the selected segment of lung parenchyma; three 50 mL aliquots of saline are instilled through the bronchoscope and, after each instillation, the lavage fluid is retrieved using a suction pressure. An optimal sampling is the one that allows to retrieve more than 30% of the instilled fluid. The BAL fluid recovered was then used for microbiological analysis, included the research of SARS-CoV-2 RNA [9].

CT acquisition Technique

The chest CT scans have been acquired in a single full inspiratory breath hold in supine position. We used a 128-slice CT (Philips Ingenuity Core, Philips Healthcare, Netherlands). The scan technical average parameters were: tube voltage: 120 kV; tube current modulation: 183 mAs; spiral pitch factor: 1.02; collimation width 0.625, matrix 512 for the mediastinal window and 768 for the

lung window. In patients younger than 40 years the tube voltage was adequately reduced to 80–100 KV and the tube current modulation was opportunely adjusted based on the scout image.

Recorded data

For each patient the following data were recorded: demographics (age, sex), days from the symptom's onset, in-hospital stay (hospitalization days, admission unit), last negative nasopharyngeal swab execution date, bronchoscopy execution date and indication (inconclusive non-invasive COVID-19 diagnosis, concern for a management-changing alternative aetiology of respiratory disease, suspicion of superinfection, atelectasis mucus plugging-related [6]). Information obtained from the bronchoscopy were recorded in each patients, such as microbiological results (SARS-CoV-2 positivity/negativity, other respiratory viruses, bacteria and fungi detected), endoscopic findings (secretions, bronchial inflammation, endobronchial lesions) and technical procedure (bronchoscopy site, procedure duration, sedation and anaesthesia details). We noted also the laboratory data on peripheral blood (blood cells count, c-reactive protein, procalcitonin) and the main CT alterations (bilateral, peripheral, posterior or multilobar involvement, presence of ground-glass opacities, consolidations, crazy paving, reversed halo sign pleural or pericardial effusions or lymph node enlargements).

Each CT was evaluated by two expert radiologist and for each case the likelihood of COVID-19 pneumonia was reported, based on STR/RSNA and CO-RADS standards [2, 4]. In particular, STR/RSNA provides for 4 categories (typical, indeterminate, atypical appearance and negative for pneumonia) and CO-RADS 7 categories (from 0 to 6, with level of suspicion for pulmonary involvement by SARS-CoV-2 increasing with the score). We excluded from analysis CO-RADS 0 because of didn't describe a probability of SARS-CoV-2 pneumonia; we excluded also CO-RADS 6 because radiologists calculated the score independently by swab results.

Statistical analysis

Descriptive statistics were reported using absolute and relative frequencies or median and interquartile range, as appropriate. Demographic and clinical differences between subjects with identified and not-identified SARS-CoV-2 were compared for categorical and continuous variables by a Chi square of Fisher Exact test and Mann-Whitney U test, respectively.

To validate the two different probability scales of COVID-19 pneumonia (STR/RSNA and CO-RADS), the association between BAL results for the presence of SARS-CoV-2 RNA and the two

scores was evaluated using Chi Square or Fisher Exact tests. The Cochran-Armitage tests were also performed to further investigate if the series of SARS-CoV-2 identified proportions varied linearly with the ordinal score variables. Secondly, the receiver operating characteristic (ROC) curves were used to compare the two scales with BAL results, considered the gold standard. Particularly, we plot the true positive rate (Sensitivity) against the false positive rate (Specificity) for all possible cut-off values. The areas under the curve (AUC) and the 95% confidence intervals (95% CI) were also computed as measure of accuracy of the diagnostic tests. Finally, the result of non-parametric approach to compare the two ROC curve was reported.

P-values less than 0.05 were considered statistically significant and all analysis were performed using SAS software, version 9.4.

Results

Study population

Study design and flow chart is represented in figure 1 (Figure 1).

Figure 1. Study design and flow.chart.

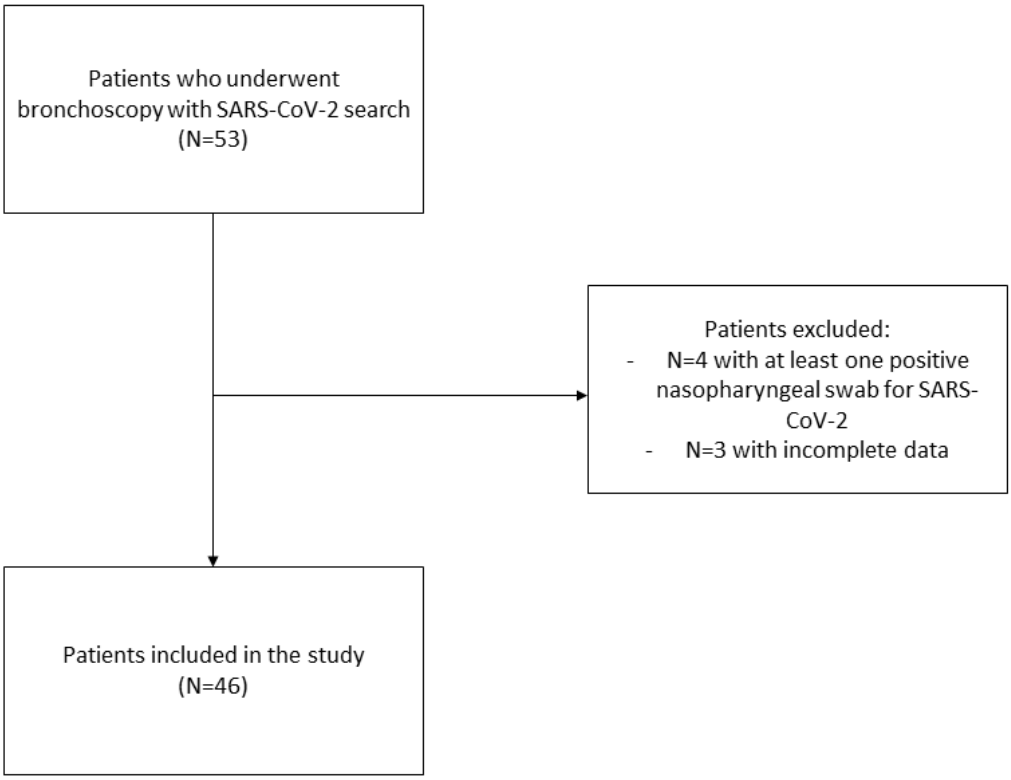

The patients' population is described in Table 1 (Table 1).

Table 1. Demographics and patients' characteristics.

	ALL (N=46)	**Non identified SARS-CoV-2 N=28**	**Identified SARS-CoV-2 N=18**	**p-value**
Sex				
Female	15 (31.25)	9 (32.14)	6 (33.33)	0.933
Male	31 (67.39)	19 (67.86)	12 (66.67)	
Age, years				
<65	27 (58.70)	14 (50.00)	13 (72.22)	0.1519
65-75	10 (20.83)	6 (21.43)	4 (22.22)	
>75	9 (20.83)	8 (28.57)	1 (5.56)	
Median [IQR]	59.61 [50.02-71.80]	65.47 [51.95-78.56]	55.34 [46.73-70.80]	0.1471
Hospital unit				
Internistic ward	31 (67.39)	21 (75.00)	10 (55.56)	0.3696
Subintensive	10 (21.74)	5 (17.86)	5 (27.78)	
Other	5 (10.87)	2 (7.14)	3 (16.67)	
Indication for bronchoscopy				
Suspected SARS-CoV-2 infection	27 (58.70)	11 (39.29)	16 (88.89)	0.0029

Suspected superinfection	12 (26.09)	10 (35.71)	2 (11.11)	
Alternative diagnosis	7 (15.22)	7 (25.00)	0 (0.00)	
Symptoms				
No	7 (15.22)	7 (25.00)	0 (0.00)	0.0319
Yes	39 (84.78)	21 (75.00)	20 (100.00)	
Days from symptoms'onset to bronchoscopy (N=41)				
Median [IQR]	14 [7-23]	15 [7-31]	12 [7-19]	0.5160
Days from nasopharyngeal swab to bronchoscopy (N=41)				
Median [IQR]	1.00 [1-3]	1 [1-3]	2 [1-4.5]	0.6905
WBC, x10^3/µL				
Median [IQR]	6.80 [5.58-9.55]	6.98 [5.45-9.81]	6.24 [5.84-8.93]	0.7797
C reactive protein, mg/dL				
Median [IQR]	7.29 [1.47-12.75]	5.08 [0.86-13.97]	7.88 [4.05-10.79]	0.5689
Procalcitonin, ng/mL				
Median [IQR]	0.10 [0.05-0.21]	0.09 [0.05-0.55]	0.10 [0.05-0.16]	0.6968
Number of CT alterations				
Median [IQR]	5 [4-7]	5 [3.5-6]	6 [5-7]	0.0348

In our study we included 46 consecutive patients; the majority were male (n 31, 67.4%), with a median age of 59.6 years. 67.4% (n 31) of them were hospitalized in an internal medicine ward. At the time of bronchoscopy, most patients were symptomatic (n 39, 84.8%). The bronchoscopy was on average performed 14 days [median IQR 7-23] from symptoms' onset, 1.5 days [IQR 1-3] from the last nasopharyngeal swab, and 3.2 days after the chest CT scan (range 0-7 days). In our cohort the indications for a bronchoscopy were: 58.7% (N=27) suspected SARS-CoV-2 infection, 26.1% (N=12) suspected superinfection and 15.2% (N=7) alternative indication (i.e. lung cancer, cryptogenetic organizing pneumonia). No cases of bronchoscopy for lung atelectasis due to mucous plugging were recorded. Considering the whole sample, in eight cases (16.7%) an endoscopic erythematous bronchial mucosa was observed and in eleven cases (22.9%) endobronchial secretions were reported.

SARS-CoV-2 was isolated on BAL in 18 cases (39.1%) despite the negative RT-PCR testing performed on two nasopharyngeal swabs. A coinfection was demonstrated in 4/18 patients (22.2%); the co-infecting pathogens were different in all patients and they were Staphylococcus Aureus in the

first patient, both Escherichia coli and Mycoplasma pneumoniae in the 2nd patient, Klebsiella pneumoniae in the 3rd patient and both Herpes simplex virus and Cytomegalovirus in the 4th patient.

Performing a microbial research on the BAL lavage fluid we were able to identify at least an alternative pathogen in 12/28 patients in whom SARS-CoV-2 RNA was not found (42.9%) (Table 2).

Table 2. Other pathogens isolated on BAL.

Pathogens	**N 16 (%)**
Bacteria	6 (37.50%)
Escherichia coli	2
Staphylococcus aureus	1
Klebsiella pneumoniae	1
Chlamydia pneumoniae	1
Pseudomonas aeruginosa	1
Viruses	5 (31.25%)
Human Herpesvirus 6	2
Herpes Simplex Virus 1	1
Metapneumovirus	1
Respiratory Syncytial Virus	1
Fungi	5 (31.25%)
Candida albicans	5

The radiologists were able to correctly identify those infections as non COVID-19 in 7/12 cases, assigning an atypical pattern based on STR/RSNA classification. The CT scans of 2 patients with BAL-demonstrated Candida Albicans infection were considered negative, while 3 other CT scans were classified as indeterminate (2/12, metapneumovirus and Herpes Simplex Virus infection) or typical (1/12, Pseudomonas aeruginosa infection). Finally, among patients with negative SARS-CoV-2 on BAL, cyto-histological analysis allowed the diagnosis of four lung carcinoma and two alveolar haemorrhages (6/28 patients). Finally, in 10 cases we did not reach a definitive diagnosis (10/46, 21.7%).

The clinicians suspected COVID-19 infection in 27/46 patients included in the study based on clinical, laboratory and epidemiologic findings. We were able to identify SARS-CoV-2 RNA through BAL in 16 of them, while the bronchoscopy was negative in the other 11 subjects with clinically suspected COVID-19. The sensitivity, specificity and accuracy of the clinical analysis in our population were therefore 88.9%, 60.7% and 71.7% respectively.

All subjects with BAL-identified SARS-CoV-2 had symptoms, while 21/28 patients in who the BAL was unable to identify the virus' RNA reported cough, fever and dyspnoea. As regards laboratory findings, the WBC count and the presence of elevated C reactive protein and procalcitonin were not significantly associated with the identification of SARS-CoV-2 RNA (p-values 0.7797, 0.5689, 0.6968).

CT findings

CT findings are represented in Table 3 (Table 3). Statistically significant differences were found in the biological CT characteristics of patients with identified and non-identified SARS-CoV-2 (p-value 0.0348): subjects with the virus had higher number of alterations (6 [5-7] vs 5 [3.5-6]) (Table 1).

Table 3. Biological chest CT characteristics.

Biological CT characteristics	**ALL (N=46)**	**SARS-2-CoV not identified (N=28)**	**SARS-2-CoV identified (N=18)**	**p-value**
Bilateral	31 (64.58)	16 (57.14)	15 (75.00)	0.2362
Peripheral	31 (64.58)	15 (53.57)	16 (80.00)	0.0736
Posterior	36 (75.00)	20 (71.43)	16 (80.00)	0.7365
Ground-glass	39 (81.25)	22 (78.57)	17 (85.00)	0.7161
Consolidation	35 (72.92)	19 (67.86)	16 (80.00)	0.5124
Multilobar	34 (70.83)	19 (67.86)	15 (75.00)	0.7502
Crazy paving	7 (14.58)	1 (3.57)	6 (30.00)	0.0158
Reversed halo	2 (4.17)	0 (0.00)	2 (10.00)	0.1684
Pleural effusion	11 (22.92)	9 (32.14)	2 (10.00)	0.0920
Pericardial effusion	1 (2.08)	1 (3.57)	0 (0.00)	>0.999
Lymph Nodes	14 (29.17)	7 (25.00)	7 (35.00)	0.5282
Median [IQR]	5 [4-7]	5 [3.5-6]	6 [5-7]	0.0475

STR/RSNA identified 32.6% (N=15) typical COVID-19 patterns, 23.9% (N=11) indeterminate patterns and 37% (N=17) atypical appearances; while 3 (6.5%) CT scans were negative for pneumonia. CO-RADS score indicated very high and high levels of suspicion in 23.9% (N=11) of cases each, whereas other 37% (N=17) of cases showed lower or very lower levels of suspicion. We found a positive association between the two scores ($p<0.001$); in particular all cases identified as very high levels of suspicion by CO-RADS were defined as typical by STR/RSNA; moreover the cases identified as atypical according to STR/RSNA consensus statement showed a CO-RADS score ≤ 3 (Table 4).

Table 4. Bronchoalveolar lavage, CO-RADS and STR/RSNA CT probability scores results.

Bronchoalveolar lavage fluid	**N (%)**
SARS-CoV-2 not identified	28 (60.9)
SARS-CoV-2 identified	18 (39.1)
CO-RADS	
Very lower level of suspicion – 1	3 (6.5)
Low level of suspicion – 2	14 (30.4)
Equivocal findings – 3	7 (15.2)
High level of suspicion – 4	11 (23.9)
Very high level of suspicion – 5	11 (23.9)
STR/RSNA	
Negative for pneumonia	3 (6.5)
Atypical appearance	17 (37.0)
Indeterminate appearance	11 (23.9)
Typical appearance	15 (32.6)

The 18 patients with BAL identified SARS-CoV-2 RNA presented the following CT patterns according to STR/RSNA consensus statement: typical 11/18; indeterminate 4/18; atypical 3/18. On the other hand, the CO-RADS classification categorized the patients in the following way: CO-RADS 5 8/18; CO-RADS 4 5/18; CO-RADS 3 3/18; CO-RADS 2 2/18 (Table 5).

Table 5. Association between STR/RSNA and CO-RADS CT probability scores and SARS-CoV-2 positivity on BAL.

	ALL (N=46)	**SARS-CoV-2 not identified (N=28)**	**SARS-CoV-2 identified (N=18)**	**p-value**
STR/RSNA				
Negative for pneumonia	3	3 (100%)	0 (0%)	0.005
Atypical appearance	17	14 (82.3%)	3 (17.7%)	
Indeterminate appearance	11	7 (63.7%)	4 (36.3%)	
Typical appearance	15	4 (26.7%)	11 (73.3%)	
CO-RADS				
Very lower level of suspicion – 1	3	3 (100%)	0 (0%)	0.0266
Low level of suspicion – 2	14	12 (85.7%)	2 (14.3%)	
Equivocal findings – 3	7	4 (57.2%)	3 (42.8%)	
High level of suspicion – 4	11	6 (54.6%)	5 (45.4%)	
Very high level of suspicion – 5	11	3 (27.3%)	8 (72.7%)	

Consequently, we identified SARS-CoV-2 RNA on BAL in the 73.3% of patients with typical CT STR/RSNA pattern (n 11/15), while the BAL was negative for SARS-CoV-2 RNA in the 82.4% of patients with atypical pattern (n 14/17). STR/RSNA is significantly associated with the presence of SARS-CoV-2 on BAL (p=0.0055) and the trend is statistically significant (p=0.0005).

Typical pattern displayed a sensitivity of 61.1% (95% CI 35.8- 82.7), a specificity of 85.7% (95% CI 67.3-96) and a PPV of 73.3% (95% CI 50.8-88). Atypical and negative patterns in our small population showed a NPV of 82.3% (95% CI 58.6-96.4) and 100% respectively.

When CO-RADS score identified a very high level of suspicion for SARS-CoV-2 infection we identified the virus on BAL in the 72.7% of cases (8/11); on the contrary, in case of low or very low level of suspicion (CO-RADS scores 1 and 2) the BAL was negative in 85.7% and 100% of cases respectively (n 12/14 and 3/3). Poorer results were found for the other levels of suspicion (Table 5). We found a significant association between CO-RADS score and presence of SARS-CoV-2 on BAL (p=0.0266) and even the trend was statistically significant (p=0.0012) (Table 5).

CO-RADS score accuracy has been calculated considering a score ≥4 as positive for COVID 19 and a score ≤ 3 as negative, on the model of Hermans et al. [9]. The resulting sensitivity, specificity, PPV and NPV were 72.2% (95% CI 46.5-90.3), 67.8% (95% CI 47.7-84.1), 59.1% (95% CI 44-72.7) and 79.2% (95% CI 63.4-89.3).

Notably, BAL was able to identify the presence of SARS-CoV-2 RNA in 10/11 patients with both a typical STR/RSNA pattern and a white blood cell (WBC) count <11,000 cells/μL. BAL also identified the presence of SARS-CoV-2 RNA in 7/8 patients with both a CO-RADS 5 classification and a WBC count <11,000 cells/μL. Notably the only patient affected by COVID-19 and not identified by these combined parameters had a coinfection from Klebsiella Pneumoniae (Table 6).

Table 6. BAL positive: STR/RSNA and CO-RADS vs WBC count.

	ALL (N=18)	**WBC<11.000**	**WBC>11.000**	**p-value**
STR/RSNA				
Atypical appearance	3	0	3	0.0052
Indeterminate appearance	4	4	0	
Typical appearance	11	10	1	
CO-RADS				
Low level of suspicion – 2	2	0	2	0.0301
Equivocal findings – 3	3	2	1	
High level of suspicion – 4	5	5	0	
Very high level of suspicion – 5	8	7	1	

The association of typical STR/RSNA pattern and a normal WBC count had therefore a sensitivity of 55.6% (95% CI 30.8-78.5), a specificity of 96.4% (95% CI 81.7-99.9) and a PPV of 90.9% (95% CI 58.3-98.6). The association of CO-RADS 5 and a normal WBC count displayed a sensitivity of 38.9% (95% CI 17.3-64.2), a specificity of 96.4% (95% CI 81.7-99.9), and a PPV of 87.5% (95% CI 48.4-98.1).

Figure 2 shows the ROC curves. The values of AUC were similar for STR/RSNA and CO-RADS (p=0.6716): 0.789 (95% CI 0.661-0.919) and 0.775 (95% CI 0.644-0.908), respectively (Figure 2).

Figure 2. ROC curves of STR/RSNA and CO-RADS score associations with BAL results: comparison of sensitivity and specificity.

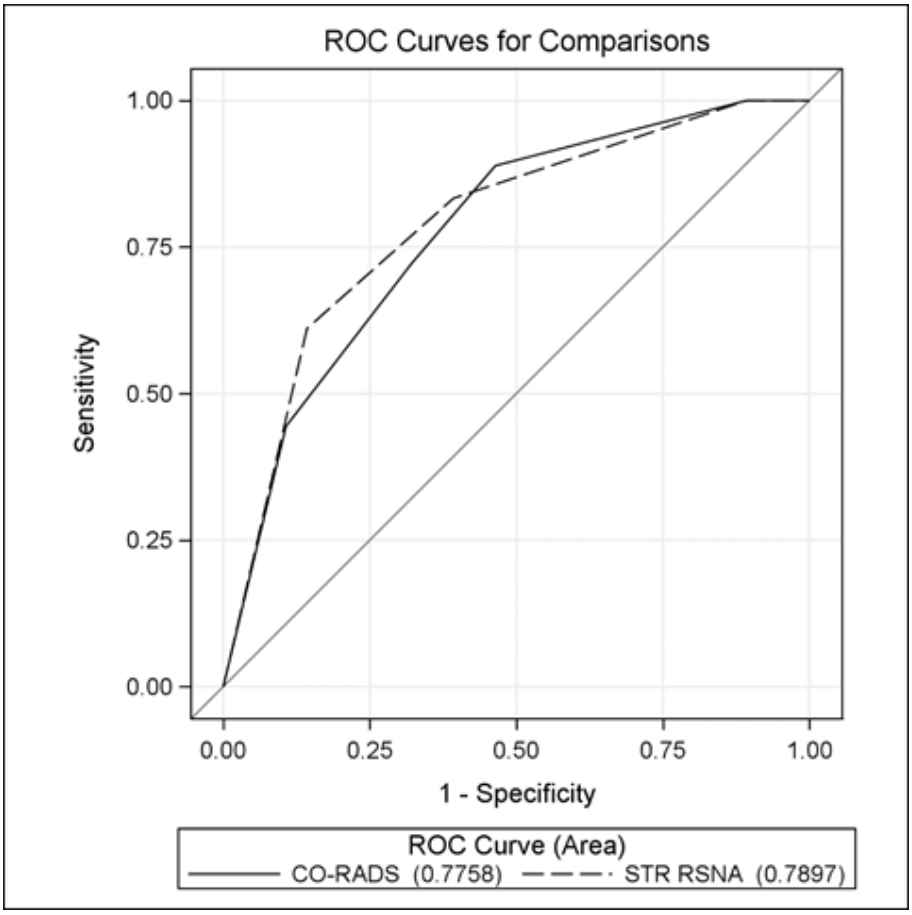

Discussion

The issue of RT-PCR sensitivity in the diagnosis of COVID-19 and the supposed number of false negatives is still debated, since at the present day the RT-PCR performed on a nasopharyngeal swab sample remains the only globally validated gold standard for the diagnosis of COVID-19 [10, 11]. Some Chinese authors already pointed out the risk of misdiagnosis [12], especially when a chest CT indicating interstitial pneumonia is present [13]. A large study conducted in 610 patients from the province of Wuhan who underwent up to five RT-PCR testing pointed out that 12% of COVID-19 positive patients, as demonstrated by at least one positive nasopharyngeal swab, were negative after the first test [14]. Moreover, the study showed how the RT-PCR may turn repeatedly from positive to negative. These results suggest the isolation of any patients with clinical, epidemiological and radiographic features suspected for COVID-19 even if in case of negative RT-PCR [5].

Studies that evaluated the concordance between nasopharyngeal swabs and BAL results confirmed a moderate agreement [15, 16]; moreover Ora et al. demonstrated that three negative swabs along

with negative antibodies, independently of a suggestive CT scan, can rule out SARS-CoV-2 infection in suspected patients [17]. In our cohort BAL was able to identify SARS-CoV-2 RNA in almost 40% patients with two negative RT-PCRs performed on nasopharyngeal swabs. Although some of these patients could theoretically have contracted the infection in the time interval between the nasopharyngeal swab and the BAL we believe this is unlikely, since the amount of time was on average very short and the symptoms' onset was about two weeks before the procedure. Moreover, we must consider that BAL was performed with different indications and when it was done for a suspected SARS-CoV-2 infection, the positivity rate was 59.2%.

These results seem therefore to confirm the hypothesis made by Li et al. and by Xie et al. [12, 14]: the diagnosis of COVID-19 should not rely exclusively on the RT-PCR testing, since the results of the nasopharyngeal swab samples are variable and potentially unsteady. We therefore examined the association between the CT images, as classified by the CO-RADS score and the STR/RSNA consensus statement, and the BAL results. In fact, in our cohort the integration of clinical, radiological and BAL results brought us to a definitive diagnosis in 78.2% of cases (36/46 patients): 18 SARS-CoV-2 pneumonia, 12 other infective pneumonia and 6 other diagnosis (mainly lung cancer).

STR/RSNA consensus statement diagnostic accuracy was evaluated through ROC curve and proved to be moderately accurate in identifying SARS-CoV-2 infection, with an AUC of 0.790. The sensitivity, specificity and PPV of the typical pattern were slightly lower than those described by a larger study assessing the diagnostic accuracy of STR/RSNA consensus statement [18], in which those values are reported as 71.6%, 91.6% and 87.8% respectively. On the other hand, the NPV of atypical and negative pattern are similar, being 89.6% end 86.2%. We believe that this offset may be due to the fact that our population is smaller and includes only patients with a negative nasopharyngeal swab, who therefore would have been considered false positives or true negatives in a traditional CT accuracy study like the ones so far conducted in Italy [5, 18]. Additionally, as we explained in the results, a high percentage of patients suffered from alternative infections which confounded the radiological diagnosis in 3 cases.

In our population the CO-RADS score was found also to underperform in comparison with the previous studies, in particular with the one recently conducted in the Netherlands [9] which reported a sensitivity, specificity, PPV and accuracy of 90.2%, 88.2%, 84.5% and 92.7% considering a CO-RADS score ≥ 4 as positive for COVID 19 and a score a score ≤ 3 as negative. We trust that the

reasons are the same that lead to a minor accuracy for the STR/RSNA consensus statement, given also the strong positive association between the two scores.

In our experience the association of a typical STR/RSNA pattern or a CO-RADS 5 and a normal WBC count (<11,000 cells/μL) proved to be extremely specific in identifying SARS-CoV-2 infection when not complicated by a bacterial superinfection. This is in keeping with the findings published by Terpos et. Al. [19] and with the recent meta-analysis written by Henry et al. [20], which point out how COVID-19 is most often associated to a depleted WBC count, while leukocytosis is most often found when a bacterial infection is present [21, 22]. The association of the 2 parameters may therefore help the clinician distinguishing between COVID-19 and an interstitial pneumonia with bacterial etiology.

Our study suffers from several limitations. The first is the retrospective nature of the research, in that patients at different stages of the disease reported autonomously to Emergency Department where they performed a CT scan. The second limitation is the fact that a large percentage of patient who performed BAL for a suspected SARS-CoV-2 infection and resulted negative did not received an alternative diagnosis, therefore it remains not completely clear the real incidence of true negative results. We didn't have the results of specific antibodies (IgM and IgG) against SARS-CoV-2 because the routine use was introduced during the last phase of our observation period: their implementation in clinical practice probably reduced the number of bronchoscopies performed in those patients with negative nasopharyngeal swabs and indeterminate chest CT. The last limitation is the relatively small number of patients included, therefore larger studies are needed to confirm the conclusions.

In conclusion, our results suggest that patients with suspected COVID-19 should not be automatically considered negative after two negative RT-PCRs and indicate that a typical STR/ACR/RSNA pattern or a CO-RADS 5 maintains a great diagnostic value even in this subgroup of patients. The integration of BAL in diagnostic flow-chart of suspected COVID-19 patients with negative RT-PCRs could lead to a definitive diagnosis in almost 80% of patients. The association with WBC count may greatly improve the CT specificity; further research is obviously needed in order to validate our findings.

References

1. Corman VM, Landt O, Kaiser M, Molenkamp R, Meijer A, Chu DK, et al. Detection of 2019 Novel Coronavirus (2019-nCoV) by Real-Time RT-PCR. Euro Surveill. 2020 Jan;25(3):2000045
2. Prokop M, van Everdingen W, van Rees Vellinga T, van Ufford JQ, Stoger L, Beenen L, et al. CO-RADS – A categorical CT assessment scheme for patients with suspected COVID-19: definition and evaluation. Radiology. 2020 Aug;296(2):E97-E104.
3. Rubin GD, Ryerson CJ, Haramati LB, et al. The Role of Chest Imaging in Patient Management during the COVID-19 Pandemic: A Multinational Consensus Statement from the Fleischner Society. Radiology. Radiology. 2020 Jul;296(1):172-180.
4. Simpson S, Kay FU, Abbara S, Bhalla S, Chung JH, Chung M, et al. Radiological Society of North America Expert Consensus Statement on Reporting Chest CT Findings Related to COVID-19. Endorsed by the Society of Thoracic Radiology, the American College of Radiology, and RSNA. J Thorac Imaging. 2020 Jul;35(4):219-227.
5. Falaschi Z, Danna PSC, Arioli R, Pasché A, Zagaria D, Percivale I, et al. Chest CT accuracy in diagnosing COVID-19 during the peak of the Italian epidemic: A retrospective correlation with RT-PCR testing and analysis of discordant cases. Eur J Radiol. 2020 Sep;130:109192.
6. Lentz RJ, Colt H. Summarizing Societal Guidelines Regarding Bronchoscopy During the COVID-19 Pandemic. Respirology. 2020 Jun;25(6):574-577.
7. Patrucco F, Albera C, Bellocchia M, Foci V, Gavelli F, Castello LM, et al. SARS-CoV-2 Detection on Bronchoalveolar Lavage: An Italian Multicenter experience. Respiration. 2020;99(11):970-978.
8. von Elm E, Altman DG, Egger M, Pocock SJ, Gøtzsche PC, Vandenbroucke JP, et al. The Strengthening the Reporting of Observational Studies in Epidemiology (STROBE) Statement: Guidelines for Reporting Observational Studies. J Clin Epidemiol. 2008 Apr;61(4):344-9.
9. Du Rand IA , Blaikley J, Booton R, Chaudhuri N, Gupta V, Khalid S, et al.; British Thoracic Society Bronchoscopy Guideline Group. British Thoracic Society guideline for diagnostic flexible bronchoscopy in adults: accredited by NICE. Thorax 2013;68 (Suppl 1):i1–44.
10. Chen H, Ai L, Lu H, Li H. Clinical and imaging features of COVID-19 [published online ahead of print, 2020 Apr 27]. Radiol Infect Dis. 2020;10.1016/j.jrid.2020.04.003.

11. Ai T, Yang Z, Hou H, et al. Correlation of Chest CT and RT-PCR Testing for Coronavirus Disease 2019 (COVID-19) in China: A Report of 1014 Cases. Radiology. 2020;296(2):E32-E40.
12. Xie X, Zhong Z, Zhao W, Zheng C, Wang F, Liu J. Chest CT for Typical Coronavirus Disease 2019 (COVID-19) Pneumonia: Relationship to Negative RT-PCR Testing. Radiology. 2020;296(2):E41-E45. doi:10.1148/radiol.2020200343
13. Long C, Xu H, Shen Q, et al. Diagnosis of the Coronavirus disease (COVID-19): rRT-PCR or CT?. Eur J Radiol. 2020;126:108961.
14. Li Y, Yao L, Li J, Chen L, Song Y, Cai Z, et al. Stability issues of RT-PCR testing of SARS-CoV-2 for hospitalized patients clinically diagnosed with COVID-19. J Med Virol. 2020;92(7):903-908.
15. Geri P, Salton F, Zuccatosta L, Tamburrini M, Biolo M, Busca A, et al. Limited role for bronchoalveolar lavage to exclude Covid-19 after negative upper respiratory tract swabs: a multicenter study. Eur Respir J. 2020 Aug 6;2001733.
16. Wang W, Xu Y, Gao R, Lu R, Han K, Wu G, Tan W. Detection of SARS-CoV-2 in Different Types of Clinical Specimens. JAMA. 2020 Mar 11;323(18):1843-4.
17. Ora J, Puxeddu E, Cavalli F, Giorgino FM, Girolami A, Chiocchi M, et al. Does bronchoscopy help the diagnosis in COVID-19 infection? Eur Respir J. 2020;56(2):2001619.
18. Ciccarese F, Coppola F, Spinelli D, Galletta GL, Lucidi V, Paccapelo A, et al. Diagnostic Accuracy of North America Expert Consensus Statement on Reporting CT Findings in Patients with Suspected COVID-19 Infection: An Italian Single Center Experience. Radiology: Cardiothoracic Imaging. 2020; 2. Published online Jul 23 2020. https://doi.org/10.1148/ryct.2020200312
19. Terpos E, Ntanasis-Stathopoulos I, Elalamy I, et al. Hematological findings and complications of COVID-19. Am J Hematol. 2020;95(7):834-847. doi:10.1002/ajh.25829
20. Henry BM, de Oliveira MHS, Benoit S, Plebani M, Lippi G. Hematologic, biochemical and immune biomarker abnormalities associated with severe illness and mortality in coronavirus disease 2019 (COVID-19): a meta-analysis. Clin Chem Lab Med. 2020;58(7):1021-1028. doi:10.1515/cclm-2020-0369
21. Lavoignet CE, Le Borgne P, Chabrier S, Bidoire J, Slimani H, Chevrolet-Lavoignet J, et al. White blood cell count and eosinopenia as valuable tools for the diagnosis of bacterial infections in the ED. Eur J Clin Microbiol Infect Dis. 2019;38(8):1523-1532.

22. Feng M, Zhang SL, Liang ZJ, Wang YL, Zhao XC, Gao C, et al. Peripheral neutrophil CD64 index combined with complement, CRP, WBC count and B cells improves the ability of diagnosing bacterial infection in SLE. Lupus. 2019;28(3):304-316.

Title: Mycotic infection prevalence among patients undergoing bronchoalveolar lavage with search of SARS-CoV-2 after two negative nasopharyngeal swabs

Background

The final diagnosis of Severe Acute Respiratory Coronavirus 2 (SARS-CoV-2) infection is based on virus positivity on real-time reverse-transcriptase-polymerase chain reaction (RT-PCR) processed on nasopharyngeal swabs (NP) [1-3]. However, this method is characterized by a high rate of false negative results, with a sensitivity ranging between 42% and 83% [4]. Due to bronchoalveolar lavage (BAL) low positivity rate for SARS-CoV-2 identification [5-7], its use in the diagnosis of SARS-CoV-2 infection should be reserved only to those cases with indeterminate or atypical radiological computed tomography (CT) manifestations with high clinical suspicion [8].

In a pandemic setting fungal pulmonary infections may be misdiagnosed as SARS-CoV-2 pneumonia. The symptoms, such as fever, cough and dyspnoea are notoriously similar [9, 10], and even the radiologic appearance may be difficult to distinguish, since a lot of atypical Coronavirus Disease 2019 (COVID-19) radiologic signs can mimic mycotic infections like invasive pulmonary aspergillosis [11].

It is rising evidence that COVID-19 patients have a high incidence of fungal complications, in particular aspergillosis, candidemia and pneumocystosis [12, 13]. COVID-19-associated invasive pulmonary aspergillosis (CAPA) affects nearly 30% of critically ill patients and it is associated with higher mortality rates [14]. Moreover, critically ill COVID-19 patients are exposed to other mycotic pathogens such as Candida species and Pneumocystis jirovecii: the incidence of these isolations among COVID-19 patients is variable in literature and their etiological value is still debated [15].

Unlike COVID-19, many mycotic infections may benefit from a timely and targeted pharmacological treatment, and patients with a fungal superinfection in COVID-19 pneumonia have poorer outcomes [16, 17]. Therefore, recognizing and treating these life-threatening complications is particularly relevant.

Consequently to the results of our previous research projects [5, 8], the aim of our study is to describe the incidence of fungal pathogens isolated on bronchoalveolar lavage among the patients admitted in internal medicine wards who underwent bronchoscopy with BAL for the research of

SARS-CoV-2 and other pathogens after a double RT-PCR NP test; the second aim is to describe the clinical characteristics and main outcomes of these patients with fungal pathogens.

Material and Methods

Study population

We conducted a single centre, retrospective and observational study of consecutive patients undergoing both a chest CT scan with two consecutive NP swabs in our institution, and a bronchoscopy with BAL with the RT-PCR testing for SARS-CoV-2 RNA and microbiologic culture. Data were collected between March 16th and November 30th, 2020. Patients underwent bronchoscopy with different indications: inconclusive diagnosis of SARS-CoV-2 infection after previous examinations, concerns about an alternative etiology of respiratory diseases which would alter the management, suspicion of superinfection (viral, bacterial, fungal), bronchial or lung atelectasis caused by mucous plugs [5]. We excluded from the analysis those cases with incomplete or non-retrievable data or with at least one positive nasopharyngeal swab. The patients who underwent bronchoscopy more than 7 days after the chest CT scan were also excluded. The study was approved by the local Institutional Review Board (approval protocol number CE 97/20) and was conducted in accordance with Strengthening the Reporting of Observational studies in Epidemiology (STROBE) statement for observational studies [18].

During flexible bronchoscopy the tip of the instrument is placed in wedge position through the tributary bronchus of the selected segment of lung parenchyma; three 50 mL aliquots of saline are instilled through the bronchoscope and, after each instillation, the lavage fluid is retrieved using a suction pressure. An optimal sampling is the one that allows one to retrieve more than 30% of the instilled fluid. In our study the BAL fluid recovered was used for microbiological analysis, including the research of SARS-CoV-2 RNA [19].

RT-PCR testing was performed on nasopharyngeal swabs and BAL fluid (Xpert [Cepheid]). After cytospin and direct examination, all samples underwent culture and incubation for bacteria and fungi evaluation; identification of mycotic agents was achieved by mass spectrometry. Aspergillus fumigatus and Pneumocystis jirovecii DNA were extracted and PCR performed in duplicate: a single positive well was considered as positive. Galactomannan was dosed on BAL; it was

determined by enzyme immunoassay and considered as positive, after two determinations performed on the same sample, when the index was equal or greater than 1.

Chest CT execution technique

The Chest CT scans were acquired during a single full inspiratory breath hold, with the patient in supine position. We used a 128-slice CT (Philips Ingenuity Core, Philips Healthcare, Netherlands). Scan parameters were: tube voltage: 120 kV; 210 mAs; collimation width 0.625; spiral pitch factor: 1.08; matrix 512 (mediastinal window) and 768 (lung window). The images were subsequently reconstructed with a slice thickness of 1 mm.

Recorded data

For each patient the following data were recorded: demographics (age, sex), days from the symptoms' onset, in-hospital stay (hospitalization days, admission unit), last negative nasopharyngeal swab date, bronchoscopy date, white blood cells count (WBC, in x103/µL), C-reactive protein (CRP, in mg/dL) and procalcitonin (PCT, in ng/mL) blood levels. Information obtained from the bronchoscopy were recorded in each patient: mycotic isolation, SARS-CoV-2 positivity/negativity, other respiratory viruses and bacteria detected. We also noted the laboratory data on peripheral blood (blood cells count, CRP, PCT) and the main CT alterations (bilateral, peripheral, posterior or multilobar involvement, presence of ground-glass opacities, consolidations, crazy paving, reversed halo sign pleural or pericardial effusions or lymph node enlargements). For each patient we calculated, at Emergency Department admission, the Novara-COVID score for the stratification of in-hospital clinical instability and mortality of patients with suspected COVID-19 [20]

Each CT was evaluated by two expert radiologists (ZF and FF) and for each case the likelihood of COVID-19 pneumonia was reported, based on Society of Thoracic Radiology / Radiological Society of North America (STR/RSNA) standards [4], which provides for 4 categories (typical, indeterminate, atypical appearance and negative for pneumonia).

For the diagnosis of aspergillosis and other mold infections, we used the European Organization for Research and Treatment of Cancer (EORTC)/Mycosis Study Group (MSG) criteria for patients affected by immunosuppressive underlying conditions [21]. Other non-immunosuppressed patients were classified as having a putative invasive pulmonary mold infection (IPMI) or false positive/clinically non relevant colonization: in particular, those patients with positive antigen test

or PCR without a positive culture on BAL fluid and without clinical deterioration (stability or improvement of symptoms, stability or reduction of pulmonary infiltrates and inflammatory markers) or correlated to mold infection were considered as false positive or clinically non relevant colonization [12].

Statistical analysis

Descriptive statistical analyses were conducted. We reported frequency and percentage (%) mean and standard deviation (SD) or median and interquartile range [IQR] for categorical and continuous variables. Association between CT pattern and bronchoalveolar lavage isolation was evaluated using Chi Square or Fisher Exact test as appropriate.

Results

Between March 16 and November 30, 2020, a total of 118 subjects underwent BAL with search of SARS-CoV-2 RNA and in 33.1% (n=39/118) of them we isolated at least one mycotic agent while in 23.7% (n=28/118) we identified SARS-CoV-2. The 39 included patients were predominantly male (n=27, 69.2%) and had a median age of 71.7 years [IQR 60.0-80.7]. Most of them were admitted in an internal medicine ward (69.2%); they were hospitalized and underwent bronchoscopy for a median time of 3 [IQR 2-5] and 7 [IQR 5-13] days after symptoms' onset. Mean Novara-COVID score was 3.66 [SD ±0.77]. Almost all patients were symptomatic for respiratory tract infection (94.9%) with increased inflammatory markers (mean CRP and PCT respectively 9.58 mg/dL and 2.18 ng/mL). According to STR/RSNA standards for SARS-CoV-2 pulmonary infection, chest CT was defined as: typical 7.7%, indeterminate 28.2%, atypical appearance 56.4% and negative for pneumonia 7.7% (Table 1).

Table 1. Patients' characteristics

	N (%)
Demographics of patients with an isolated mycotic species	39
Sex	
Female	12 (30.8)
Male	27 (69.2)
Age, years	
<65	15 (38.5)
65-75	8 (20.5)
>75	16 (41.0)
Median [IQR]	71.67 [60.01-80.65]
Hospital unit	
Internal Medicine ward	27 (69.2)
Infectious Diseases ward	6 (15.4)

Other non intensive care units	6 (15.4)
Symptomatic	
Yes	37 (94.9)
Days from symptoms' onset to bronchoscopy	
Median [IQR]	7 [5-13]
Days from nasopharyngeal swab to hospitalization	
Median [IQR]	3 [2-5]
Days from nasopharyngeal swab to bronchoscopy	
Median [IQR]	2 [1-3]
Blood analysis	
White blood cell count (in $x10^3/\mu L$), mean [±SD]	9.58 [±5.42]
C-reactive protein (in mg/dL), mean [±SD]	12.10 [±9.41]
Procalcitonin (in ng/mL), mean [±SD]	2.18 [±4.25]
NOVARA-COVID score	
Mean [±SD]	3.66 [±0.77]
STR/RSNA CT pattern	
Negative for pneumonia	3 (7.7)
Atypical appearance	22 (56.4)
Indeterminate appearance	11 (28.2)
Typical appearance	3 (7.7)

Comorbidities are reported in Table 2 (Table 2). Fourteen patients (35.9%) were immunosuppressed for different conditions: 7 cases of immunosuppression for stem cell transplantation, 3 patients affected by onco-hematological disorders, 3 patients in chronic steroid treatment for rheumatological diseases (two vasculitis and 1 case of systemic sclerosis), 1 renal transplanted patient.

Table 2. Patients' comorbidities

	N (%)
Immunosuppression	14 (35.9)
- Stem cell transplantation	7
- Oncohematological disorders	3
- Rheumatological disease in chronic treatment with steroids	3
- Renal transplantation	1
Hypertension	17 (43.6)
Ischemic heart disease	4 (10.2)
Cardiac arrhythmias	9 (23.1)
Diabetes	5 (12.8)
Dyslipidaemia	8 (20.5)
Other oncologic disorders	10 (25.6)
Chronic kidney failure	6 (15.4)
Neurologic disorders	4 (10.2)
Chronic respiratory diseases	5 (12.8)

Among the 118 included patients who underwent bronchoscopy for SARS-CoV-2 search, BAL was positive for SARS-CoV-2 in 28 cases (23.7%); as reported above, we isolated at least one mycotic

agent in 39 cases (in two patients we isolated 2 fungi each, for a total of 41 isolations). Eight cases of mycotic and bacterial coinfections were reported. Other viruses and bacteria present on BAL are reported in Table 3 (Table 3).

Table 3. Viruses, Bacteria and fungi isolated on bronchoalveolar lavage.

	N
Bronchoscopies performed	118
Virus	
SARS-CoV-2	28
Rhinovirus	4
Metapneumovirus	1
RSV	3
HSV6	8
HSV1	3
CMV DNA	3
EBV DNA	3
Fungi	
Aspergillus fumigatus	3
Pneumocystis jirovecii	6
Candida spp.	32
Bacteria	
Escherichia coli	2
Pseudomonas aeruginosa	2
Klebsiella pneumoniae	2
Staphylococcus aureus	1
Serratia marcescens	1

CMV Cytomegalovirus, EBV Epstein Barr Virus, HSV1 Herpes Simplex Virus 1, HSV6 Herpes Simplex Virus 6, RSV Respiratory Syncytial Virus, SARS-CoV-2 Severe Acute Respiratory Syndrome Coronavirus 2.

Prevalence of SARS-CoV-2 infection among patients with at least a fungal isolation was 15.4% (n=6/39): in these patients, STR/RSNA radiological patterns were defined as typical, atypical and indeterminate in two cases each. On the other hand, the prevalence of bacterial infection in the same group was 20.5% (n=8/39). Finally, the prevalence of other viral agents (at least one virus per patient) was 17.9% (n=7/39).

Among the 39 patients included in the analysis, we isolated 41 molds: 3 Aspergillus fumigatus, 6 Pneumocystis jirovecii and 32 Candida spp (Table 3). Most (n=4/6, 66.6%) of Pneumocystis jirovecii cases occurred in patients with previous immunosuppressive underlying conditions, 1 case in a patient under pre-emptive steroid treatment for SARS-CoV-2 infection: all these cases were appropriately treated; finally, one case was considered as false positive or clinically non relevant. Two of the three cases of Aspergillus fumigatus positivity occurred in immunosuppressed patients and received specific treatment; the remaining case was considered as clinically non relevant. Most fungal isolations (n=32) were represented by Candida spp: among these, 9 cases (n=9/32, 28.1%) were detected in immunosuppressed patients and 5 cases (n=5/32, 15.6%) in patients receiving

steroids for pre-emptive treatment of SARS-CoV-2 infection. Only 5 cases (n=5/32, 15.6%) underwent specific treatment of the infection, the other cases were considered as clinically irrelevant. With these results, according to EORTC/MSG criteria, the prevalence of mold infections was 29.3% with 12 cases of mycotic infections and 29 false positive or clinically irrelevant infections (n=29/41, 70.7%).

Patients with a mycotic infection had a more frequently atypical STR/RSNA CT radiological pattern (60.6%) than patients with SARS-CoV-2 whose most frequent pattern was typical (63.6%). Among patients with both a mycotic isolation and SARS-CoV-2 infection, the three patterns (typical, indeterminate and atypical) were homogeneously distributed ($p<0.0001$) (Table 4).

Table 4. STR/RSNA CT pattern in mycotic, SARS-CoV-2 and combined (fungi and SARS-CoV-2) bronchoalveolar lavage isolation: N (%).

	Fungi (N=33)	**SARS-CoV-2 (N=22)**	**Fungi + SARS-CoV-2 (N=6)**
STR/RSNA CT pattern			
Negative for pneumonia	3 (9.1)	0 (0.00)	0 (0.0)
Atypical appearance	20 (60.6)	3 (13.6)	2 (33.3)
Indeterminate appearance	9 (27.3)	5 (22.8)	2 (33.3)
Typical appearance	1 (3.0)	14 (63.6)	2 (33.3)
Outcomes			
In-hospital mortality	5 (16.5)	1 (4.5)	1 (16.6)
In-hospital stay, in days (±SD)	16.56 (±14.1)	16.76 (±13.6)	15.66 (±7.1)

CT Computed Tomography, SARS-CoV-2 Severe Acute Respiratory Syndrome Coronavirus 2, STR-RSNA Society of Thoracic Radiology – Radiological Society of North America

Among the 6 patients who were co-infected by SARS-CoV-2 and a mycotic agent, Candida spp. was the only co-infectant microbe: three of these cases occurred in immunocompromised patients, while one patient was in treatment with preemptive high doses of steroids for a suspected SARS-CoV-2 infection. The mean WBC count and CRP of these 6 subjects were 8.42 (±3.44) x103/µL and 12.63 (±7.21) mg/dL, respectively.

At the time of BAL, at least one antibiotic treatment was ongoing in most of the included patients: only 7 patients (n=7/39, 17.9%) were naïve for any antimicrobial treatment. The most frequently used antibiotics were azithromycin (18 times), ceftriaxone (15 times), piperacillin-tazobactam (8 times), amoxicillin clavulanate (3 times), fluoroquinolones (4 times).

In-hospital mortality in patients with a fungal infection detected by BAL was 15.3% (n=6/39) and occurred on average at 22.33 days after hospital admission (SD ±12.3, 95% IC 9.5-35.2, median 23.0); 3 patients were immunosuppressed with mycotic infections and 3 with false positive or

clinically irrelevant infection. Only one of them presented the SARS-CoV-2 co-infection. Among patients who died only in 1 cases BAL evidenced a bacterial co-infectant (Klebsiella Pnuemoniae). For completeness, the mycotic and viral (non SARS-CoV-2) coinfection of detected 7 times (7/39, 17.9%): in three cases patients died during hospitalization and previously isolated viruses wee Respiratory Syncytial Virus, Herpes Simplex Virus 6 and Epstein Barr Virus. None of them was the causative of death.

Discussion

In our cohort of patients with suspected pulmonary SARS-CoV-2 infection with two negative RT-PCR test on NP swab we observed a prevalence of fungal pathogens on BAL of 33.1% (39/118), and a positivity for SARS-CoV-2 of 23.7% (28/118). In particular, co-infection of a mycotic agent and SARS-CoV-2 was present in 15.4% (6/39) of cases. According to EORTC/MSG criteria, the prevalence of mold infection was 29.3%, with 70.7% of false positive or clinically irrelevant infections.

The high mortality rate related to COVID-19 acute respiratory distress syndrome (ARDS) is linked to other infectious complications, such as fungal infections [22]. Recently, it has been demonstrated that patients affected by severe SARS-CoV-2-related pneumonia, without underlying immunosuppression, have a low risk of pulmonary invasive fungal infection, when caused by Aspergillus spp [12]. Nevertheless, up to now only few and no specific data are present in the literature regarding the prevalence of mycotic infections among patients who are hospitalized for suspected SARS-CoV-2 pulmonary infection with pulmonary infiltrates, outside the intensive care unit (ICU). Although in many clinical situations a non-invasive approach can be considered sufficient for the diagnostic work-up [23], some studies have investigated the role of bronchoscopy for diagnosis in COVID-19 patients: most of them confirmed the limited place of BAL in SARS-CoV-2 diagnosis, suggesting a role in resolving diagnostic complex cases [7]. In these studies, mycotic infections represent a relevant part of pathogens isolated on BAL: in the paper of Barberi et al. among 166 negative BAL for COVID-19, a mycotic agent was identified 38 times (22.9%), with Aspergillus fumigatus and Candida spp being the most isolated ones [24]. Even in the study of Ora et al. on 28 patients, the authors found 5 BAL positivities for Candida spp, 2 for Pneumocystis jirovecii and described 6 cases with galactomannan >0.8 but without information regarding neither the culture nor CRP [7]. In our cohort, the prevalence of mycotic isolation is in line with the results reported in these studies in patients with the same indication and setting.

Mycotic pulmonary infections are associated with a higher mortality rate for patients with nosocomial infection or complicating respiratory failure [25]; moreover, mycotic and bacterial coinfections increase mortality in severely ill COVID-19 patients [26]. In our cohort we reported an in-hospital mortality rate of 15.3% with increased inflammatory markers; multiple cells and molecules are involved in host's response to fungal infection in the lung, resulting in a complex network of inflammatory pathways [27].

Also, the mycotic infections prevalence we observed is in line with the one reported in studies including patients admitted to ICU for severe COVID-19 pneumonia, mainly caused by Aspergillus, [12, 14, 28, 29]. These similar results, despite being reported in different settings, could support some assumptions:

a) SARS-CoV-2 can infect immunocompromised patients, a population particularly susceptible to fungal infections, although it may be difficult to differentiate COVID-19 superinfection from pre-existing fungal colonization in this category [12]: the prevalence of immunocompromised patients is generally homogeneous among hospital wards [30] and these patients have worse hospital outcomes with increased risk of clinical deterioration [31-33].

b) Viral pneumonia could be complicated by invasive aspergillosis [34, 35]: Fekkar et al. reported an incidence of CAPA of 4.8% among patients admitted to ICU for severe COVID-19 pneumonia [12]; in our cohort we did not observed cases of CAPA even though we observed two cases of invasive aspergillosis who required the specific treatment. This fact probably confirms that both hospitalization and underlying clinical conditions (in these cases immunosuppression) could independently identify these patients as a high-risk populations for SARS-CoV-2 infection, in which BAL is fundamental to rule out the viral infection. Moreover, all the 3 patients had a radiological CT pattern either atypical or indeterminate, which may require further investigations to determine the causative agent.

c) The isolation of Candida spp in the respiratory tract is usually interpreted as contaminant because of its high isolation rate on BAL, and invasive pneumonia is usually a rare complication [36]; nevertheless, even when considered as an innocent bystander, Candida may contribute to the worsening of underlying respiratory disease, especially in critically ill patients, prolonging ICU stay and hospitalization [37]. In our cohort, patients with coinfection of SARS-CoV-2 and Candida spp had a higher even if non-significant longer hospital stay compared to those who had only COVID-19 without other co-infectants (15.0 ±7.7 vs 17.3 ±15.2 days, p=0.75). However, we must

acknowledge that this result could be influenced by the low number of subjects included in the study.

Interestingly, among patients with mycotic isolation on BAL, only six were in pre-emptive treatment with steroids (oral prednisone or intravenous methylprednisolone) for a suspected SARS-CoV-2 infection, which could have promoted the growth of mould on the respiratory tract, independently from their immune status.

Our results on a limited number of patients seem to indicate that the STR/RSNA consensus statement [4] is fairly accurate in discriminating lung mycotic infections from SARS-CoV-2 pneumonia, having correctly assigned about 60% of the patients with the former infection to the atypical category and 63% of the patients affected by the latter to the typical pattern. Nevertheless, we believe that the differential diagnosis between fungal infections and COVID-19 remains a challenge even for the experienced thoracic radiologists. For example, distinguishing COVID-19 from Pneumocystis jirovecii pneumonia is particularly challenging given the predominantly "ground glass" alterations present in both the conditions, while the different perihilar distribution is sometimes hard to evaluate [38]. As far as it concerns the diagnosis of SARS-CoV-2 pneumonia superinfected by a mycotic agent, we think that our results confirm the opinions expressed by Koehler et al. [11] about CAPA: currently, radiology alone cannot effectively identify this subset of patients since many atypical COVID-19 findings overlap with several fungal infections. In this setting keep suggesting that performing a BAL on patients with two consecutive NP RT-PCR tests who have a clinically suspected SARS-COV-2 infection and a radiological atypical/indeterminate pattern (clinically suspected, according with radiologic images and bio-humoral findings) may help to confirm or rule out this dangerous complication.

Our study has some limitations: first, the retrospective nature of the study, with patients presenting to the Emergency Department where they performed a CT scan and were stratified for the risk of SARS-CoV-2 infection at different stages of the disease. Second, the number of patients with a SARS-CoV-2 and mycotic co-infection is small, limiting the possibility to draw definitive conclusions in these patients hospitalized in a non-intensive care setting. However, to our knowledge this is the first published study that investigates the prevalence of mycotic co-infectants in patients hospitalized in an internal medicine ward, undergoing bronchoscopy with BAL for the research of SARS-CoV-2. All the subjects included were categorized on the basis of their immune status and mycotic infection defined as clinically relevant or irrelevant on the basis of recent guidelines, even if retrospectively [21].

However, our results confirm that the STR/RSNA CT appearance suggests, even if not definitively, the probability of SARS-CoV-2 infection, as well as it determines the need to proceed with further examinations in those cases with indeterminate or atypical appearance [8].

In conclusion, mycotic isolation on lower respiratory tract may be interpreted as an innocent bystander, but its identification on BAL could negatively influence the prognosis of patients, especially COVID-19 patients. CAPA and other invasive mycotic infection (especially Candida spp), in patients affected by SARS-CoV-2 pneumonia, represent a fearsome complication that should be investigated, particularly in immunocompromised hosts, independently from CT radiological features. We emphasize the role of BAL in resolving clinical complex cases, without limiting its role in ruling out SARS-CoV-2 infection.

References

1. Corman VM, Landt O, Kaiser M, Molenkamp R, Meijer A, Chu DK, et al. Detection of 2019 Novel Coronavirus (2019-nCoV) by Real-Time RT-PCR. Euro Surveill. 2020 Jan;25(3):2000045

2. Sawano M, Takeshita K, Ohno H, Oka H. A short perspective on a COVID-19 clinical study: 'diagnosis of COVID-19 by RT-PCR using exhale breath condensate samples'. J Breath Res. 2020 Oct 6;14(4):042003.

3. Lamote K, Janssens E, Schillebeeckx E, Lapperre TS, De Winter BY, van Meerbeeck JP. The scent of COVID-19: viral (semi-)volatiles as fast diagnostic biomarkers? J Breath Res. 2020 Jul 21;14(4):042001.

4. Prokop M, van Everdingen W, van Rees Vellinga T, van Ufford JQ, Stoger L, Beenen L, et al. CO-RADS – A categorical CT assessment scheme for patients with suspected COVID-19: definition and evaluation. Radiology. 2020 Aug;296(2):E97-E104.

5. Patrucco F, Albera C, Bellocchia M, Foci V, Gavelli F, Castello LM, et al. SARS-CoV-2 Detection on Bronchoalveolar Lavage: An Italian Multicenter experience. Respiration. 2020;99(11):970-978.

6. Geri P, Salton F, Zuccatosta L, Tamburrini M, Biolo M, Busca A, et al. Limited role for bronchoalveolar lavage to exclude Covid-19 after negative upper respiratory tract swabs: a multicenter study. Eur Respir J. 2020 Aug 6;2001733

7. Ora J, Puxeddu E, Cavalli F, Giorgino FM, Girolami A, Chiocchi M, et al. Does bronchoscopy help the diagnosis in COVID-19 infection? Eur Respir J. 2020;56(2):2001619.

8. Patrucco F, Carriero A, Falaschi Z, Paschè A, Gavelli F, Airoldi C, et al. COVID-19 Diagnosis in Case of Two Negative Nasopharyngeal Swabs: Association between Chest CT and Bronchoalveolar Lavage Results. Radiology. 2021 Mar;298(3):E152-E155.

9. Franquet T, Müller NL, Giménez A, Guembe P, de La Torre J, Bagué S. Spectrum of pulmonary aspergillosis: histologic, clinical, and radiologic findings. Radiographics. 2001 Jul-Aug;21(4):825-37.

10. Kunin JR, Blasco LF, Hamid A, Fuss C, Sauer D, Walker CM. Thoracic Endemic Fungi in the United States: Importance of Patient Location. Radiographics. 2021 Mar-Apr;41(2):380-398.

11. Koehler P, Bassetti M, Chakrabarti A, Chen SCA, Colombo AL, Hoenigl M, et al. Defining and managing COVID-19-associated pulmonary aspergillosis: the 2020 ECMM/ISHAM consensus criteria for research and clinical guidance. Lancet Infect Dis. 2020 Dec 14:S1473-3099(20)30847-1.

12. Fekkar A, Lampros A, Mayaux J, Poignon C, Demeret S, Constantin JM, et al. Occurrence of Invasive Pulmonary Fungal Infections in Patients with Severe COVID-19 Admitted to the ICU. Am J Respir Crit Care Med. 2021 Feb 1;203(3):307-317.

13. Macauley P, Epelbaum O. Epidemiology and Mycology of Candidaemia in non-oncological medical intensive care unit patients in a tertiary center in the United States: Overall analysis and comparison between non-COVID-19 and COVID-19 cases. Mycoses. 2021 Feb 20:10.1111/myc.13258.

14. Lahmer T, Kriescher S, Herner A, Rothe K, Spinner CD, Schneider J, et al. Invasive pulmonary aspergillosis in critically ill patients with severe COVID-19 pneumonia: Results from the prospective AspCOVID-19 study. PLoS One. 2021 Mar 17;16(3):e0238825. doi: 10.1371/journal.pone.0238825.

15. Pemán J, Ruiz-Gaitán A, García-Vidal C, Salavert M, Ramírez P, Puchades F, et al. Fungal co-infection in COVID-19 patients: Should we be concerned? Rev Iberoam Micol. 2020 Apr-Jun;37(2):41-46.

16. Garcia-Vidal C, Sanjuan G, Moreno-García E, Puerta-Alcalde P, Garcia-Pouton N, Chumbita M, et al. Incidence of co-infections and superinfections in hospitalized patients with COVID-19: a retrospective cohort study. Clin Microbiol Infect. 2021 Jan;27(1):83-88.

17. Verweij PE, Gangneux JP, Bassetti M, Brüggemann RJM, Cornely OA, Koehler P, et al. Diagnosing COVID-19-associated pulmonary aspergillosis. Lancet Microbe. 2020 Jun;1(2):e53-e55.

18. von Elm E, Altman DG, Egger M, Pocock SJ, Gøtzsche PC, Vandenbroucke JP, et al. The Strengthening the Reporting of Observational Studies in Epidemiology (STROBE) Statement: Guidelines for Reporting Observational Studies. J Clin Epidemiol. 2008 Apr;61(4):344-9.

19. Du Rand IA, Blaikley J, Booton R, Chaudhuri N, Gupta V, Khalid S, et al.; British Thoracic Society Bronchoscopy Guideline Group. British Thoracic Society guideline for diagnostic flexible bronchoscopy in adults: accredited by NICE. Thorax 2013;68 (Suppl 1):i1–44.

20. Gavelli F, Castello LM, Bellan M, Azzolina D, Hayden E, Beltrame M, et al. Clinical stability and in-hospital mortality prediction in COVID -19 patients presenting to the Emergency Department. Minerva Med 2021;112:118-23.

21. Donnelly JP, Chen SC, Kauffman CA, Steinbach WJ, Baddley JW, Verweij PE, et al. Revision and Update of the Consensus Definitions of Invasive Fungal Disease From the European Organization for Research and Treatment of Cancer and the Mycoses Study Group Education and Research Consortium. Clin Infect Dis. 2020 Sep 12;71(6):1367-1376.

22. Lamoth F, Glampedakis E, Boillat-Blanco N, Oddo M, Pagani JL. Incidence of invasive pulmonary aspergillosis among critically ill COVID-19 patients. Clin Microbiol Infect. 2020 Dec;26(12):1706-1708.

23. Patrucco F, Gavelli F, Ravanini P, Daverio M, Statti G, Castello LM, et al. Use of an innovative and non-invasive device for virologic sampling of cough aerosols in patients with community and hospital acquired pneumonia: a pilot study. J Breath Res. 2019 Mar 1;13(2):021001.

24. Barberi C, Castelnuovo E, Dipasquale A, Mrakic Sposta F, Vatteroni G, Canziani LM, et al. Bronchoalveolar lavage in suspected COVID-19 cases with a negative nasopharyngeal swab: a retrospective cross-sectional study in a high-impact Northern Italy area. Intern Emerg Med. 2021 Mar 26:1–8.

25. Chen KY, Ko SC, Hsueh PR, Luh KT, Yang PC. Pulmonary fungal infection: emphasis on microbiological spectra, patient outcome, and prognostic factors. Chest. 2001 Jul;120(1):177-84.

26. Silva DL, Lima CM, Magalhães VCR, Baltazar LM, Peres NTA, Caligiorne RB, Moura AS, Fereguetti T, Martins JC, Rabelo LF, Abrahão JS, Lyon AC, Johann S, Santos DA. Fungal and bacterial coinfections increase mortality of severely ill COVID-19 patients. J Hosp Infect. 2021 Jul;113:145-154.

27. Li Z, Lu G, Meng G. Pathogenic Fungal Infection in the Lung. Front Immunol. 2019 Jul 3;10:1524.

28. Nasir N, Farooqi J, Mahmood SF, Jabeen K. COVID-19-associated pulmonary aspergillosis (CAPA) in patients admitted with severe COVID-19 pneumonia: An observational study from Pakistan. Mycoses. 2020 Aug;63(8):766-770.

29. Bartoletti M, Pascale R, Cricca M, Rinaldi M, Maccaro A, Bussini L, et al. Epidemiology of invasive pulmonary aspergillosis among COVID-19 intubated patients: a prospective study. Clin Infect Dis. 2020 Jul 28:ciaa1065.

30. Di Pasquale MF, Sotgiu G, Gramegna A, Radovanovic D, Terraneo S, Reyes LF, et al. Prevalence and Etiology of Community-acquired Pneumonia in Immunocompromised Patients. Clin Infect Dis. 2019 Apr 24;68(9):1482-1493.

31. Belsky JA, Tullius BP, Lamb MG, Sayegh R, Stanek JR, Auletta JJ. COVID-19 in immunocompromised patients: A systematic review of cancer, hematopoietic cell and solid organ transplant patients. J Infect. 2021 Mar;82(3):329-338.

32. Yu J, Ouyang W, Chua MLK, Xie C. SARS-CoV-2 Transmission in Patients With Cancer at a Tertiary Care Hospital in Wuhan, China. JAMA Oncol. 2020 Jul 1;6(7):1108-1110.

33. Lewis MA. Between Scylla and Charybdis - Oncologic Decision Making in the Time of Covid-19. N Engl J Med. 2020 Jun 11;382(24):2285-2287.

34. Schauwvlieghe AFAD, Rijnders BJA, Philips N, Verwijs R, Vanderbeke L, Van Tienen C, et al. Invasive aspergillosis in patients admitted to the intensive care unit with severe influenza: a retrospective cohort study. Lancet Respir Med 2018;6:782–792.

35. Schwartz IS, Friedman DZP, Zapernick L, Dingle TC, Lee N, Sligl W, et al. High rates of influenza-associated invasive pulmonary aspergillosis may not be universal: a retrospective cohort study from Alberta, Canada. Clin Infect Dis 2020;71:1760–1763.

36. Pendleton KM, Huffnagle GB, Dickson RP. The significance of Candida in the human respiratory tract: our evolving understanding. Pathog Dis. 2017 Apr 1;75(3):ftx029.

37. Azoulay E, Timsit JF, Tafflet M, de Lassence A, Darmon M, Zahar JR, et al. Candida colonization of the respiratory tract and subsequent pseudomonas ventilator-associated pneumonia. Chest. 2006 Jan;129(1):110-7.

38. Hochhegger B, Zanon M, Altmayer S, Mandelli NS, Stüker G, Mohammed TL, et al. COVID-19 mimics on chest CT: a pictorial review and radiologic guide. Br J Radiol. 2021 Feb 1;94(1118):20200703.

Title: Effects of anti-fibrotic drug nintedanib on blood monocytes and monocyte-derived macrophages of patients with Idiopathic Pulmonary Fibrosis (IPF) naïve for treatment and healthy subjects

Background

Idiopathic pulmonary fibrosis (IPF) is a chronic, progressive fibrotic disorder affecting the lower respiratory tract of adults over the age of 40 years [1]. Histopathologic pattern associated with diagnosis of IPF is the "usual interstitial pneumonia" (UIP), also seen in other fibrotic progressive lung diseases such as connective tissue disorders with pulmonary manifestations, chronic hypersensitivity pneumonia, asbestosis [1]. The histopathological features of UIP in patients with IPF include the proliferation of mesenchymal cells, progressive increase of interstitial fibrosis, overproduction and disorganized deposition of collagen and extracellular matrix, resulting in a distortion of the pulmonary architecture, forming subpleural cystic airspaces called honeycomb cysts. Moreover, fibroblast foci are the main cluster of fibrosis, and myofibrolasts, located near fibroblast foci, are a characteristic histologic feature of UIP. These manifestations are associated with a mild, patchy chronic inflammatory cell infiltrate [2].

The initiation of histopathologic process observed in IPF remains unknown, but several risk factors have been associated with the development of IPF such as cigarette smoking, environmental pollutants, chronic gastric aspiration, viral infections and some drugs; also, genetic predisposition is linked to the development of IPF as suggested by reports of families with members affected. However, none of the above-mentioned risk factors explain the remodelling and progression of IPF [3].

Inflammation

As demonstrated in animal models [4], the inflammation precedes the development of a fibrotic response, and the inflammatory alveolitis reduces the subsequent fibrotic response. The alveolitis of early pulmonary fibrosis in animal models is sustained by alveolar macrophages, neutrophils, eosinophils and lymphocytes [5]. Alveolar macrophages are considered one of the main responsible for initiating the fibrotic process due to their ability to secrete proinflammatory and profibrotic cytokines that affect mesenchymal cell proliferation and promote collagen deposition [6].

Macrophages

Macrophages are mainly involved in the maintenance of homeostasis and resistance to invasion by pathogen [7]. They are present in different tissue and undergo M1 (classical) or M2 (alternative) activation, characterised by different phenotype and function depending of the stimuli to which they are exposed: classical M1 activation are stimulated by toll-like receptor ligands and INF-γ, while alternative M2 activation are stimulated by IL-4 and IL-13 [8].

The M1 phenotype is characterized by the expression of proinflammatory cytokines, production of reactive nitrogen and oxygen intermediates, promotion of Th1 response and microbiological and tumoricidal activity; on the other hand, M2 macrophages are involved in parasite containment and promotion of tissue remodelling, tumor progression and have immunoregulatory functions. M2 are characterized by phagocytic activity, expression of scavenging molecules, mannose and galactose receptors, production of ornithine and polyamines through the arginase pathway, and an IL-12lo, IL-10hi, IL-1decoyRhi, IL-1RAhi phenotype [8].

Macrophage polarization is a dynamic process that can be reproduced in vitro too [9, 10] and it has been demonstrated that several pathologies reflect changing in macrophage activation, with classically activated M1 cells implicated in starting and continuing inflammation, while M2 macrophages are associated with resolution or smouldering of chronic inflammation [11].

Monocytes-macrophage differentiation is sustained by a network of signalling molecules, transcription factors, epigenetic mechanisms and posttranscriptional regulators [8] (Figure 1).

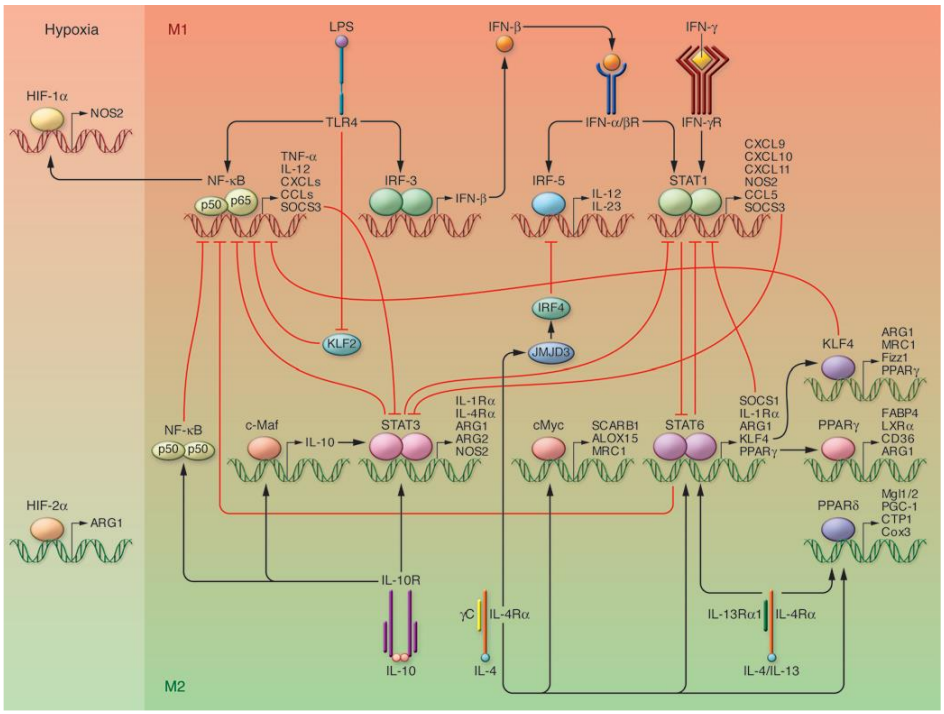

Figure 1: Mechanisms and major pathways of macrophage polarization [8].

Pulmonary Macrophages

Pulmonary macrophages are classified in two categories: alveolar macrophages (AMs) residing in the alveoli, and interstitial macrophages (IMs) which are sited in lung parenchyma. AMs colonize the lung tissue shortly after the birth and have self-renewal proprieties independent of the input from the blood monocyte at steady state. IMs derives from both yolk-sac macrophages and bone marrow-derived monocytes (BMDMs). AMs are the main effectors of immune responses and have both proinflammatory and anti-inflammatory proprieties; on the other hand, IMs maintain immune homeostasis in the respiratory tract including immune tolerance to antigens [12].

Macrophages represent the most abundant cells in the lungs and play a vital role in airway remodelling in pulmonary fibrosis. Also pulmonary macrophages can differentiate into classically activated macrophages (M1) or alternatively activated macrophages (M2) (Figure 2) [12].

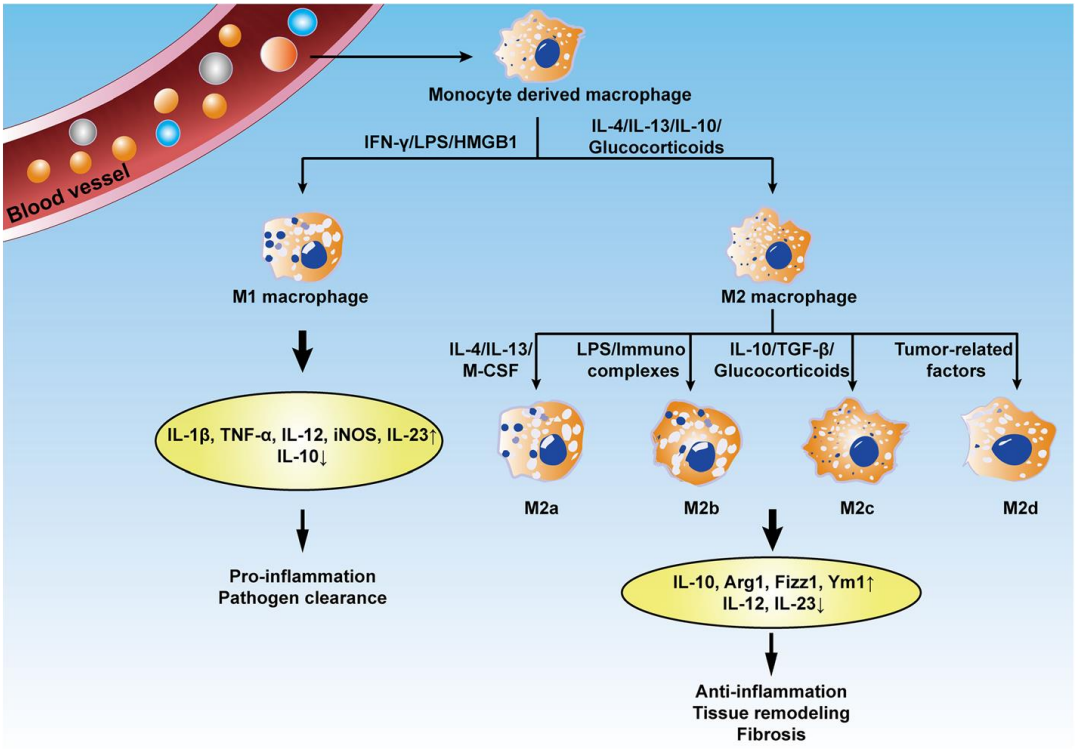

Figure 2: Schematic diagram of macrophage subtypes. BV, blood vessel; M0, monocyte; LPS, lipopolysaccharide; IL, interleukin [12].

M1 Macrophages in IPF

M1 macrophages in IPF patients contribute to the host defence generating reactive nitric oxide (NO) via inducible nitric oxide synthase (iNOS) and releasing proinflammatory cytokines and chemokines (IL-1β, IL-12, IL-23, CCL2 and TNF-α). Phenotypically, these cells are characterized by the expression of high levels of CD80, TLR4, MHCII and CD86. They have a strong anti-microbial and anti-tumoral activity, mediate tissue damage and initiate inflammatory response. Granulocyte-macrophage colony-stimulating factor (GM-CSF) stimulate the generation of M1 from naïve M0 or polarized M2 [12, 13].

In the current opinion of IPF pathogenesis, pulmonary fibrosis process is the final pathological outcome of aberrant healing responses to persistent lung injury. Pulmonary cellular damage induced by several factors (environmental particulates, infections, mechanical damage) results in the disruption of lung parenchymal architecture. At the early inflammatory stages, acute lung injury promotes an M1 phenotype under the control of interferon regulatory factor 5 (IRF-5) with expression of high levels of iNOS and proinflammatory cytokines: these are associated with Th1 immune response and responds to INF-γ and TLR ligands to maximize the cytotoxic activity. However, persistent and sustained inflammatory responses act as a trigger to initiate the fibrotic

response in the lung. Interestingly, as demonstrated in a murine model [14, 15], during the healing process there is an early and sustained concentration of exudate macrophages (ExM) and their precursors, the Ly-6Chi monocytes; type II alveolar cells (AEC II) injury induces a modest inflammatory response that is nonetheless significantly enriched for alternatively activated and profibrotic ExM and Ly-6Chi monocytes. The accumulation of these cells and the development of fibrosis in response to the alveolar injury is CCR2 dependent, implicating ExM and Ly-6Chi monocytes [12].

M2 Macrophages in IPF

M2 polarization could be induced by several mediators such as IL-4, IL-13, TGF-β, IL-10, all of them implicated in the wound-healing fibrosis cascade [16]. M2 macrophages are characterized by low levels of MHCII, CD86, iNOS2 and high levels of arginase-1 and cell surface receptors such as macrophage mannose receptor, also called CD206 [12]. CD206 is expressed on alveolar macrophages and exert an important function in the phagocytosis of M2 cells via increasing efferocytosis of invading pathogens and apoptotic cells [12].

During the development and progression of IPF, the predominant infiltration of M2 macrophages in fibrotic areas acts as a vital regulator of fibrogenesis; in particular, M2 macrophages produce profibrotic mediators such as TGFβ and PDGF by which they induce continuous fibroblast activation and promote myofibroblast proliferation (Figure 3). Moreover, IL-10 generates a Th2 microenvironment which involves fibrocyte recruitment and M2 macrophage activation, leading to excessive extracellular matrix deposition [12].

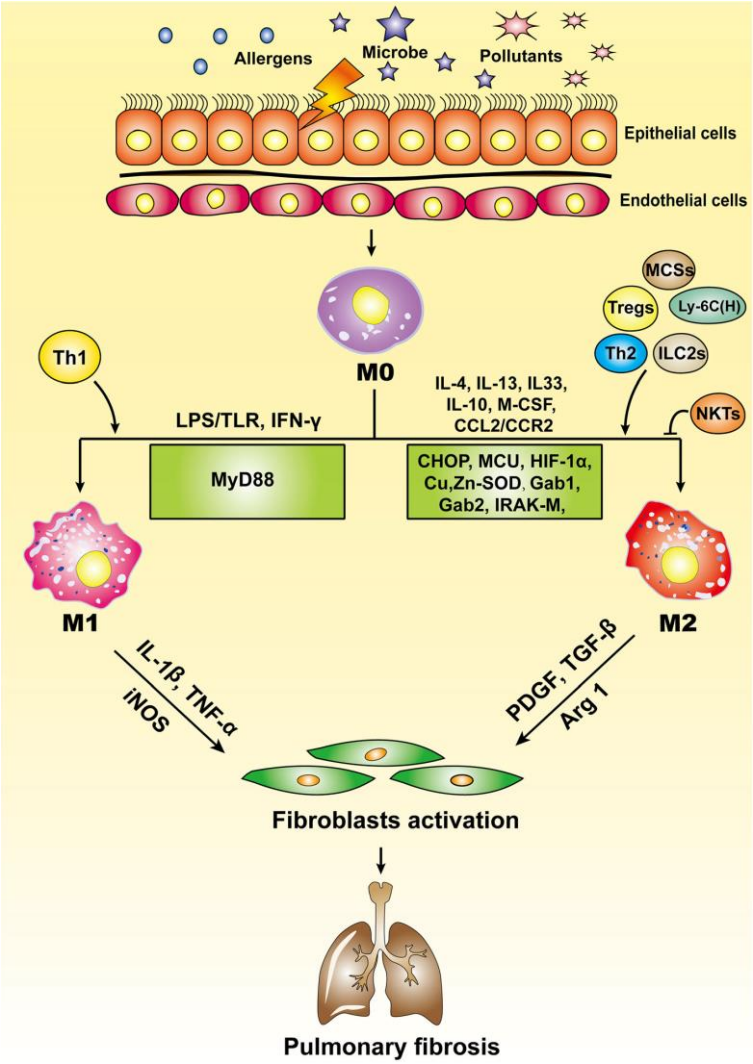

Figure 3: Macrophages in the pathogenesis of pulmonary fibrosis. Ly-6C (H), Ly-6Chigh monocytes; MCS, mesenchymal stem cells; ILC2s, lymphoid type 2 cells; NKTs, natural killer T cells; MCU, mitochondrial calcium uniporter; CHOP, C/EBP homologous protein; IRAK-M, IL-1R–associated kinase-M; Arg 1, arginase 1; iNOS, inducible nitric oxide synthase [12].

Monocytes

Monocytes are circulating blood cells characterised by the expression of the receptors CD14 and CD16 [17]. Three populations of monocytes are identified based on the presence of these surface markers: the classical (CD14++CD16-), the non-classical (CD14++CD16+) and the intermediate (CD14+CD16+). Intermediate monocytes display similar ROS production and phagocytosis potential, lower adhesion to surfaces, but higher expression of class II molecule and IL-12 production than classical monocytes [17]. Intermediate and non-classical monocytes emerge from the pool of classical monocytes [18].

Classical monocytes (CD14++CD16-) were found to be primed for phagocytosis, innate sensing/immune response and migration; intermediate (CD14+CD16+) were the only expressing

CCR5 (C-C chemokine receptor type 5) and were well-suited for antigen presentation, cytokine secretion, apoptosis regulation and differentiation; non classical monocytes (CD14++CD16+) are involved in complement and Fc gamma-mediated phagocytosis and adhesion [17] (Figure 4).

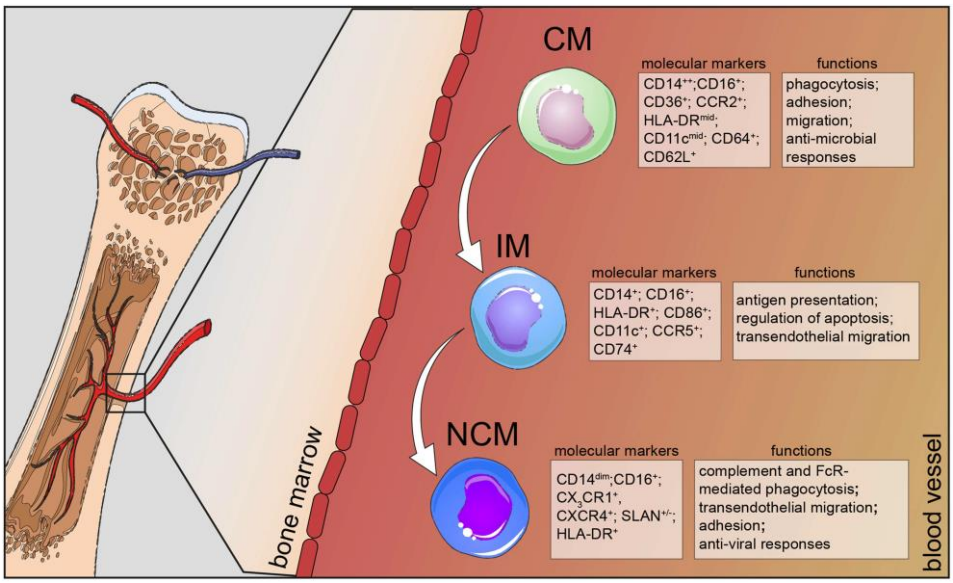

Figure 4: Human monocyte subsets in health. CM, classical monocytes; IM, intermediate monocytes; NCM, non-classical monocytes [17].

Non-classical monocytes express a distinct transcriptomic and metabolic profile in comparison to classical monocytes which utilize carbohydrate metabolism as their energy source. Non-classical, similarly to CD14+CD16+ monocytes, present antigen processing capabilities but are distinguished from classical monocytes by their association with wound healing process [19]. Moreover, they have antagonizing function to classical monocytes and promote neutrophil adhesion at the endothelial interface via the secretion of TNFα [20].

Data regarding different monocyte population in IPF are limited: classical CD14++CD16- count was demonstrated to be a prognostic marker of mortality in IPF patients [21] and total count of monocytes was correlated with fibrosis extension measured at CT scan [22]; nevertheless, no abnormalities in frequencies of intermediate, non-classical and classical subset were observed in IPF patients [22].

Prognostic value of Monocytes in IPF

Data regarding different monocyte population in IPF are limited. Classical CD14++CD16- count was demonstrated to be a prognostic marker of mortality in IPF patients [21] and total count of

monocytes was correlated with fibrosis extension measured at CT scan [22]; nevertheless, no abnormalities in frequencies of intermediate, non-classical and classical subset were observed in IPF patients [22].

The robust association of high monocyte count with mortality in other fibrotic diseases such as systemic sclerosis, hypertrophic cardiomyopathy, and myelofibrosis suggests they might contribute to pathogenesis of these diseases as well. Recruitment of monocytes to damaged tissue to aid in repair—typically a beneficial response—becomes detrimental when an organ undergoes continuous, pathogenic wound healing [23]. In IPF, monocytes migrate to the lung and differentiate into profibrotic inflammatory alveolar macrophages [24]. Consistent with this model of lung fibrosis, depletion of monocytes has been shown to strikingly reduce the degree of fibrosis following lung injury in the bleomycin treatment-induced lung fibrosis mouse model. Up to now, there are no clinically approved drugs that reduce monocyte count without causing neutropenia, and depletion of monocytes could perhaps lead to an increased risk of infection [24].

Recently, the clinical interest in monocyte peripheral count increased due to clinical implications in patients with IPF: in particular, *Scott* et al. [23] investigated whether a specific immune cell type from patients with IPF could identify those at higher risk and poor outcome. They observed that CD14+ classical monocyte percentage above the mean were associated with a shorter transplant free survival and that the threshold of 0.95 $x10^9$ cells/L or greater were associated with mortality even after the adjustment for forced vital capacity (FVC) [23]. This data was also confirmed by *Liu* et al. [25] who observed an inverse correlation between monocytes count and survival and diffusion of the lungs for carbon monoxide (DLCO); moreover, they demonstrated that in IPF patient proportions of monocytes were higher as compared to healthy controls. *Kreuter* et al. [26] retrospectively analysed three large phase III trials (ASCEND, CAPACITY, INSPIRE) to evaluate the relationship between monocyte count and different clinical outcome: they observed that those patients with monocyte count of 0.60 to <0.95 x 10^9 cells/L experienced more IPF progression, all-cause mortality and all-cause hospitalization compared to those patients with a count lower than 0.60 x 10^9 or higher than 0.95 x 10^9 cells/L. Finally, *Kawamura* et al. [27] demonstrated that IPF patients that experienced an acute exacerbation of fibrosing interstitial lung disease had a higher monocyte count at the time of antifibrotic initiation; this association was independently significant after adjusting for the initial severity of fibrotic damage.

The possibility to provide some readily measurable serum biomarkers reflecting the IPF-related pathophysiology may guide the physician towards a better clinical approach in patients with IPF. In addition to the prediction of poorer prognosis, monocyte count has been linked with the occurrence

of acute exacerbations of fibrosing ILDs, and regular monitoring may help to guide clinical decision-making with respect to the initiation of antifibrotic medications [23, 27].

Cytokines involved in lung fibrosis

TGF-β: TGF-β is one of the most potent inducers of extracellular matrix production, including collagen and other matrix proteins. TGF-β expression is elevated in both animal models of lung fibrosis and in fibrotic human lungs. The major cellular sources of TGF-β over-production during the development of lung fibrosis have been identified as alveolar macrophages, bronchial epithelium and hyper-plastic type II alveolar epithelial cells (AECs). TGF-β is involved in fibroblast proliferation, inducing fibroblast differentiation to myofibroblast which are the primary effector for lung fibrogenesis [28].

TNF- α: Data from murine models showed that development of fibrosis induces the expression of TNF- α and blockade ameliorates fibrosis. [28]. But there is strong evidence that TNF- α plays opposing roles in pulmonary fibrotic disease depending on the stage of the fibrotic process, complicating therefore its use for the treatment of ILD. A randomized double-blind trial in which human subjects with clinically progressive IPF received etanercept, a fully humanized soluble recombinant TNF receptor fusion protein, demonstrated that the treatment had no effect on lung function or quality of life endpoints; however, a decreased rate of disease progression was observed, and the treatment was well tolerated [28].

IL-1β: IL-1β is elevated in alveolar macrophages of patients with interstitial lung diseases, including IPF, sarcoidosis, and asbestosis [28]. Moreover, multiple studies have described IL-1β or IL-1βR polymorphisms in patients with fibrosing lung disease. In murine models, administration of recombinant IL-1β or transient overexpression in the lungs recapitulates many of the salient features of bleomycin-induced fibrosis, and this process is at least partially dependent on IL-17A [28].

Oxidative stress

There is growing evidence that oxidative stress plays a significant role in IPF [29]. Oxidative stress is defined as an imbalance between oxidant production and antioxidant defence in favour of oxidants, that leads to cellular dysfunction and tissue damage [29]. Due to its exposure to relatively higher oxygen tensions than other tissues, the lung is particularly sensitive to oxidative stress. Exogenous oxidants and pollutants further increase oxidant production and activate inflammatory

cells to generate free radicals. Cigarette smoke, asbestos fibers, drugs and radiations, are well-known to favour fibrotic interstitial lung reactions. Furthermore, they have been shown to trigger the production of the reactive oxygen species (ROS) as hydroxyl radical, hydrogen peroxide, and superoxide radical. In the human lung, several pathways can generate ROS, including nicotinamide adenine dinucleotide phosphate oxidases, myeloperoxidase, eosinophil peroxidase, mitochondrial electron transport chain, and xanthine oxidase. In addition, superoxide may react with nitric oxide (NO) to form various reactive nitrogen species (RNS), such as peroxynitrite. NO is principally produced by the inducible form of nitric oxide synthase (iNOS) in the lung, in particular during inflammation. Moreover, human lung cells widely also express the constitutive forms of NOS, that further contribute to NO production. In general, a complex variety of oxidants are produced in response to injury leading to pulmonary fibrosis. These oxidants can activate several genes related to cell growth, cell death, and fibroblast proliferation [29].

Since pulmonary homeostasis requires an appropriate balance between intracellular and extracellular oxidants and antioxidants, lung protection is guaranteed by several molecules that include (i) small-molecular-weight antioxidants (e.g., glutathione, vitamins, uric acid), (ii) mucins, (iii) metal-binding proteins (transferrin, lactoferrin, metallothionein, etc.), (iv) intracellular and extracellular superoxide dismutases (SODs), (v) enzymes to reduce H_2O_2 (several glutathione-associated enzymes and catalase), (vi) detoxification enzyme systems (e.g., glutathione-S-transferases), and (vii) other redox regulatory thiol proteins (e.g., thioredoxin-peroxiredoxin system and glutaredoxins) [29].

Nintedanib

Nintedanib is a small-molecule tyrosine kinase inhibitor that targets platelet-derived growth factor (PDGF) receptor-α and -β, fibroblast growth factor (FGF) receptor-1–3 and vascular endothelial growth factor (VEGF) receptor-1–3 [30]. Nintedanib binds competitively to the ATP-binding pocket of these receptors, thereby blocking intracellular signalling [30]. Nintedanib also inhibits the Src family kinase lymphocyte-specific tyrosine protein kinase (Lck), colony-stimulating factor (CSF)-1 receptor (CSF1R) and 20 other kinases with median inhibitory concentration (IC50) values <100 nM [30, 31]. Both VEGF and FGF receptors are pro-angiogenic receptor tyrosine kinases and nintedanib was firstly designed as an anti-angiogenic drug for cancer indications. The clinical development of nintedanib for cancer indications, including non small cell lung cancer, colorectal cancer and ovarian cancer, is ongoing. The inhibition of PDGF receptor-α and β is the main reason

nintedanib was selected as a potential treatment for IPF [30, 31], but other several effects have been proven on fibrotic process [32]:

- Inhibition of fibroblast proliferation and migration: the inhibitory activity of nintedanib was demonstrated in primary human lung fibroblasts from patients with IPF (IPF-HLF) and from healthy donors (N-HLF). In cells from the patients, PDGF-BB, FGF-2 and VEGF caused a significant pro-proliferative effect that was significantly reversed by nintedanib. In N-HLF, even lower concentrations of nintedanib significantly antagonised the growth factor-induced pro-proliferative effect. IPF-HLF demonstrated a stronger migratory response to all three growth factors compared to N-HLF.
- Effects on fibroblast transformation: nintedanib inhibited activation of primary human lung fibroblasts from IPF patients induced by TGF-β to differentiate into myofibroblast, as determined by the α-smooth muscle actin mRNA expression as a marker for myofibroblast differentiation
- Effects on extracellular matrix (ECM) components: nintedanib reduced TGF-β-stimulated collagen secretion and deposition by primary human lung fibroblasts from patients with IPF cultured for 48 h. Nintedanib also reduced secreted metalloproteinase-2 (TIMP-2) levels and induced the secretion of pro-matrix metalloproteinase (MMP)-2. Reduced TIMP-2 levels, together with increased pro-MMP-2, could contribute to the reduction in collagen. Inhibition of fibroblast/myofibroblast proliferation by nintedanib might also exert an indirect inhibitory effect on ECM secretion and deposition
- Effects on apoptosis: lung fibroblasts/myofibroblasts isolated from patients with IPF are reported to have an elevated resistance to apoptotic stimulation preventing resolution of fibrosis (REF). Whether nintedanib can induce apoptosis in human lung fibroblasts is currently unknown.
- Anti-angiogenic activity: by inhibition of VEGF, PDGF and FGF signalling pathways nintedanib reduces tumour microvessel density and demonstrates preclinical anti-angiogenic efficacy in an animal model of xenograft tumours in mice. Taken together, the experimental evidence supports nintedanib having anti-angiogenic efficacy; however, whether this adds to its anti-fibrotic activity in IPF still needs to be elucidated.
- Anti-fibrotic and anti-inflammatory activity: bleomycin-induced and silica-induced fibrosis are two murine models of lung fibrosis used to evaluate nintedanib efficacy on inflammation and fibrosis. Nintedanib inhibits fibrotic changes in a dose-dependent manner in the bleomycin model; moreover, mRNA expression of fibrosis-related markers was inhibited.

When administered at therapeutic regimen, nintedanib gave a near complete attenuation of fibrosis. On BALF, nintedanib reduced lymphocyte count, IL-1β levels and percentage of myeloid dendritic cells in lung tissue.

Nintedanib effects on macrophages

Huang et al. [33] recently evaluated the effects of nintedanib on macrophages activation in a fos-related antigen-2 (Fra2) mouse model of systemic sclerosis. They started from the assumption that all the pathways that are influenced by nintedanib activity (PDGFR, VEGRF and FGFR) are implicated into the pathogenesis of fibrosis and are discussed as candidates for target therapies for systemic sclerosis. Fra2 transgenic mice develop a destructive microvascular disease with apoptosis of endothelial cells, followed by systemic fibrotic manifestations. The authors hypothesised that nintedanib may inhibit M2 polarisation in Fra2 transgenic mice as previously observed after treatment with tocilizumab. They observed that nintedanib completely prevented the increase in M2 macrophages with M2 counts comparable to those in non-transgenic control. In contrast to M2 macrophages, the number of M1 macrophages did not differ. To confirm the inhibitory effects, they tested nintedanib on alternative activation of monocytes induced by M-CSF1, IL-4 and IL-13. Nintedanib reduced M2 counts with suppression of expression of M2 markers as CD163 or CD206. The expression marker CD86 or general markers of monocytes such as CD14 was unchanged or even increased by incubation of nintedanib. Finally, the authors observed that the number of macrophages positive for IL-4 or IL-13 were increased in Fra2 mice and after the treatment with nintedanib the number of IL-4 and IL-13 positive macrophages drop to levels of non-transgenic mice [33].

Fibrocytes are monocyte-derived cells and a marked increase in circulating fibrocyte has a positive correlation with the presence of fibroblastic foci in the lung of IPF patients. *Sato* et al. [34] assessed the effects of nintedanib on the differentiation of fibrocytes from monocytes. They observed that even monocytes express FGF, PDGF and VEGR even if with lower concentration than fibrocytes. They finally demonstrated that nintedanib has inhibitory effects on fibrocyte differentiation from monocytes, and the same effect was observed after the specific inhibition for FGFR, PDGFR and VEGFR. This suggest that these growth factors may play a role in the differentiation of fibrocytes in pulmonary fibrosis [34].

Bellamri et al. [35] have investigated the anti-inflammatory effects of nintedanib on human macrophages. They exposed primary cultures of human monocyte-derived macrophages, differentiated with CSF1, to nanomolar concentrations of nintedanib that were in the range of the

blood plasma drug concentrations measured in patients with IPF after a steady-state standard dosing of two times 150 mg per day. In these patients, the highest nintedanib blood concentrations were about 70 nM. The authors demonstrated that nintedanib (10–1000 nM) inhibited the phosphorylation of the colony-stimulating factor 1 (CSF1) receptor (CSF1R) and the downstream signalling pathways in human macrophages. At 200–1000 nM, nintedanib reduced the adhesion of CSF1 macrophages, without inducing cytotoxicity, and repressed the expression of CCL2. In addition, nintedanib (200–1000 nM) altered the polarization of human macrophages by decreasing the production of pro-fibrotic cytokines and the membrane expression of markers in M1 and M2 macrophages, respectively [36]. In particular, they stimulated M1 polarization with LPS/INF and M2 with IL-4/IL-13: they observed that nintedanib reduce expression of M2 macrophages membrane markers CD206 and CD209 but no results were observed for M1 markers (CD80, CD86, CD40, CD83). Moreover, nintedanib did not inhibit the induction of IL-1β and IL-8 secretion but blocked the mRNA expression for IL-10; on the other hand, nintedanib did not affects CCL18, CCL22 and PDGF expression in M2 macrophages.

Aim of the study

The aim of the study is to evaluate the effects of nintedanib on phenotype and responsiveness of human monocytes/macrophages isolated from patients affected by IPF before and after treatment with the drug. Moreover, we performed the same experiments in monocyte/macrophage isolated from healthy donor to compare the basal characteristics of cells and to evaluate the effects of nintedanib in vitro. At the time of writing this manuscript, we enrolled 10 patients of which we had the basal value of cells only. So, waiting for the cells from patients after 3 months of treatments, we treated monocyte/macrophage of patients in vitro and compared to that isolated from healthy donors.

This study is based on a preliminary evaluation we performed to define if it would be present a correlation between the monocyte count and one-year functional trend of 37 patients with IPF, after one year treatment with nintedanib. In table 1 the characteristics of the patients are shown. We included all consecutive patients who were diagnosed as IPF and who started the treatment with nintedanib between 1st January 2018 and 31st December 2019. For each of these patients we recorded the monocyte count, the % of the predicted values of FVC and DLCO on the day they

started the treatment with nintedanib (T0) and same functional values one year after the treatment (T1). We then calculated the difference between T1 and T0 for FVC and DLCO.

Number of subjects	37
Age, in years (mean ±SD)	70.28 ±6.33
Sex: M / F	33 / 4
Peripheral monocytes count, in x 10^9 cells/L (mean ±SD)	0.67 ±0.20
T0 FVC, % of the predicted value (mean ±SD)	81.40 ±15.50
T1-T0 FVC difference (mean ±SD)	-5.05 ±7.64
T0 DLCO, % of the predicted value (mean ±SD)	47.51 ±15.43
T1-T0 DLCO difference (mean ±SD)	-9.05 ±8.90

Table 1: Demographics of IPF patients; data are presented as means ± standard deviations

We observed a negative correlation between monocyte count and FVC and DLCO; in particular, for FVC was -0.34 (95% CI -0.605 and -0.028, p=0.033) and DLCO was -0.36 (95% CI -0.618 to -0.050, p=0.024) (Figure 5).

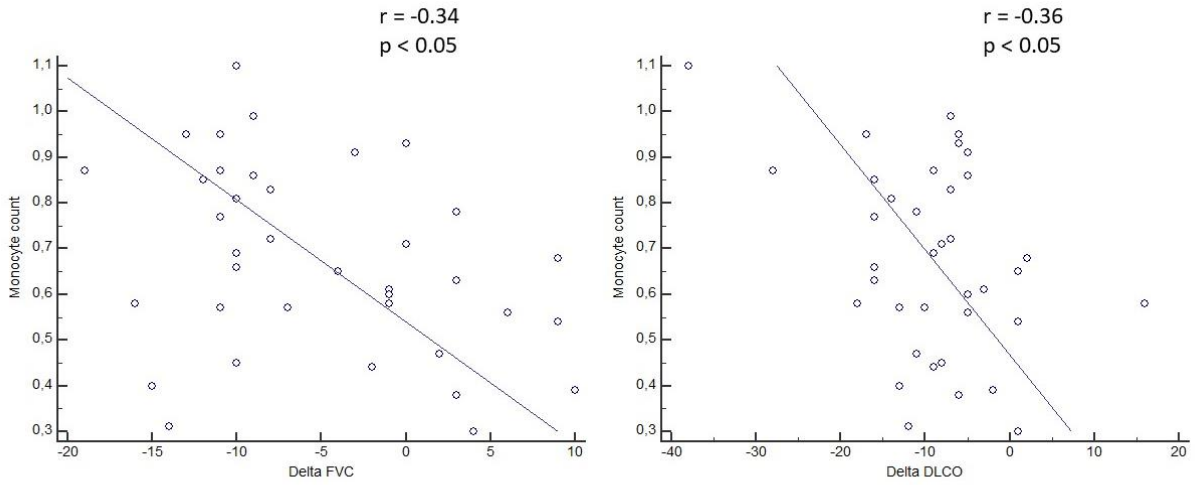

Figure 5: Correlation between monocyte count and one-year variation of FVC and DLCO in IPF patients. Delta FVC and Delta DLCO are referred to one year variation of the functional parameter; monocyte count is expressed in 10^9 cells/L. Correlation was analysed with Pearson correlation coefficient. Significance level was considered $p<0.05$.

Patients were divided in three groups on the basis of monocyte peripheral count according to a previously published study [26]: <0.60 x 10^9 cells/L, 0.60 to 0.95 x 10^9 cells/L, ≥0.95 x 10^9 cells/L (Table 2).

Monocyte count (in x 10^9 cells/L)	<0.60	0.60 to 0.95	≥0.95	p
Monocyte count (in x 10^9 cells/L) (mean ±SD)	0.46 ±0.10	0.75 ±0.10	0.98 ±0.06	<0.001
T0 FVC, % of the predicted value (mean ±SD)	80.71 ±12.48	84.42 ±16.19	69.60 ±17.03	0.160
T1-T0 FVC difference (mean ±SD)	-3.00 ±9.08*	-5.36 ±6.80	-12.20 ±3.56*	0.075
T0 DLCO, % of the predicted value (mean ±SD)	40.28 ±8.71	52.36 ±15.70	47.80 ±22.51	0.076
T1-T0 DLCO difference (mean ±SD)	-6.35 ±8.45$	-9.36 ±7.09	-17.8 ±12.98$	0.046

Table 2: differences among monocyte peripheral count. Data are presented in means ± standard deviations analysed by one-way ANOVA with Kruskal–Wallis test for multiple comparison. Significance level was considered p<0.05. * monocyte count <0.60 vs ≥0.95 x 10^9 cells/L: p=0.031, $p=0.016

In our cohort, we observed that patients with a monocyte count greater than 0.95 x 10^9 cells/L had a higher one-year FVC and DLCO reduction than those with a monocyte count lower than 0.60 x 10^9 cells/L.

Materials and methods:

Enrolment of patients

We prospectively enrolled 10 patients with a diagnosis of definite IPF, based on international guidelines [1], who accessed at Interstitial Lung Disease Ambulatory of Respiratory Disease Division of AOU Maggiore della Carità Hospital, after approval of the Research Protocol by the

Ethic Committee of Azienda Ospedaliera Maggiore della Carità, Novara (Prot. 264/CE), and informed written consent. All patients were naïve from an antifibrotic treatment. Enrolled patients must be suitable for the treatment with nintedanib and in particular they should have a FVC ≥50% and a DLCO ≥30%.

For each patient we recorded: demographics (age, gender, body mass index), comorbidities (i.e. cardiovascular, respiratory, oncologic, endocrinologic, nephrologic), pulmonary function test results (FVC, forced expiratory volume in the first second FEV1, total lung capacity TLC, and DLCO).

IPF diagnosis was on international guidelines cases [1].

For each patient we collected 40 mL of venous peripheral blood.

As control group, we enrolled 5 subjects who met subsequent criteria: never smoker, no past history of respiratory diseases (i.e. asthma, emphysema, chronic obstructive pulmonary disease), no chronic respiratory therapies or in treatment with steroids or immunosuppressant, no recent use of non-steroidal anti-inflammatory drugs, no pregnant women. Moreover, at the enrolment, they should be asymptomatic, without any respiratory symptoms.

Isolation and differentiation of monocytes

Human monocytes were isolated from IPF patients and healthy volunteers by standard technique of dextran sedimentation and Histopaque (density = 1.077 g/cm^3, Sigma-Aldrich, Milano, Italy), gradient centrifugation (400 x g, 30 minutes, room temperature) and recovered by fine suction and the interface, as previously described [37]. Purified monocytes populations were obtained by adhesion (90 min, 37°C, 5% CO2) in serum-free RPMI 1640 medium (Sigma-Aldrich) supplemented with 2 mM glutamine and antibiotics. Cell viability (trypan blue dye exclusion) was usually >98%. To differentiate monocytes into M1 macrophages, cells were cultured in 10% FBS-enriched medium with human (hr) GM-CSF (50 ng/mL) for 5 days, and then IFN-γ (20 ng/mL) and LPS (50 ng/mL) were added for an additional 24 h. To obtain M2 macrophages, monocytes were cultured in 10% FBS-enriched medium containing hrM-CSF (50 ng/mL) for 5 days, and then hrIL4, hrIL13 and hrIL10 (20 ng/mL) were added for an additional 24 h. Cell phenotype characterization was evaluated by the expression of specific surface marker CD86 and CD80 (M1) and CD206 and CD163 (M2). Cells were treated with nintedanib at different concentrations [35].

All experiment were performed in triplicate using cell isolated from each single subject.

Cell viability

To evaluate any potential toxicity of nintedanib in monocytes and monocyte-derived macrophages (MDM), cell viability was evaluated using the methylthiazolyldiphenyl-tetrazolium bromide (MTT) assay. Cells (1 x 10^4 cells) were treated for 2 and 12 h with nintedanib in a concentration range between 2.5 and 50 nM; then the medium was replaced by the MTT assay solution (1 mg/mL; 2 h, 37°C 5% CO_2; Sigma-Aldrich). The supernatant was removed and DMSO (Sigma-Aldrich) was added to dissolve the purple formazan; the absorbance was read at 580 and 675 nm [37].

Superoxide anion (O_2^-) production

500.000 cells (density 1 x 10^6 cells/ml) were treated for 1 h with nintedanib and then stimulated with PMA (Sigma-Aldrich) 1 µM for 30 minutes. PMA is a stimulus that induces a strong and significant respiratory burst via PKC activation [38]. PMA can be used to explore antinflammatory efficacy of any substance. Superoxide anion production was evaluated by the SOD-sensitive cytochrome C (CytC) reduction assay and expressed in nmol CytC reduced x 10^{-6} cell/30 min, using an extinction coefficient of 21.1 nM. To avoid interference with spectrophotometrical recordings, cells were incubated with RPMI 1640 without phenol red, antibiotics and FBS.

We also evaluated the percentage of cells producing O_2^- using the ROS/Superoxie Detection Assay Kit according to the manufacturer's instructions (AbCam, Cambridge, UK). Results were acquired and analysed by Attune NXT flow cytometer and software (life Technologies) and expressed as mean fluorescence intensity (MFI) and percentage of positive cells to O_2^- and ROS/RNS staining [37].

Flow cytometry analysis

Measurements of expression of surface markers was performed by analysed by Attune XT flowcytometer and software (life Technologies). Cells were treated with nintedanib 15 nM for 6 h. The following anti-body panels were used: FITC anti-CD16, FITC anti-CD80, PE anti-CD86, PE anti-CD163, PerCp anti-CD206 and APC anti-CD14. The monocyte and macrophage populations were defined as CD14+ cells. Data are expressed as number of CD16+, CD80+, CD86+, CD163+ or CD206+ cells over the number of CD14+ cells. CD80 and CD86 are M1-like markers, CD163 and CD 206 are M2-like markers. Monocyte populations were defined as: classical (CD14++CD16-), non-classical (CD14++CD16+) and intermediate (CD14+CD16+).

Statistical analysis

The data and statistical analysis comply with the recommendations on experimental design and analysis in pharmacology [39]. Statistical analysis was performed using GraphPad Prism 6 (GraphPad Software) and MedCalc (MedCalc Software Ltd). Data are expressed as mean ± SEM of 'n' independent experiments performed in triplicate. Different cell populations are expressed in percentages as appropriate. Statistical significance among different cell treatment was assessed by Student's paired t-test or one-way repeated measures ANOVA. Statistical significance was defined as $P < 0.05$.

Results:

Effects of nintedanib on cell viability:

To avoid possible confounding effects of cell toxicity, we firstly evaluated the effects of nintedanib on cell viability by using MTT assay. We started the cell viability test of monocytes at 150 nM and, after 24 hours, we observed that nintedanib induced toxicity and no cells were alive (data not shown). Therefore, monocytes and macrophages M1 and M2 from IPF patients and healthy donors were challenged with different concentrations of nintedanib (2.5 nM, 7.5 and 15 nM) for 2 and 12 hours. As shown in figure 6, nintedanib did not demonstrated cytotoxic effects (Figure 6).

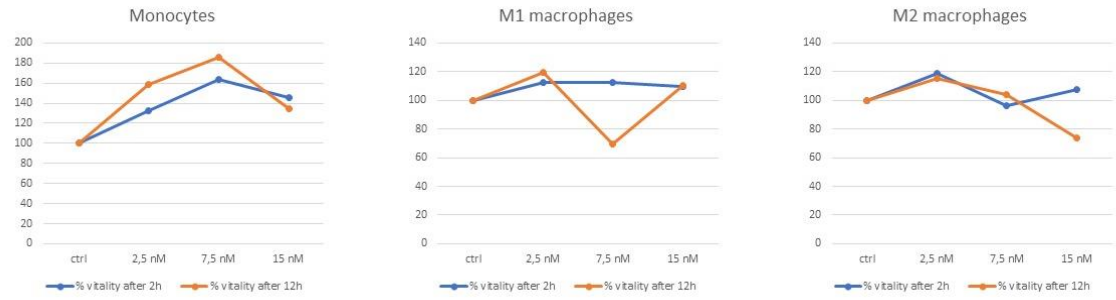

Figure 6: MTT assay for viability test on monocytes and monocyte-derived macrophages. Effects of increasing nintedanib concentrations on cell viability of monocytes and monocyte-derived macrophages M1 and M2. Data are means of triple independent experiments from distinct donors.

Effects of nintedanib on oxidative stress in monocytes, M1 and M2 macrophages:

Both monocytes and macrophages, as major phagocytes, release basal amounts of O_2^- that increase after stimulation. We analysed the effects of nintedanib on this parameter by evaluation of the nmol of reduced CytC in monocyte/macrophage from IPF patients and healthy donors.

In IPF patients we observed a higher basal superoxide production in monocytes (Figure 7A), in M1(Figure 7B) and M2 (Figure 7C) macrophages, as well as after PMA burst (Figure 7).

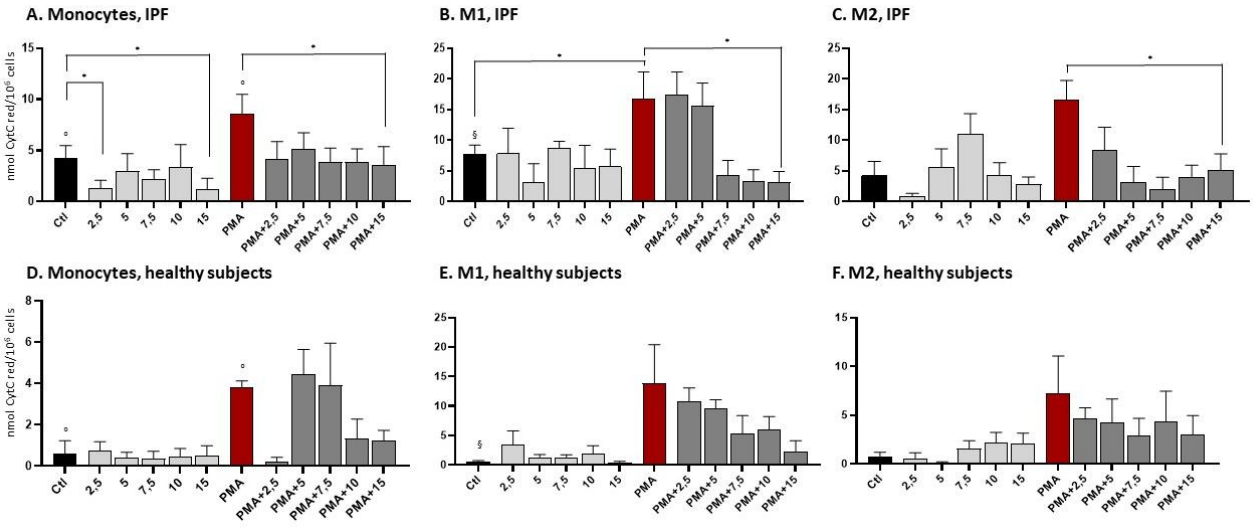

Figure 7. Effects of nintedanib on oxidative stress. Monocytes, M1 and M2 macrophages of IPF patients (A, B, C) and healthy subjects (D, E, F) were treated with nintedanib at different concentrations, in the presence and absence of PMA. Data are presented in mean ± S.E.M. on nmol CytC red/10^6 cells: in black basal production (Ctl) in light gray increasing nM doses of nintedanib, in red after PMA burst and in dark gray PMA plus increasing nM doses of nintedanib. Ctl of IPF *vs* healthy subjects (°, $p<0.05$), PMA stimulus of IPF *vs* healthy subjects (°, $p<0.05$); Ctl of IPF M1 macrophages vs M1 of healthy subjects (§, $p<0.05$); IPF patients Ctl *vs* different nM nintedanib doses and PMA *vs* PMA + 15 nM nintedanib (*, $p<0.05$). Data are results of triple independent experiments from distinct donors.

As shown in figure 7, basal O_2^- production from unstimulated monocytes (controls, ctl) isolated from patients (figure 7A), macrophages M1 (Figure 7B) and M2 (figure 7C) was about 4-fold higher than the respective cells from healthy donors (figure 7D, 7E and 7F). Interestingly, nintedanib at any concentrations affected basal O_2^- production both in monocytes from patients and healthy donors. In particular, nintedanib at 2.5nM and 1.5 nM significantly reduced the basal O_2 production in monocytes from patients by 77.3% and -77.9%, respectively (Figure 7A). Treatment of cell with PMA 1 µM for 30 minutes induced a double increase in the basal O_2^- production (+72.7%) both in monocytes from patients and healthy donors, that nintedanib reverted in a dose-dependent way.

In M1 macrophages, we did not observe significant effects of ninentedanib on basal O_2^- production in either patients or controls (Figure 7B and C). After PMA burst, we observed a significant increase of reduced Cytc production that nintedanib reduced in a dose dependent manner.

In M2 macrophages of patients (Figure 7C) nintedanib induced an increase of basal production and the effects was bell-shaped with a peak at 7.5nM but not significant, while in M2 macrophages from healthy donors (Figure 7F), nintedanib showed dose-dependent increase but not significant. The PMA burst induced an increase of superoxide production, significant in the patient cells. Nintedanib reduced the PMA-induced O_2^- production with a significant effect at the highest concentration in M2 macrophages patients.

We then evaluated the PMA-induced burst responsiveness in monocytes (Figure 8A) macrophages M1 (Figure 8B) and M2 (figure 8C) from patients via FACS analysis.

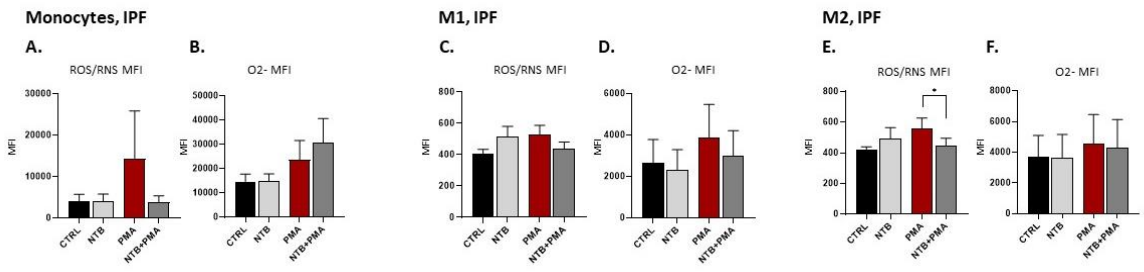

Figure 8. Effects of nintedanib on oxidative stress expressed as mean fluorescence intensity with FACS analysis. In black basal (Ctrl), in light gray after 15 nM of nintedanib, in red after PMA burst, in dark gray PMA plus 15 nM of nintedanib. Data are expressed in means ± S.E.M. of three independent experiments from distinct donors, analysed by t-test. Significance levels: * $p<0.05$ PMA vs PMA + 15 nM nintedanib in M2 macrophages of IPF patients.

As shown in figure 8, in monocytes and in M1 we did not observe a reduction of O_2^- nor ROS/RNS MFI levels after introduction of nintedanib (Figure 8 A, B, C, D). In M2 macrophages the introduction of nintedanib after the PMA stimulus brought ROS/RNS MFI levels to basal ones (-14.4%, p=0.034) (Figure 8E).

Effects of nintedanib on monocyte populations in IPF patient and healthy patients:

As specified above, monocyte populations were defined as: classical (CD14++CD16-), non-classical (CD14++CD16+) and intermediate (CD14+CD16+). Compared to healthy donors (Figure 9A), the most prominent population of monocytes is the CD14++CD16- (Figure 9B). Interestingly,

nintedanib induced a decrease of monocytes CD14++CD16+ in IPF patients (Figure 9B) while it did not show effects on monocytes from healthy donors (Figure 9A).

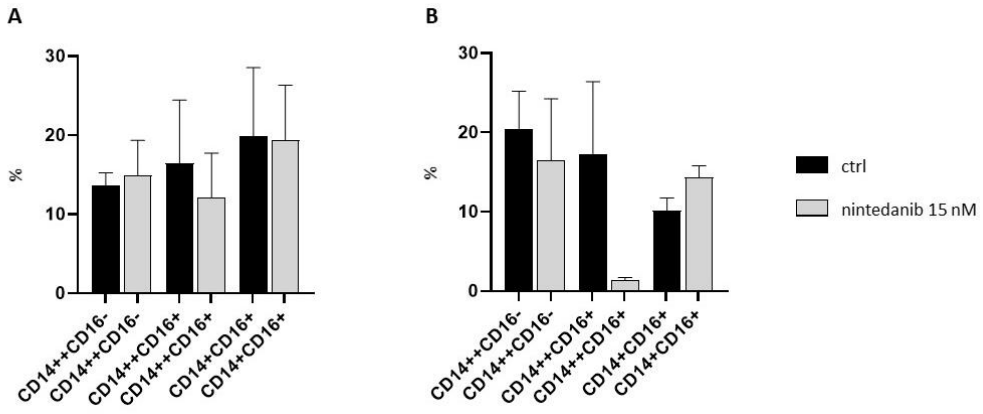

Figure 9. Effects of nintedanib on monocyte populations in healthy subjects (A) and IPF patients (B). Data are expressed in means ± S.E.M. of of three independent experiments of different monocyte populations' percentages: in black basal (ctrl) and light gray after stimulation with 15 nM of nintedanib.

Effects of nintedanib on surface markers expression in macrophages from IPF patients and healthy donors:

We then evaluated the effect of nintedanib on macrophage polarization analysing the specific surface markers for M1 and M2 phenotype. As shown in Figure 10, the percentage of cells expressing CD80 and CD86 is very similar between healthy donors (Figure 10A) and IPF patients (Figure 10B) with an interesting difference regarding the expression of CD206, that is higher in the M1 macrophage of patients ($p<0.05$). Treatment of M1 macrophages with nintedanib did not affect surface marker expression in either healthy donors or patients, apart from a slight reduction in CD80 and CD86. Regarding the M2 macrophages group, there are not important differences between healthy donors (Figure 10C) and patients (Figure 10D), apart a major expression of CD80 in the M2 macrophages from patients. Interestingly, nintedanib induced a significant reduction of CD206 expression (-14.2%) in M2 population of the IPF patients.

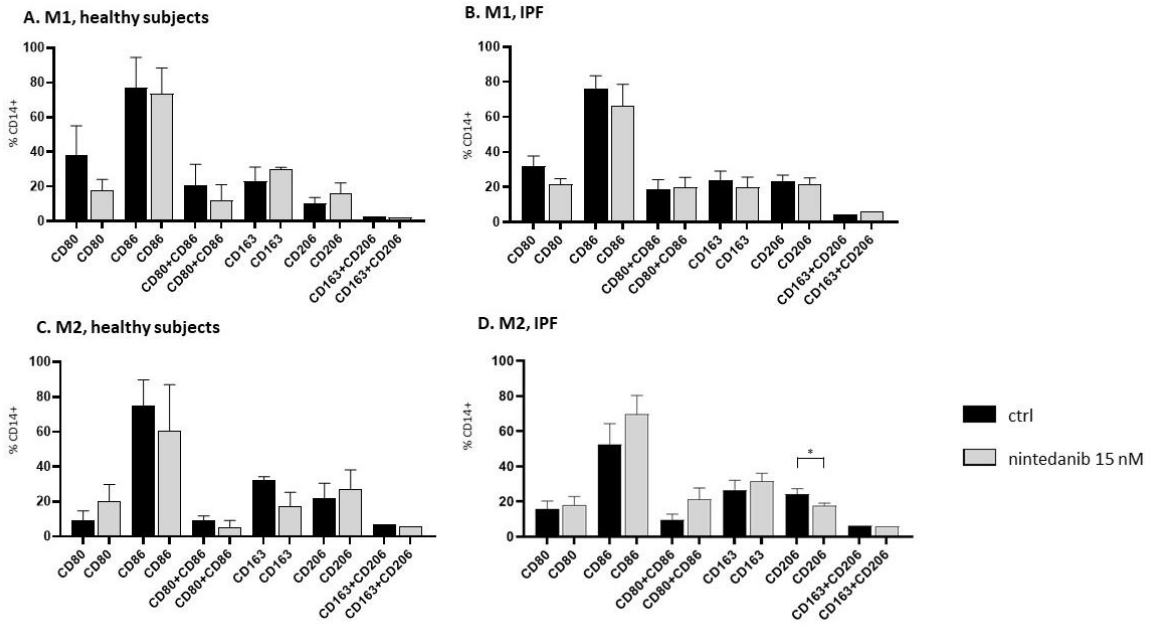

Figure 10. Effects of nintedanib on macrophage populations in healthy subjects and IPF patients. Data are expressed in means (± S.E.M.) of three independent experiments of percentage CD14 positive cells: in black basal (ctrl) and light gray after stimulation with 15 nM of nintedanib. Data were analysed using t-test. Significance levels: * $p<0.05$ CD206 pre and post nintedanib stimulation.

Discussion

In literature there is growing evidence that monocyte play an important role in predicting a poorer outcome in IPF patients [23]. In our historical cohort of patient with IPF we demonstrated an inverse correlation between monocyte count, FVC and DLCO and that patients with a higher one-year functional loss (both FVC and DLCO) had a higher basal monocyte count (data not published). This result is in line with *Kreuter* et al. study [26]. These observations established the basis for the evaluation of nintedanib effects on peripheral monocyte and monocyte-derived macrophages. Nintedanib highest blood concentrations in IPF patients were about 70 nM after a steady-state dosing of two times 150 mg per day [40]: the mean concentrations at steady state measured for each nintedanib concentrations were evaluated in patients who were assuming nintedanib, but the concentrations were halved in case of 100 mg twice daily. *Bellarmi* et al. [35] demonstrated that nintedanib at 10-1000 nM concentration inhibited the phosphorylation of CSF1R and downstream signalling pathways induced by CSF1 in human macrophages. This result led us to perform the viability test at 150 nM but we observed that after 12 hours nintedanib induced toxicity in all cells. Therefore, for the rest of experiments, we used concentrations increasing up to the highest of 15nM at which cells were all alive after 12 hours. This is probably due to the different protocol used

Several evidence demonstrate the effects of nintedanib on monocytes but the majority of them evaluated the effects on specific grow factor receptors expression (i.e. PDGFR, VEGFR) [34]. We firstly reported the effects of nintendanib on monocytes superoxide anion production and their polarization in IPF patients. We demonstrated that in monocytes the stimulation with nintedanib reduce the basal production of oxidative stress measured in nmol of Cytc reduced. Interestingly, at 15 nM of nintedanib, the production of oxidative stress in IPF patients is very similar to the production in healthy volunteers. These results could build the basis to verify it the monocyte production of oxidative stress would influence phenotype macrophages polarization. In fact, it has long been recognized that depletion of circulating monocytes (e.g., using Ccr2−/− mice or via the systemic administration of liposomal clodronate) ameliorates fibrosis severity in the lung and other organs [41]. To explain these findings, investigators have suggested that during injury, monocytes rapidly differentiate into monocyte-derived alveolar macrophages and they are polarized toward a profibrotic or M2 phenotype in the fibrotic lung. This macrophage polarization model is based on limited evidence and is conceptually incomplete [41].

Non classical monocytes are associated with wound healing process, and they have an opposite function to classical monocytes, promoting neutrophil adhesion and endothelial interface via secretion of TNFα [19, 20]. Non classical monocytes in our cohort of IPF patients were highly present, confirming their role in wound heling process. After the treatment with nintedanib we observed a great reduction of non classical monocytes percentage, with a relative reduction of classical monocytes. This is in line with the effects of nintedanib in IPF patients. Moreover, classical monocyte count was demonstrated to be a prognostic marker of mortality in IPF patients [21] and our result is in line with nintedanib effects on lung fibrosis and mortality of patients.

In patients with interstitial lung diseases (ILDs) PMA induces phagocytes to secrete myeloperoxidase (MPO) and activates their membrane-bound NADPH oxidase, thus generating superoxide anion, which subsequently dismutates into H_2O_2, a substrate for MPO [42]. Moreover, oxidative stress values were significantly higher in IPF patients with acute exacerbation than in those with stable disease, with an inverse correlation with FVC and DLCO [43]. Up to now, no studies evaluated the effects of nintedanib on monocyte-derived macrophages M1 and M2 from IPF patients. In our cohort nintedanib did not significantly affect the basal O_2^- production in M1 neither in M2, but it reduced in a dose dependent manner the PMA-induced burst in both macrophage populations. This result possibly supports the effects of nintedanib in reducing the risk of acute exacerbations [44]. Moreover, it has been previously demonstrated an affect of nintedanib in reducing the concentration of several systemic circulating markers of oxidative stress [45].

Alternatively activated M2 macrophages were demonstrated to be present in fibrotic lesions of IPF patients, producing high amount of pro-inflammatory and pro-fibrotic cytokines (i.e. IL-10, IL-6, TNF-α, and TGF-β1) [46, 47]. Among surface markers of M2 cells, CD206 is demonstrated to exert important function in the phagocytosis by increasing efferocytosis of invading pathogens and apoptotic cells [12]. *Huang* et al. demonstrated, in a murine model of systemic sclerosis, that nintedanib reduced M2 counts with suppression of the expression levels of CD206 [33]. Interestingly, we observed a reduction of CD206 expression in M2 macrophages of IPF subjects after nintedanib stimulation. Our results therefore seem to support the antifibrotic effects of nintedanib also by reduction of CD206 profibrotic marker expression by M2 cells.

Our study has several limitations. First, the number of subjects included in the analysis cannot allow us to draw firm conclusions; however, we observe a clear trend in the effects of nintedanib on the reduction of oxidative stress in both monocytes and macrophages and the effects on the expression of M2 cell surface markers. The increase in the number of patients with IPF and of healthy subjects will be crucial to better define the immunomodulatory effects of nintedanib. We don't know if these results are reproducible in alveolar macrophages of IPF patients, which are one of the terminal effectors of fibrosis deposition. The lung environment would play an important role on these cells, influencing their polarization as well as the effects of the drug. For this reason, we are collecting specimens of BAL of IPF patients, but their number is too small to draw any conclusion. Finally, we did not explore the production of pro-inflammatory and pro-fibrotic cytokines produced by monocytes and monocyte-derived peripheral macrophages: the quantification of these mediators would add some important information about the effects induced by nintedanib.

In conclusion, we firstly reported the effects on oxidative stress and cells polarization of nintedanib on monocytes and monocyte-derived macrophages in IPF patients; nintedanib significantly reduced the oxidative stress produced by monocytes and restore basal release of O_2^- in M1 and M2 macrophages. Moreover, nintedanib reduce non-classical monocytes and pro-fibrotic surface marker expressed by M2 macrophages, both significantly involved in wound healing in IPF.

References:

1. Raghu G, Remy-Jardin M, Myers JL, Richeldi L, Ryerson CJ, Lederer DJ, et al. Diagnosis of Idiopathic Pulmonary Fibrosis. An Official ATS/ERS/JRS/ALAT Clinical Practice Guideline. Am J Respir Crit Care Med. 2018 Sep 1;198(5):e44-e68. Navaratnam V, Fleming KM, West J,

Smith CJ, Jenkins RG, Fogarty A, et al. The rising incidence of idiopathic pulmonary fibrosis in the U.K. Thorax. 2011 Jun;66(6):462-7.

2. Homer RJ, Elias JA, Lee CG, Herzog E. Modern concepts on the role of inflammation in pulmonary fibrosis. Arch Pathol Lab Med. 2011 Jun;135(6):780-8.

3. Naik PK, Moore BB. Viral infection and aging as cofactors for the development of pulmonary fibrosis. Expert Rev Respir Med. 2010;4(6):759.

4. Snider GL. Interstitial pulmonary fibrosis. Chest. 1986;89(3 Suppl):115S.

5. Reynolds HY, Fulmer JD, Kazmierowski JA, Roberts WC, Frank MM, Crystal RG. Analysis of cellular and protein content of broncho-alveolar lavage fluid from patients with idiopathic pulmonary fibrosis and chronic hypersensitivity pneumonitis. J Clin Invest. 1977;59(1):165.

6. Degryse AL, Lawson WE. Progress toward improving animal models for idiopathic pulmonary fibrosis. Am J Med Sci. 2011;341(6):444.

7. Davies LC, Jenkins SJ, Allen JE, Taylor PR. Tissue-resident macrophages. Nat Immunol. 2013 Oct;14(10):986-95.

8. Sica A, Mantovani A. Macrophage plasticity and polarization: in vivo veritas. J Clin Invest. 2012 Mar;122(3):787-95.

9. Saccani A, Schioppa T, Porta C, Biswas SK, Nebuloni M, Vago L, et al. p50 nuclear factor-kappaB overexpression in tumor-associated macrophages inhibits M1 inflammatory responses and antitumor resistance. Cancer Res. 2006 Dec 1;66(23):11432-40.

10. Guiducci C, Vicari AP, Sangaletti S, Trinchieri G, Colombo MP. Redirecting in vivo elicited tumor infiltrating macrophages and dendritic cells towards tumor rejection. Cancer Res. 2005;65(8):3437–3446.

11. Martinez FO, Helming L, Gordon S. Alternative activation of macrophages: an immunologic functional perspective. Annu Rev Immunol. 2009;27:451–483.

12. Zhang L, Wang Y, Wu G, Xiong W, Gu W, Wang CY. Macrophages: friend or foe in idiopathic pulmonary fibrosis? Respir Res. 2018 Sep 6;19(1):170.

13. Sierra-Filardi E, Vega MA, Sanchez-Mateos P, Corbi AL, Puig-Kroger A. Heme Oxygenase-1 expression in M-CSF-polarized M2 macrophages contributes to LPS-induced IL-10 release. Immunobiology. 2010;215:788–95.

14. Gibbons MA, MacKinnon AC, Ramachandran P, Dhaliwal K, Duffin R, Phythian-Adams AT, et al. Ly6Chi monocytes direct alternatively activated profibrotic macrophage regulation of lung fibrosis. Am J Respir Crit Care Med. 2011;184:569–81.

15. Xiang GA, Zhang YD, Su CC, Ma YQ, Li YM, Zhou X, et al. Dynamic changes of mononuclear phagocytes in circulating, pulmonary alveolar and interstitial compartments in a mouse model of experimental silicosis. Inhal Toxicol. 2016;28:393–402.

16. Zhong B, Yang X, Sun Q, Liu L, Lan X, Tian J, et al. Pdcd4 modulates markers of macrophage alternative activation and airway remodeling in antigen-induced pulmonary inflammation. J Leukoc Biol. 2014;96:1065–75.

17. Kapellos TS, Bonaguro L, Gemünd I, Reusch N, Saglam A, Hinkley ER, et al. Human Monocyte Subsets and Phenotypes in Major Chronic Inflammatory Diseases. Front Immunol. 2019 Aug 30;10:2035.

18. Patel AA, Zhang Y, Fullerton JN, Boelen L, Rongvaux A,Maini AA, et al. The fate and lifespan of human monocyte subsets in steady state and systemic inflammation. J Exp Med. 2017 Jul 3;214(7):1913-1923.

19. Chimen M, Yates CM, McGettrick HM, Ward LSC, Harrison MJ, Apta B, et al. Monocyte Subsets Coregulate Inflammatory Responses by Integrated Signaling through TNF and IL-6 at the Endothelial Cell Interface. J Immunol. 2017 Apr 1;198(7):2834-2843.

20. Scott MKD, Quinn K, Li Q, Carroll R, Warsinske H, Vallania F, et al. Increased monocyte count as a cellular biomarker for poor outcomes in fibrotic diseases: a retrospective, multicentre cohort study. Lancet Respir Med. 2019 Jun;7(6):497-508.

21. Fraser E, Denney L, Antanaviciute A, Blirando K, Vuppusetty C, Zheng Y, et al. Multi-Modal Characterization of Monocytes in Idiopathic Pulmonary Fibrosis Reveals a Primed Type I Interferon Immune Phenotype. Front Immunol. 2021 Mar 5;12:623430.

22. Broekelmann TJ, Limper AH, Colby TV, McDonald JA. Transforming growth factor beta 1 is present at sites of extracellular matrix gene expression in human pulmonary fibrosis. Proc Natl Acad Sci USA. 1991;88:6642–6646.

23. Scott MKD, Quinn K, Li Q, Carroll R, Warsinske H, Vallania F, Chen S, et al. Increased monocyte count as a cellular biomarker for poor outcomes in fibrotic diseases: a retrospective, multicentre cohort study. Lancet Respir Med. 2019 Jun;7(6):497-508.

24. Scott CL, Henri S, Guilliams M. Mononuclear phagocytes of the intestine, the skin, and the lung. Immunol Rev. 2014;262:9–24.

25. Liu YZ, Saito S, Morris GF, Miller CA 3rd, Li J, Lefante JJ. Proportions of resting memory T cells and monocytes in blood have prognostic significance in idiopathic pulmonary fibrosis. Genomics. 2019 Dec;111(6):1343-1350.

26. Kreuter M, Lee JS, Tzouvelekis A, Oldham JM, Molyneaux PL, Weycker D, et al. Monocyte Count as a Prognostic Biomarker in Patients with Idiopathic Pulmonary Fibrosis. Am J Respir Crit Care Med. 2021 Jul 1;204(1):74-81.

27. Kawamura K, Ichikado K, Anan K, Yasuda Y, Sekido Y, Suga M, et al. Monocyte count and the risk for acute exacerbation of fibrosing interstitial lung disease: A retrospective cohort study. Chron Respir Dis. 2020 Jan-Dec;17:1479973120909840.

28. Byrne AJ, Maher TM, Lloyd CM. Pulmonary Macrophages: A New Therapeutic Pathway in Fibrosing Lung Disease? Trends Mol Med. 2016 Apr;22(4):303-316.

29. Fois AG, Paliogiannis P, Sotgia S, Mangoni AA, Zinellu E, Pirina P, et al. Evaluation of oxidative stress biomarkers in idiopathic pulmonary fibrosis and therapeutic applications: a systematic review. Respir Res. 2018 Mar 27;19(1):51.

30. Hilberg F, Roth GJ, Krssak M, Kautschitsch S, Sommergruber W, Tontsch-Grunt U, et al. BIBF 1120: triple angiokinase inhibitor with sustained receptor blockade and good antitumor efficacy. Cancer Res 2008; 68: 4774–4782.

31. Hilberg F, Tontsch-Grunt U, Baum A, Le AT, Doebele RC, Lieb S, et al. Triple angiokinase inhibitor nintedanib directly inhibits tumor cell growth and induces tumor shrinkage via blocking oncogenic receptor tyrosine kinases. J Pharmacol Exp Ther 2018; 364: 494–503.

32. Wollin L, Wex E, Pautsch A, Schnapp G, Hostettler KE, Stowasser S, et al. Mode of action of nintedanib in the treatment of idiopathic pulmonary fibrosis. Eur Respir J. 2015 May;45(5):1434-45.

33. Huang J, Maier C, Zhang Y, Soare A, Dees C, Beyer C, et al. Nintedanib inhibits macrophage activation and ameliorates vascular and fibrotic manifestations in the Fra2 mouse model of systemic sclerosis. Ann Rheum Dis. 2017 Nov;76(11):1941-1948.

34. Sato S, Shinohara S, Hayashi S, Morizumi S, Abe S, Okazaki H, et al. Anti-fibrotic efficacy of nintedanib in pulmonary fibrosis via the inhibition of fibrocyte activity. Respir Res. 2017 Sep 15;18(1):172.

35. Bellamri N, Morzadec C, Joannes A, Lecureur V, Wollin L, Jouneau S, et al. Alteration of human macrophage phenotypes by the anti-fibrotic drug nintedanib. Int Immunopharmacol. 2019 Jul;72:112-123.

36. Richeldi L, Costabel U, Selman M, Kim DS, Hansell DM, Nicholson AG, et al. Efficacy of a tyrosine kinase inhibitor in idiopathic pulmonary fibrosis. N Engl J Med. 2011 Sep 22;365(12):1079-87.

37. Talmon M, Rossi S, Pastore A, Cattaneo CI, Brunelleschi S, Fresu LG. Vortioxetine exerts anti-inflammatory and immunomodulatory effects on human monocytes/macrophages. Br J Pharmacol. 2018 Jan;175(1):113-124.

38. Myers MA, McPhail LC, Snyderman R. Redistribution of protein kinase C activity in human monocytes: correlation with activation of the respiratory burst. J Immunol. 1985 Nov;135(5):3411-6.

39. Curtis MJ, Bond RA, Spina D, Ahluwalia A, Alexander SP, Giembycz MA, et al. Experimental design and analysis and their reporting: new guidance for publication in BJP. Br J Pharmacol. 2015 Jul;172(14):3461-71.

40. Ogura T, Taniguchi H, Azuma A, Inoue Y, Kondoh Y, Hasegawa Y, et al. Safety and pharmacokinetics of nintedanib and pirfenidone in idiopathic pulmonary fibrosis. Eur Respir J. 2015 May;45(5):1382-92.

41. Misharin AV, Morales-Nebreda L, Reyfman PA, Cuda CM, Walter JM, McQuattie-Pimentel AC, et al. Monocyte-derived alveolar macrophages drive lung fibrosis and persist in the lung over the life span. J Exp Med. 2017;214:2387–404.

42. Pennathur S, Vivekanandan-Giri A, Locy ML, Kulkarni T, Zhi D, Zeng L, et al. Oxidative Modifications of Protein Tyrosyl Residues Are Increased in Plasma of Human Subjects with Interstitial Lung Disease. Am J Respir Crit Care Med. 2016 Apr 15;193(8):861-8.

43. Matsuzawa Y, Kawashima T, Kuwabara R, Hayakawa S, Irie T, Yoshida T, et al. Change in serum marker of oxidative stress in the progression of idiopathic pulmonary fibrosis. Pulm Pharmacol Ther. 2015 Jun;32:1-6.

44. Crestani B, Huggins JT, Kaye M, Costabel U, Glaspole I, Ogura T, et al. Long-term safety and tolerability of nintedanib in patients with idiopathic pulmonary fibrosis: results from the open-label extension study, INPULSIS-ON. Lancet Respir Med. 2019 Jan;7(1):60-68.

45. Fois AG, Sotgiu E, Scano V, Negri S, Mellino S, Zinellu E, et al. Effects of Pirfenidone and Nintedanib on Markers of Systemic Oxidative Stress and Inflammation in Patients with Idiopathic Pulmonary Fibrosis: A Preliminary Report. Antioxidants (Basel). 2020 Oct 30;9(11):1064.

46. Lodyga M, Cambridge E, Karvonen HM, Pakshir P, Wu B, Boo S, et al. Cadherin-11-mediated adhesion of macrophages to myofibroblasts establishes a profibrotic niche of active TGF-beta. Sci Signal 2019: 12(564).

47. Novak ML, Koh TJ. Macrophage phenotypes during tissue repair. J Leukoc Biol 2013: 93(6): 875-881.

Title: Use of Remote Dielectric Sensing (ReDS™) in patients with idiopathic pulmonary fibrosis: correlation with clinical, radiological and pulmonary functional parameters.

Background:

Idiopathic pulmonary fibrosis (IPF) is the most common idiopathic interstitial pneumonia and at histopathologic examination presents features of usual interstitial pneumonia (UIP) [1]. IPF causes worsening dyspnoea and progressive loss of pulmonary function with a median survival time of approximately 3-5 years [1, 2].

Pulmonary function tests (PFT) and high-resolution CT (HRCT) are fundamental for the diagnosis of IPF. Typical UIP pattern on HRCT is defined by the presence of honeycombing and reticular opacities, with or without traction bronchiectasis, in subpleural and basal predominance in both lungs. The presence of typical UIP patterns on HRCT is sufficient for the diagnosis of IPF in the appropriate clinical setting. Moreover, HRCT can be used to evaluate the extent of IPF and its radiological progression [1].

IPF is characterized by a spirometric functional restrictive pattern, defined by a reduction of total lung capacity (TLC); nevertheless, due to its reproducibility, forced vital capacity (FVC) has been used as the standard spirometric measure of pulmonary function in IPF for many decades. Longitudinal change in serial measures of lung volume (either FVC or vital capacity) is a widely accepted reflection of disease progression in patients with IPF and a commonly used primary endpoint in therapeutic studies in IPF [3]. Forced vital capacity (FVC) is generally accepted as a reliable and valid measure of clinical status in patients with IPF [1]; it is often obtained and followed as a surrogate of disease severity and progression in clinical practice and research, though does not appear to either correlate with any specific radiological feature or present CT pattern [3].

Lung volumes determined by functional respiratory imaging directly correlate with FVC as their relative changes: loss of lobe volumes, increase of fibrotic tissue and airway radius measured at TLC correlated with changes in FVC, but these changes already occur in the lower lobes when FVC is still within normal limits [4].

In lung fibrosis CT measurements, including densitometric measures, quantitative interstitial score, quantitative honeycombing measure and visual fibrosis score were strongly correlated with both FVC and diffusion lung capacity for carbon monoxide (DLCO): in particular, there is an inverse correlation between quantitative densitometry of lung and FVC (measured with lung attenuation and percent high attenuating area) as well as percentage of fibrosis (inverse correlation between

fibrosis score and FVC) [5]. However, Park et al. showed the absence of correlation between FVC and 'consistent' UIP CT pattern. This was not the case with DLCO where inverse correlation was seen [1].

Even if the ability to identify IPF in chest CT is well known, the availability and radiation limitations make it unsuitable for serial assessment of lung content. This is the reason why it is important to develop new non-invasive, reproducible and easy-to-use technologies.

Remote Dielectric Sensing (ReDS™) technology (Sensible Medical Innovations Ltd. Kfar Neter, Israel) measures the dielectric properties of tissues, quantifying the content of fluids inside the scan volume. Low power electro-magnetic signals are emitted across the thorax through the lung and the characteristics of the signals received after passing through the tissue are related to their dielectric properties, which are mostly determined by the lung's fluid content [6]. The dielectric property of biological tissue is a basic biophysical parameter [7]: they change mainly with the amount of air, blood and parenchyma and the air content can be described by the measured end derived filling factor, F [6, 7]. The dielectric coefficient of a material is represented by a frequency-dependent number describing its interactions with electromagnetic energy, including absorption, reflection and transmission of the energy. The dielectric coefficient of the intact lung is very sensitive to the ratio between volumes of air and water, thus this number is a direct indicator of fluid concentration [7] (Figure 1).

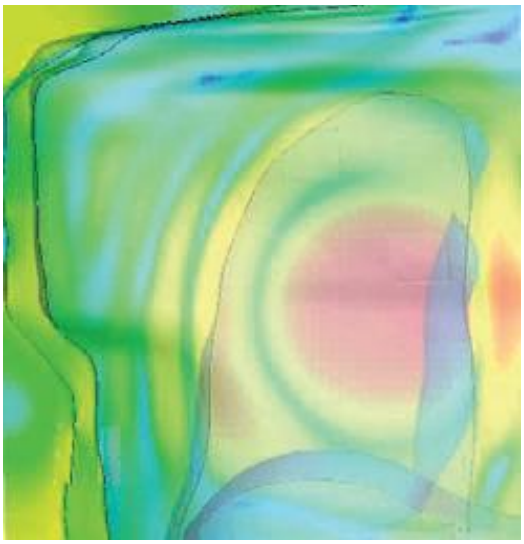

Figure 1. An example of region of interest size and location (color-coded red) as calculated by an electromagnetic simulation tool

In lung fibrosis, the volume of air is reduced while the tissue volume is increased compared to a normal lung; we also know that the more fibrosis increases, the more FVC, TLC and DLCO are reduced because FVC and TLC are proportional to fibrosis [2].

Amir et al. provided a direct validation of the accuracy of ReDS™ when compared to CT in patients with acute and chronic congestive heart failure: the authors demonstrated that ReDS™ and CT have comparable accuracy to determine fluid content variations with an absolute difference in measurements between the two methods of 3.75% [6].

Given the proven correlation between CT and ReDS™, we aimed to investigate the/a possible correlation of ReDS™ score and clinical, radiological and functional measures in patients with IPF.

Methods:

Study population

We conducted a single centre prospective observational study, including all consecutive patients with a definitive diagnosis of IPF, followed at Interstitial Lung Diseases Ambulatory of Maggiore della Carità Hospital, Novara, a middle-size teaching hospital in the North-West of Italy. Recruitment period started at 1st September 2021 and finished at 30th November 2021. This study was conducted in accordance with STROBE statement for observational cohort studies [8].

We included all patients with a definitive diagnosis of IPF based on international guidelines [9] and who signed the specific information consent form. We excluded those patients who had a previous history of pulmonary arterial hypertension (primitive or secondary to the pulmonary disease), congestive heart failure and those who were not able to perform the spirometric evaluation at the moment of the ReDS™ measure.

For each patient we recorded: demographics (age, gender, height and weight), CT pattern (UIP definite, UIP probable, UIP indeterminate), dyspnoea score measured with mMRC scale and respiratory functional data. In particular we measured: FVC (in L/min and %predicted value), vital capacity (VC, in L/min and %predicted value), forced expiratory volume in the first second (FEV1, in L/min and %predicted value), FEV1/FVC (in %), FEV1/VC (in %), peak expiratory flow (PEF, in L/s), TLC (in L and %predicted value), DLCO (in ml/min/mmHg and %predicted value), alveolar volume (AV, in liters) and DLCO/AV (in ml/min/mmHg/L and %predicted value).

Each patient, at the enrolment time, underwent ReDS™ measurement; ReDS™ Wearable System (Sensible Medical Innovations Ltd., Netanya, Israel) is composed by two sensors integrated in a

wearable vest which is applied to the thorax of the patient. After having wear it, the two sensor are located on the front and back of the thorax without the need for direct contact skin. The measurement starts when the upfront sensor inflates and last for nearly 60 seconds after which the results is displayed on ReDS™ screen (Figure 2).

Figure 2. Instructions on ReDS™ use and illustration of the ReDS™ technology.

The two sensors analyze signal that reflects dielectric proprieties of the section of the lung interposed between the two sensors; as specified above, dielectric coefficient of a material is represented by a frequency-dependent number describing its interactions with electromagnetic energy, including absorption, reflection and transmission of the energy. Water has a high dielectric coefficient and dielectric coefficients of tissues are determined mainly by their fluid content. In particular, the dielectric coefficient of pulmonary tissue is determined by the dielectric coefficient of its components (air, blood, parenchyma) and their relative concentrations. In normal conditions, it is accepted that lung is primarily composed of air and water components: the dielectric coefficient of the intact lung is very sensitive to the ratio between the volumes of air and water, thus this number is a direct indicator of fluid concentration [6]. The measure result is reported as percentage of fluid content in the scan volume: derived from its clinical validation use, ReDS™ score normality ranges between 20 and 35% [10].

Statistical methods

Categorical variables are presented as absolute value and percentage, while for continuous ones we reported mean ± SD or median and interquartile range [IQR], as appropriate. Statistical comparison

between different groups were made with Student's t test. Correlation between functional parameters or clinical continuous variables and ReDS™ results were calculated using Pearson correlation coefficient. A two-tailed test was considered for the hypothesis testing procedure and statistically significant values were considered to reach a P value <0.05. Statistical analysis was performed using MedCalc (MedCalc Software Ltd, Belgium).

Results:

We included in our analysis results of 41 measurements of 41 consecutive patients whose characteristics are reported in Table 1 (Table 1). Restrictive defect was moderate (TLC 56.92%) with a moderate reduction of DLCO (40.63%) and FVC was mildly reduced (75.92%). Mean measured ReDS™ score was 33.32%

Table 1. Characteristics of included subjects.

	N (%)
Number of subjects	41
Age (in years ±SD)	75.27 ± 5.53
Gender Male / Female	35 (85.36%) / 6 (14.64%)
UIP CT pattern • Definite • Probable	 29 (70.73%) 12 (29.27%)
Dyspnea scale mMRC	2.14 ± 0.76
FVC (L/min)	2.73 ± 0.82
FVC %	75.92 ± 18.79
VC (L/min)	2.78 ± 0.83
VC %	77.21 ± 18.86
FEV1 (L/min)	2.23 ± 0.66
FEV1 %	82.41 ± 20.05
FEV1/FVC	82.03 ± 8.01
FEV1/VC %	87.24 ±12.91
TLC (L)	3.64 ± 0.97
TLC %	56.92 ± 12.51

DLCO (ml/min/mmHg)	9.68 ± 3.82
DLCO %	40.63 ± 14.82
AV (L)	3.43 ± 1.05
AV %	58.13 ± 15.98
DLCO/AV (ml/min/mmHg/L)	2.89 ± 1.02
DLCO/AV %	70.51 ± 18.14
ReDS™ score %	33.32 ± 5.85

We observed an inverse correlation between ReDS™ score and FVC%, VC%, TLC, TLC%, DLCO, DLCO%, AV and AV%; strongest correlation was observed with FVC% (R = -0.4029), VC% (R = -0.4302), TLC% (R = -0.5060) and DLCO% (R = -0.4346). On the other hand, we observed a direct correlation between ReDS™ score and FEV1/FVC and mMRC score whose correlations were respectively R = 0.3832 and R = 0.4720 (Table 2 and Figure 3).

Table 2. All IPF patients: clinical and functional correlations.

	R	95% IC	p
FVC	-0.2401	-0.5101 to 0.0729	0.1305
FVC%	**-0.4029**	**-0.6322 to -0.1087**	**0.0090**
VC	-0.2639	-0.5286 to 0.0476	0.0955
VC%	**-0.4302**	**-0.6516 to -0.1413**	**0.0050**
FEV1	-0.1222	-0.4143 to 0.1927	0.4465
FEV1%	-0.2702	-0.5335 to 0.0408	0.0875
FEV1/FVC	**0.3832**	**0.0856 to 0.6180**	**0.0134**
FEV1/VC	0.2277	-0.0859 to 0.5003	0.2277
TLC	**-0.3363**	**-0.5836 to 0.0319**	**0.0316**
TLC%	**-0.5060**	**-0.7040 to -0.2349**	**0.0007**
DLCO	**-0.3453**	**-0.5902 to -0.0421**	**0.0270**
DLCO%	**-0.4346**	**-0.6547 to -0.1466**	**0.0045**
DLCO/AV	-0.0385	-0.3422 to 0.2723	0.8109
DLCO/AV%	-0.1815	-0.4633 to 0.1336	0.2562
AV	**-0.3542**	**-0.5968 to -0.0522**	**0.0231**
AV%	**-0.4049**	**-0.6336 to -0.1111**	**0.0086**
Dyspnoea mMRC	**0.4720**	**0.1923 to 0.6808**	**0.0018**
Height	0.1622	-0.1531 to 0.4475	0.3111

Weight	0.1097	-0.2049 to 0.4037	0.4948

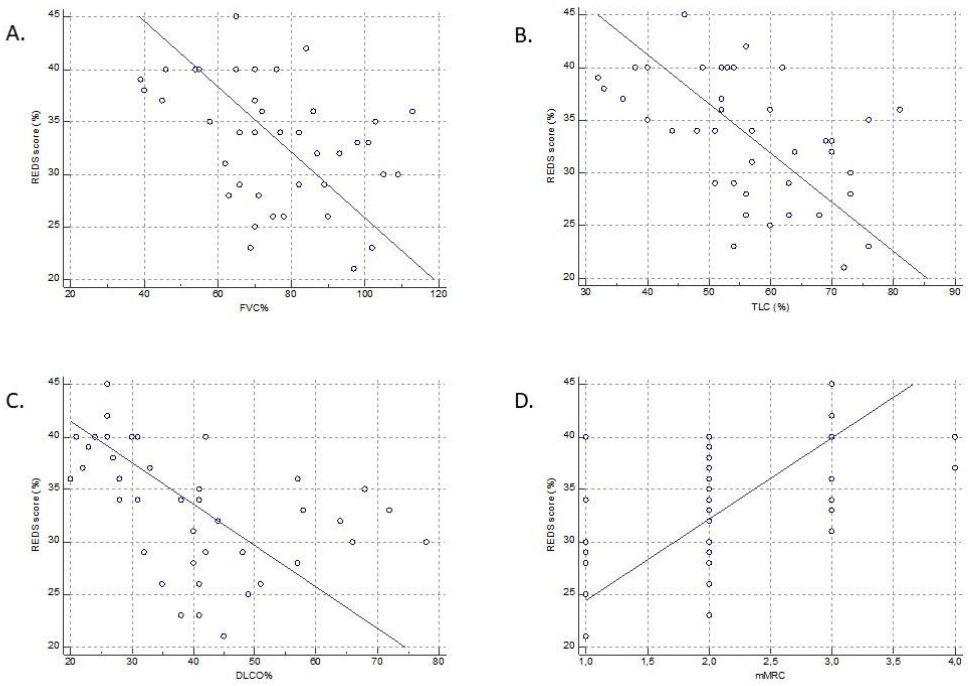

Figure 3. Main results of correlation between ReDS™ score and functional parameters and mMRC dyspnea score.

When we selected only IPF patients with a definitive UIP pattern at CT (29 subjects) inverse correlation was maintained between ReDS™ score and FVC%, VC% and TLC%; conversely a direct correlation was present for mMRC dyspnoea scale (Table 2).

Table 2. IPF patients with UIP definite CT pattern: clinical and functional correlations.

	R	95% IC for r	p
FVC	-0.2773	-0.5844 to 0.0993	0.1454
FVC%	**-0.4655**	**-0.7108 to -0.1194**	**0.0109**
VC	-0.2801	-0.5864 to 0.0962	0.1411
VC%	**-0.4746**	**-0.7165 to -0.1308**	**0.0093**
FEV1	-0.1429	-0.4841 to 0.2360	0.4596
FEV1%	-0.2859	-0.5906 to 0.0900	0.1327
FEV1/FVC	**0.5168**	**0.1854 to 0.7427**	**0.0041**
FEV1/VC	0.2608	-0.1169 to 0.5726	0.1719
TLC	-0.3104	-0.6077 to 0.0633	0.1013
TLC%	**-0.4860**	**-0.7236 to -0.1454**	**0.0075**
DLCO	-0.2675	-0.5774 to 0.1098	0.1607

DLCO%	-0.3487	-0.6342 to 0.0241	0.0637
DLCO/AV	0.0295	-0.3406 to 0.3918	0.8790
DLCO/AV%	-0.1130	-0.4605 to 0.2644	0.5593
AV	-0.3367	-0.6259 to 0.0340	0.0741
AV%	-0.3490	-0.6344 to 0.0201	0.0635
Dyspnoea mMRC	**0.4389**	**0.0862 to 0.6938**	**0.0172**
Height	-0.0099	-0.3751 to 0.3578	0.9591
Weight	0.05186	-0.3207 to 0.4106	0.7893

Finally, when we selected only IPF patients with a UIP probable CT pattern (12 subjects), the only correlations with ReDS™ score were DLCO, DLCO%, AV% (inversely correlated) and mMRC (directly correlated) (Table 3).

Table 3. IPF patients with UIP probable CT pattern: clinical and functional correlations.

	R	95% IC for r	p
FVC	-0.0840	-0.6277 to 0.5147	0.7950
FVC%	-0.2377	-0.7142 to 0.3893	0.4569
VC	-0.2164	-0.7030 to 0.4082	0.4994
VC%	-0.3387	-0.7641 to 0.2920	0.2816
FEV1	-0.0137	-0.5830 to 0.5646	0.9663
FEV1%	-0.2256	-0.7079 to 0.4001	0.4808
FEV1/FVC	0.1713	-0.4465 to 0.6785	0.5946
FEV1/VC	0.2587	-0.3701 to 0.7250	0.4168
TLC	-0.4390	-0.8091 to 0.1804	0.1534
TLC%	-0.5710	-0.8623 to 0.0043	0.0525
DLCO	**-0.5953**	**-0.8715 to -0.0325**	**0.0411**
DLCO%	**-0.6755**	**-0.9003 to -0.1658**	**0.0159**
DLCO/AV	-0.3233	-0.7568 to 0.3077	0.3053
DLCO/AV%	-0.4182	-0.8001 to 0.2049	0.1761
AV	-0.4451	-0.8117 to 0.1731	0.1471
AV%	**-0.5800**	**-0.8657 to -0.0091**	**0.0481**
Dyspnoea mMRC	**0.5769**	**0.0045 to 0.8646**	**0.0495**
Height	0.6136	0.0612 to 0.8782	0.0338
Weight	0.2343	-0.3924 to 0.7124	0.4637

When we stratified patients for functional severity based on TLC (% of the predicted value), we observed a significant difference in ReDS™ scores among patients with a mild and severe restrictive pattern. Same results were reported in case of FVC (% of the predicted value) alterations when the difference was observed for values lower than 50% and greater than 80%: in this case, when we divided ReDS™ results for FVC% above and below 50% we confirmed the statistically significant difference. Similar results were observed for DLCO (% of the predicted value) when the difference was observed for value greater than 60% and lower than 40%. On the other hand, considering mMRC dyspnoea functional classes, grouping ReDS™ score of patients with mMRC 3 and 4, we observed a significant difference between patients with mMRC 1 and 3-4 scores. Finally, we did not observe differences among ReDS™ score of UIP definite versus probable CT pattern (Table 4).

Table 4. ReDS™ score among different radiological, functional and clinical groups.

	Mean (± SD) ReDS™ score	p
UIP definite UIP probable	33.13 ±6.12 33.75 ±5.37	0.669
TLC ≥60% TLC 40-60% TLC ≤40%	29.93 ±5.02 * 34.85 ±5.82 38.60 ±1.14 *	0.002 0.002*
FVC ≥80% FVC 50-80% FVC <50%	31.31 ±5.18 * 33.85 ±6.27 38.60 ±1.14 *	0.043 0.016*
FVC ≥50% FVC <50%	32.75 ±5.88 38.40 ±1.14	0.040
DLCO ≥60% DLCO 40-60% DLCO <40%	32.00 ±2.12 30.35 ±5.51* 36.31 ±5.47*	0.005 0.043*
mMRC 1 mMRC 2 mMRC 3 and 4	29.57 ±6.13* 32.39 ±5.43 37.63 ±4.17*	0.006 0.002*

Discussion

In our study we demonstrated an inverse correlation between ReDS™ score and functional parameters indicative for a pulmonary restrictive pattern: in particular, we observed an inverse correlation with FVC, VC, TLC, AV and DLCO. All these parameters are typically reduced in patients with IPF and each of them correlates with pulmonary fibrosis [8]. In lung fibrosis the volume of air is reduced while the tissue volume is increased compared to a normal lung; we also

know that the more fibrosis increases, the more FVC, TLC and DLCO are reduced and that FVC and TLC are proportional to fibrosis (as demonstrated by chest CT comparison analysis) [3-5].

The ReDS™ is a non-invasive technology that measures lung fluid content quickly and accurately. The result is displayed in percent units (%), representing the volume of fluid in the lung out of the lung volume. The readings range is 15-60%. The system utilizes low power electromagnetic waves for a simple up to 90-second measurement. The electromagnetic waves are transmitted and received by two dedicated sensors applied on patient thorax (chest and back) without the need for direct skin contact. The system also includes a bedside portable console for operating the sensors unit and calculating the result. The traveling electromagnetic signal is affected by tissues' conductivity and capacitance properties: since these properties are most affected by the presence of fluids, the signal was demonstrated to be representative of tissue fluid content. The signal properties are then analyzed using a dedicated algorithm which provides the result: when applying on the chest, the fluid in the lung fluid can be assessed [6, 10, 11].

As specified above in methods section, ReDS™ measures the combination of dielectric proprieties (relative permittivity and conductivity) of the lungs which are determined by the volumetric concentrations of fluids. *Nopp* et al. defined that the filling factor (F) is the ratio of air volume (Va) to lung tissue volume (Vc) (F = Va / Vc) [12]. Filling factor (F) and Relative Permittivity and Conductivity are inversely correlated; the decrease of conductivity and relative permittivity was explained by alveolar walls thinning as well as the deformation of the epithelial cells and blood vessels through the expansion of the alveoli [7].

Based on the assumption that in lung fibrosis Va is reduced and Vc is increased, for the formula F = Va / Vc, F is directly proportional to FVC and therefore FVC is inversely proportional to dielectric properties (conductivity and permittivity).

If the equation of ReDS™ measurement is ReDS™ = 1 / (1+F) and, after simplifications, ReDS™ = Vc / (Va+Vc)

Then if lung air volume is reduced as measured in FVC (or TLC) ReDS™ is higher,

And if Vc increases and Va decreases due to fibrosis, therefore ReDS increases even more.

This would demonstrate the reason why in our patients the % of ReDS™ score increases with the reduction of FVC and TLC (and collaterally also DLCO).

Amir et al. demonstrated that the mean ReDS™ score in subjects without acute decompensated heart failure was 27.3% and that it was significantly lower than the one measured in patients with

acute decompensated heart failure (mean 39.8%) [6]. In our cohort of IPF patients the mean ReDS™ score was higher, with a 33.3% in the IPF cohort of patients, even if we do not dispose of a control arm.

The rate of decline in FVC was the most common primary end-point outcome in clinical trials in IPF, expressed either in milliliters per year [13] or as percentage of the predicted value and the prognosis of IPF patients is worse in those ones with lower FVC or DLCO [14-16]. In our study we observed a significant difference between mean ReDS™ scores among patients stratified on functional parameters FVC, TLC and DLCO, even if this significance was maintained only for mild and severe functional impairment probably due to the small size of the cohort.

FVC measured with a daily home spirometry in IPF and non-IPF ILD patients facilitates the identification of FVC variability, which was associated with disease progression [17]. ReDS™ system measures can be performed at home, as conducted by *Amir* et al. in the monitoring of patients with heart failure [18]. ReDS™ system could then be used in the home monitoring of patients with IPF due to its ease of use and the reproducibility of its measurements [6]: moreover, thanks to the unnecessary coordination between patient and measure system, this could be useful in patients with a difficult coordination to perform reproducible spirometric measurements or in case of severe respiratory failure, when desaturation could be harmful. Finally, during coronavirus-19 disease (COVID-19) pandemic, telemedicine could represent a bridge to monitor patients with chronic diseases, offering to clinician the possibility to evaluate patients sparing/avoiding them to long voyages and possible contagions [19].

Interestingly, considering the whole population of IPF patients, the ReDS™ score was directly correlated with the dyspnea score measured with mMRC scale: in particular there was a significant difference of ReDS™ scores among patients with mMRC 1 and 3 and 4 groups. Previously published data, particularly in patients with a severe functional impairment, demonstrated that there was a poor correlation between the 6MWT distance and both FVC% and DLCO% [20], but dyspnoea measured with MRC scale, was correlated with functional parameters FVC, TLC and DLCO [21]. Dyspnoea, measured with mMRC scale, was also correlated with a poorer survival in IPF patients: the mMRC had a hazard ratio of 2.402, resulting as independent variable to predict survival [22]. Our results suggest that by measuring indirectly the reduced volume of air in lungs of IPF patients and possibly fibrotic amount, ReDS™ score correlates with dyspnoea, with a non-invasive method.

UIP definite pattern is characterized by the presence of honeycombing with or without peripheral traction bronchiectasis or bronchiolectasis with subpleural and basal predominant alterations; in

UIP probable pattern the reticular pattern with peripheral traction bronchiectasis or bronchiolectasis does not have honeycombing alterations [9]. A direct correlation between radiological pattern and functional abnormalities was never demonstrated even if there is a correlation between CT densitometric measures and FVC and DLCO [5]. Nevertheless, there is a strong correlation between CT-derived automated lung volume and TLC and a significant correlation between manual CT measurements and FVC% in patients with IPF [23]. Up to now, no studies demonstrated differences in lung volumes at CT scan among UIP definite and probable patterns, as well as FVC is comparable among them [24, 25]. Even in our cohort of patients FVC, TLC and DLCO were similar among two groups without significant differences. With these premises, the differences we observed in ReDS™ scores could be derived by the higher presence at CT scan of honey combing and traction bronchiectasis that are present in UIP pattern. An augmentation in the amount of fibrotic tissue increases mean lung density and decrease the histogram kurtosis and skew and, consequently, reduce the air volume [26]; however, several studies failed to demonstrate differences of kurtosis, skewness and mean lung attenuation between UIP pattern fibrosis/IPF patients and patients with HP and/or unclassifiable idiopathic interstitial pneumonia [27, 28]. We suppose that the differences of correlation between ReDS™ scores of patients with UIP definite and probable pattern could be due to the different disposition of the alterations in the lungs: in particular, the electromagnetic waves are emitted in the upper part of the thorax, frontally, and pass through the lung until reaching the sensor located in the lower part of the thorax, dorsally (Figure 4). The differences among significant correlations of functional parameters among the two CT pattern groups, as well as the lack of differences of ReDS™ scores, indicates that the ReDS™ system is a quantitative measurement, not qualitative. Interestingly, both groups maintain the correlation between dyspnoea scale.

Figure 4. Sagittal view of ReDS™ sensor position: left image of a normal lung and right image sagittal CT scan view of UIP definitive pattern of IPF patient.

Our study has several limitations: firstly, we did not acquire CT images in occasion of ReDS™ measurement; this would confirm our suppositions about the correlation between functional parameters, CT density and fibrotic score, and their correlation with ReDS™ results. This hypothesis is only a speculation but is based on the indirect assumption, previously demonstrated, that FVC, TLC and DLCO are correlated with fibrosis at CT in IPF patients [23], and that lung water was correlated with density at CT scan [5, 6]. In second, we make a punctual observation of functional parameters and ReDS™ scores; the longitudinal evaluation of ReDS™ scores trend, and its correlation with functional parameters, would give us a predictive instrument for IPF patients. Thirdly, we did not perform a comparison between IPF population and a healthy cohort of subjects. Finally, we excluded from our analysis patients with secondary pulmonary hypertension (3 patients), to avoid a confounding factor that would increase the ReDS™ score; nevertheless, its measurement, with other bio humoral and clinical evaluations, would give to the clinician and important information, due to its prognostic value in patients with acute heart decompensation [6].

In conclusion, we demonstrate a correlation of ReDS™ scores with some functional (mainly indicative or diagnostic for a restrictive pattern) and clinical parameters in patients with IPF; the score is correlated with the density of tissues that the electromagnetic waves emitted by ReDS™ pass through, reflecting their dielectric proprieties. Due to its ease to use, invasiveness and non-necessity of patients' collaboration to obtain an adequate measurement, ReDS™ could be used as

an adjunction to classical spirometric evaluation in IPF patients. Larger and longitudinal studies are needed to confirm these promising preliminary results.

References list:

1. Park HJ, Lee SM, Song JW, Oh SY, Kim N, Seo JB. Texture-based automated quantitative assessment of regional patterns on initial CT in patients with idiopathic pulmonary fibrosis: Relationship to decline in forced vital capacity. American Journal of Roentgenology. 2016 Nov 1;207(5):976–83.

2. Plantier L, Cazes A, Dinh-Xuan AT, Bancal C, Marchand-Adam S, Crestani B. Physiology of the lung in idiopathic pulmonary fibrosis. Vol. 27, European Respiratory Review. European Respiratory Society; 2018.

3. du Bois RM, Weycker D, Albera C, Bradford WZ, Costabel U, Kartashov Aet al. Forced vital capacity in patients with idiopathic pulmonary fibrosis: test properties and minimal clinically important difference. Am J Respir Crit Care Med. 2011 Dec 15;184(12):1382-9.

4. Clukers J, Lanclus M, Mignot B, Van Holsbeke C, Roseman J, Porter S, et al. Quantitative CT analysis using functional imaging is superior in describing disease progression in idiopathic pulmonary fibrosis compared to forced vital capacity. Respir Res. 2018 Nov 6;19(1):213.

5. Ash SY, Harmouche R, Vallejo DL, Villalba JA, Ostridge K, Gunville R, et al. Densitometric and local histogram based analysis of computed tomography images in patients with idiopathic pulmonary fibrosis. Respir Res. 2017 Mar 7;18(1):45.

6. Amir O, Azzam ZS, Gaspar T, Faranesh-Abboud S, Andria N, Burkhoff D, et al. Validation of remote dielectric sensing (ReDS^{TM}) technology for quantification of lung fluid status: Comparison to high resolution chest computed tomography in patients with and without acute heart failure. International Journal of Cardiology. 2016 Oct 15;221:841–6.

7. Wang JR, Sun BY, Wang HX, Pang S, Xu X, Sun Q. Experimental study of dielectric properties of human lung tissue in vitro. Journal of Medical and Biological Engineering. 2014;34(6):598–604.

8. von Elm E, Altman DG, Egger M, Pocock SJ, Gøtzsche PC, Vandenbroucke JP; STROBE Initiative. The Strengthening the Reporting of Observational Studies in Epidemiology

(STROBE) statement: guidelines for reporting observational studies. PLoS Med. 2007 Oct 16;4(10):e296.

9. Raghu G, Remy-Jardin M, Myers JL, Richeldi L, Ryerson CJ, Lederer DJ, et al. Diagnosis of idiopathic pulmonary fibrosis: an official ATS/ERS/JRS/ALAT clinical practice guideline. Am J Respir Crit Care Med 2018; 198(5):e44-e68.

10. Uriel N, Sayer G, Imamura T, Rodgers D, Kim G, Raikhelkar J, et al. Relationship Between Noninvasive Assessment of Lung Fluid Volume and Invasively Measured Cardiac Hemodynamics. J Am Heart Assoc. 2018 Nov 20;7(22):e009175.

11. Offer A, Tuvia BG, Weinstein JM, Schliamser J, Burkhoff, D Abbo, A, Abraham WT, International Journal of Cardiology: Evaluation of remote dielectric sensing (ReDS) technology-guided therapy for decreasing heart failure re-hospitalizations, 2017, 240, 279-284

12. Nopp P, Rapp E, Pfützner H, Nakesch H, Ruhsam C. Dielectric properties of lung tissue as a function of air content. Phys Med Biol. 1993 Jun;38(6):699-716.

13. Richeldi L, du Bois RM, Raghu G, Azuma A, Brown KK, Costabel U, et al. Efficacy and safety of nintedanib in idiopathic pulmonary fibrosis. N Engl J Med 2014; 370: 2071–2082.

14. King TE Jr, Bradford WZ, Castro-Bernardini S, Fagan EA, Glaspole I, Glassberg MK, et al. A phase 3 trial of pirfenidone in patients with idiopathic pulmonary fibrosis. N Engl J Med 2014; 370: 2083–2092.

15. Parker JM, Glaspole IN, Lancaster LH, Haddad TJ, She D, Roseti SL, et al. A phase 2 randomized controlled study of tralokinumab in subjects with idiopathic pulmonary fibrosis. Am J Respir Crit Care Med 2018; 197: 94–103.

16. Raghu G, Martinez FJ, Brown KK, Costabel U, Cottin V, Wells AU, et al. CC-chemokine ligand 2 inhibition in idiopathic pulmonary fibrosis: a phase 2 trial of carlumab. Eur Respir J 2015; 46: 1740–1750.

17. Veit T, Barnikel M, Crispin A, Kneidinger N, Ceelen F, Arnold P, et al. Variability of forced vital capacity in progressive interstitial lung disease: a prospective observational study. Respir Res. 2020 Oct 19;21(1):270.

18. Amir O, Ben-Gal T, Weinstein JM, Schliamser J, Burkhoff D, Abbo A, et al. Evaluation of remote dielectric sensing (ReDS) technology-guided therapy for decreasing heart failure re-hospitalizations. Int J Cardiol. 2017 Aug 1;240:279-284.

19. Coskun F, Hanta I, Cilli A, Ozkaya G, Ursavas A, Sevinc C. Effects of the COVID-19 pandemic on the follow-up and treatment of patients with idiopathic pulmonary fibrosis: a cross-sectional, multicentre phone call survey. BMJ Open. 2021 Aug 12;11(8):e050578.

20. Pastre J, Barnett S, Ksovreli I, Taylor J, Brown AW, Shlobin OA, Ahmad K, Khangoora V, Aryal S, King CS, Nathan SD. Idiopathic pulmonary fibrosis patients with severe physiologic impairment: characteristics and outcomes. Respir Res. 2021 Jan 6;22(1):5.

21. Papiris SA, Daniil ZD, Malagari K, Kapotsis GE, Sotiropoulou C, Milic-Emili J, et al. The Medical Research Council dyspnea scale in the estimation of disease severity in idiopathic pulmonary fibrosis. Respir Med. 2005 Jun;99(6):755-61.

22. Nishiyama O, Taniguchi H, Kondoh Y, Kimura T, Kato K, Kataoka K, et al. A simple assessment of dyspnoea as a prognostic indicator in idiopathic pulmonary fibrosis. Eur Respir J. 2010 Nov;36(5):1067-72.

23. Robbie H, Wells AU, Jacob J, Walsh SLF, Nair A, Srikanthan A, et al. Visual and Automated CT Measurements of Lung Volume Loss in Idiopathic Pulmonary Fibrosis. AJR Am J Roentgenol. 2019 Aug;213(2):318-324.

24. Fukihara J, Kondoh Y, Brown KK, Kimura T, Kataoka K, Matsuda T, et al. Probable usual interstitial pneumonia pattern on chest CT: is it sufficient for a diagnosis of idiopathic pulmonary fibrosis? Eur Respir J. 2020 Apr 9;55(4):1802465.

25. Salisbury ML, Tolle LB, Xia M, Murray S, Tayob N, Nambiar AM, et al. Possible UIP pattern on high-resolution computed tomography is associated with better survival than definite UIP in IPF patients. Respir Med. 2017 Oct;131:229-235.

26. Weatherley ND, Eaden JA, Stewart NJ, Bartholmai BJ, Swift AJ, Bianchi SM, et al. Experimental and quantitative imaging techniques in interstitial lung disease. Thorax. 2019 Jun;74(6):611-619.

27. Sverzellati N, Zompatori M, De Luca G, Chetta A, Bnà C, Ormitti F, et al. Evaluation of quantitative CT indexes in idiopathic interstitial pneumonitis using a low-dose technique. Eur J Radiol. 2005 Dec;56(3):370-5.

28. Sverzellati N, Calabrò E, Chetta A, Concari G, Larici AR, Mereu M, et al. Visual score and quantitative CT indices in pulmonary fibrosis: Relationship with physiologic impairment. Radiol Med. 2007 Dec;112(8):1160-72.